Supporting Information

The Chemistry of Kratom [*Mitragyna speciosa*]: Updated Characterization Data and Methods to Elucidate Indole and Oxindole Alkaloids

Laura Flores-Bocanegra, Huzefa A. Raja, Tyler N. Graf, Mario Augustinović, E. Diane Wallace, Shabnam Hematian, Joshua J. Kellogg, Daniel A. Todd, Nadja B. Cech, and Nicholas H. Oberlies*

Index of Figures

Index of Tables

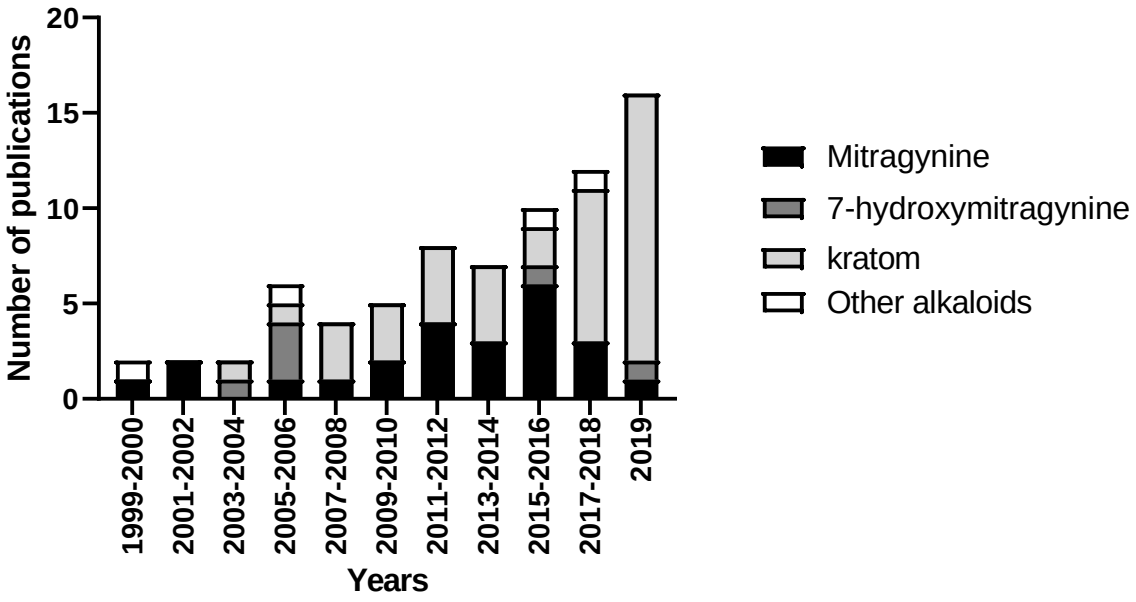

Figure S1. Histogram showing the number of papers about the pharmacological properties for kratom (presumably an extract of *M. speciosa*) and/or the kratom alkaloids mitragynine, 7-hydroxymitragynine and others, published in the past 20 years. This search was performed using "SciFinder" and "PubMed" with the research topic "Kratom" and "*Mitragyna speciosa*". The search was refined by looking only at those papers published that applied *in vitro* and/or *in vivo* pharmacological studies as well as those for case reports.

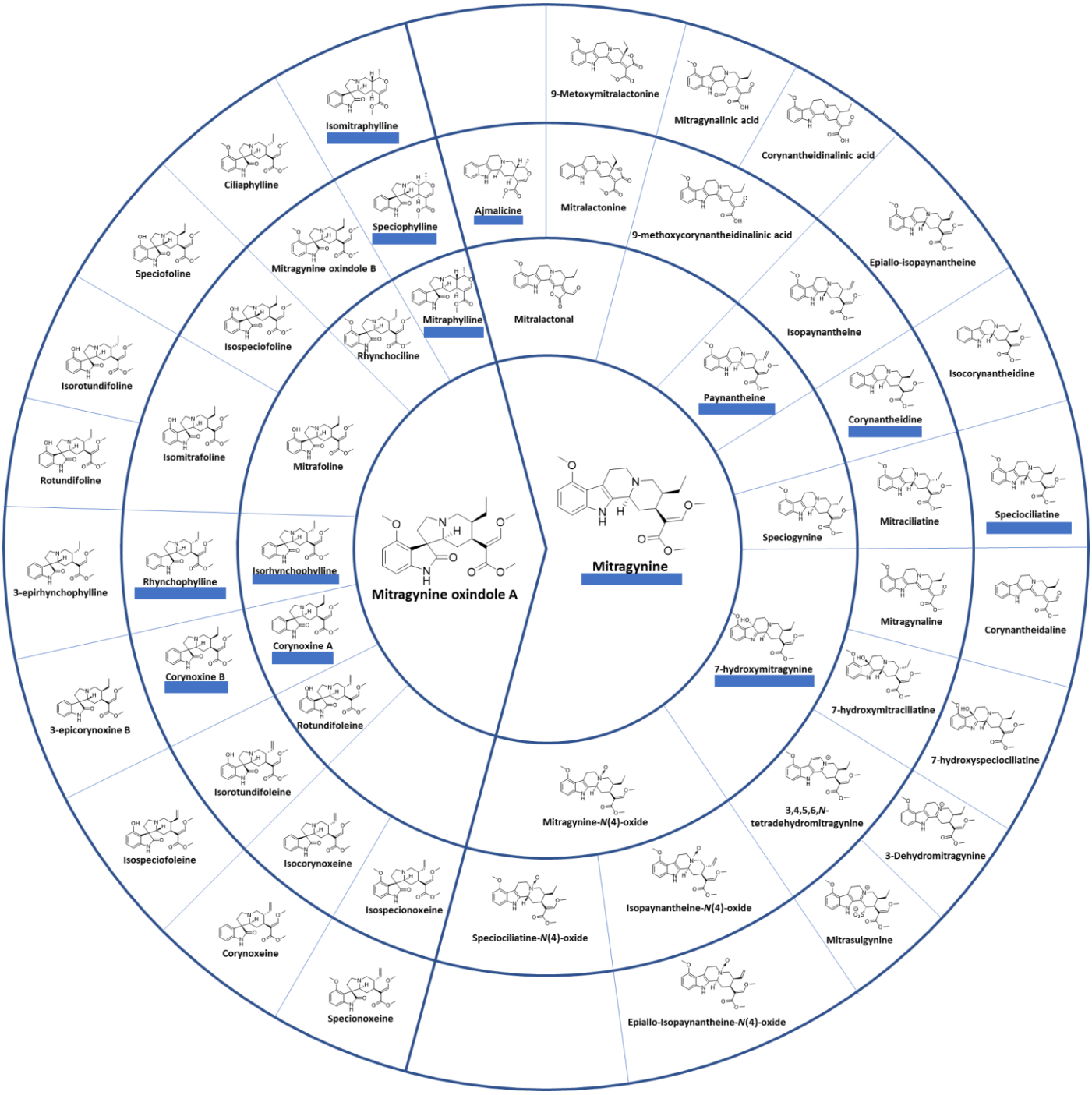

Figure S2. Schematic representation of the 54 compounds that have been reported from *Mitragyna speciosa*, showing the interrelatedness of the structures. Compounds to the right are indole alkaloids, while those to the left are oxindole alkaloids. Compounds underlined in blue are commercially available (as of 2019); however, we strongly recommend verifying both the purity and identity of any purchased standards.

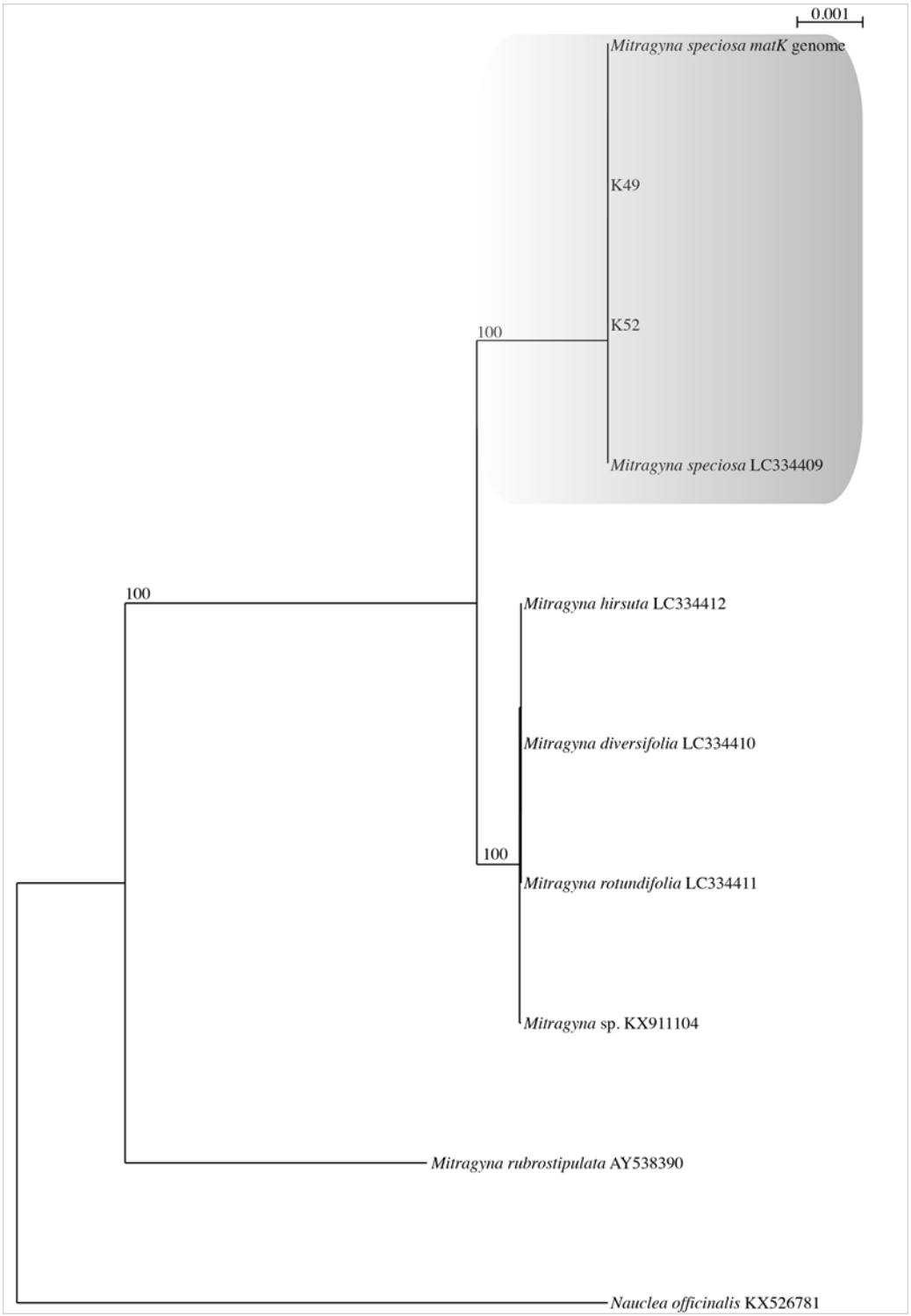

Figure S3. Phylogenetic tree (RAxML; -lnL = 2220.13) inferred from the DNA sequence data from the plastid region (*matK*; 1525 bp). K49 and K52 form a strongly supported clade with published sequence data of *Mitragyna speciosa*, including a partial sequence of *matK* from the *Mitragyna speciosa* genome assembly; BioProject: PRJNA325670 (Center for Food Safety and Applied Nutrition (CFSAN), part of the FDA). Numbers refer to RAxML bootstrap support values ≥ 70% based on 1000 replicates. Clades with samples from the present study are highlighted in gray. Bar indicates nucleotide substitutions per site. The tree was rooted to *Nauclea officinalis*

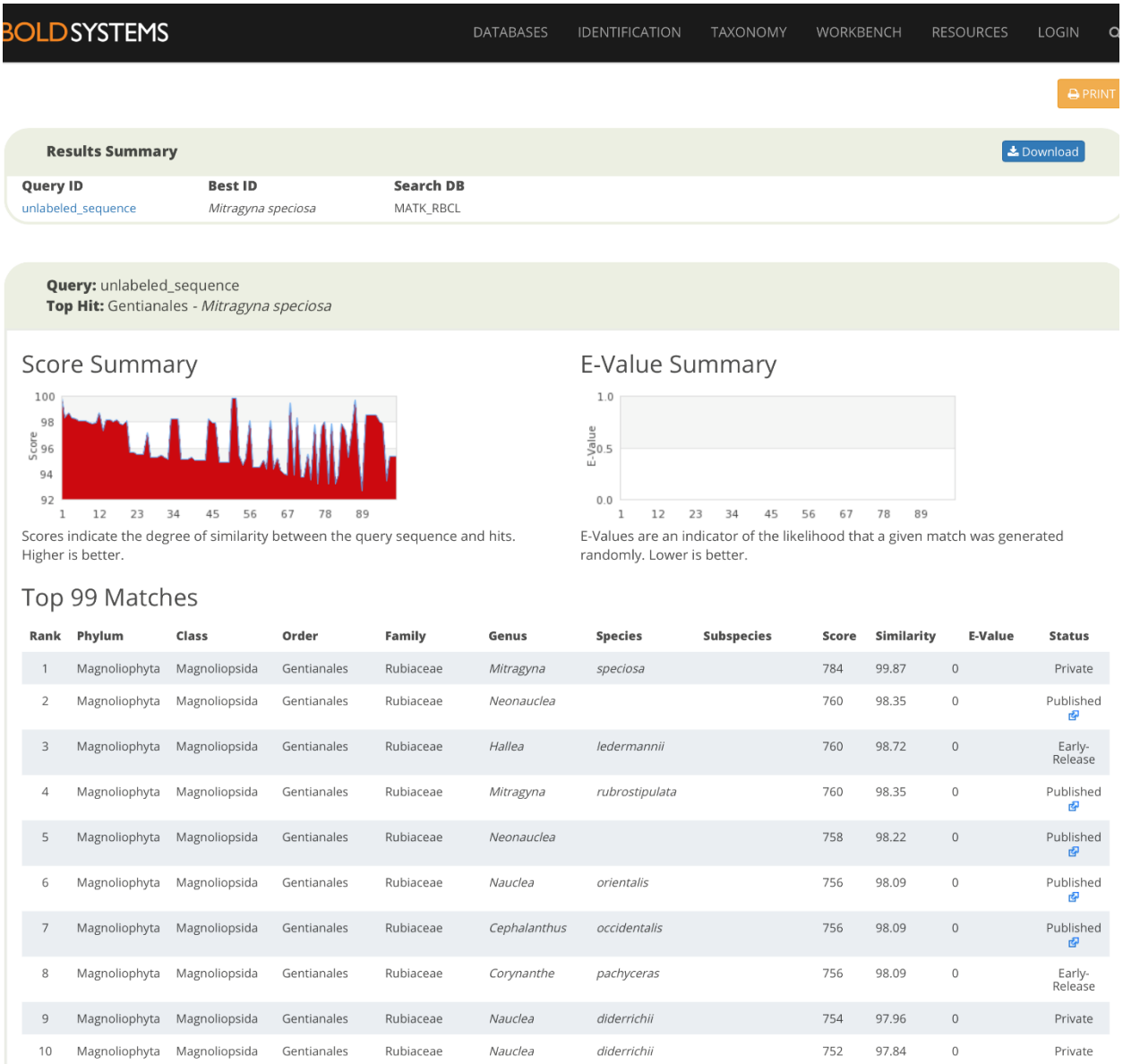

Rank	Phylum	Class	Order	Family	Genus	Species	Subspecies	Score	Similarity	E-Value	Status
1	Magnoliophyta	Magnoliopsida	Gentianales	Rubiaceae	*Mitragyna*	*speciosa*		784	99.87	0	Private
2	Magnoliophyta	Magnoliopsida	Gentianales	Rubiaceae	*Neonauclea*			760	98.35	0	Published
3	Magnoliophyta	Magnoliopsida	Gentianales	Rubiaceae	*Hallea*	*ledermannii*		760	98.72	0	Early-Release
4	Magnoliophyta	Magnoliopsida	Gentianales	Rubiaceae	*Mitragyna*	*rubrostipulata*		760	98.35	0	Published
5	Magnoliophyta	Magnoliopsida	Gentianales	Rubiaceae	*Neonauclea*			758	98.22	0	Published
6	Magnoliophyta	Magnoliopsida	Gentianales	Rubiaceae	*Nauclea*	*orientalis*		756	98.09	0	Published
7	Magnoliophyta	Magnoliopsida	Gentianales	Rubiaceae	*Cephalanthus*	*occidentalis*		756	98.09	0	Published
8	Magnoliophyta	Magnoliopsida	Gentianales	Rubiaceae	*Corynanthe*	*pachyceras*		756	98.09	0	Early-Release
9	Magnoliophyta	Magnoliopsida	Gentianales	Rubiaceae	*Nauclea*	*diderrichii*		754	97.96	0	Private
10	Magnoliophyta	Magnoliopsida	Gentianales	Rubiaceae	*Nauclea*	*diderrichii*		752	97.84	0	Private

Figure S4. Graphical overview of the BLAST results (January 2020) in BOLD database using *matK* (core locus of The Consortium for the Barcode of Life; CBOL). Sample K49 shows ≥ 99% similarity with *Mitragyna speciosa*. Only the top 10 results are shown.

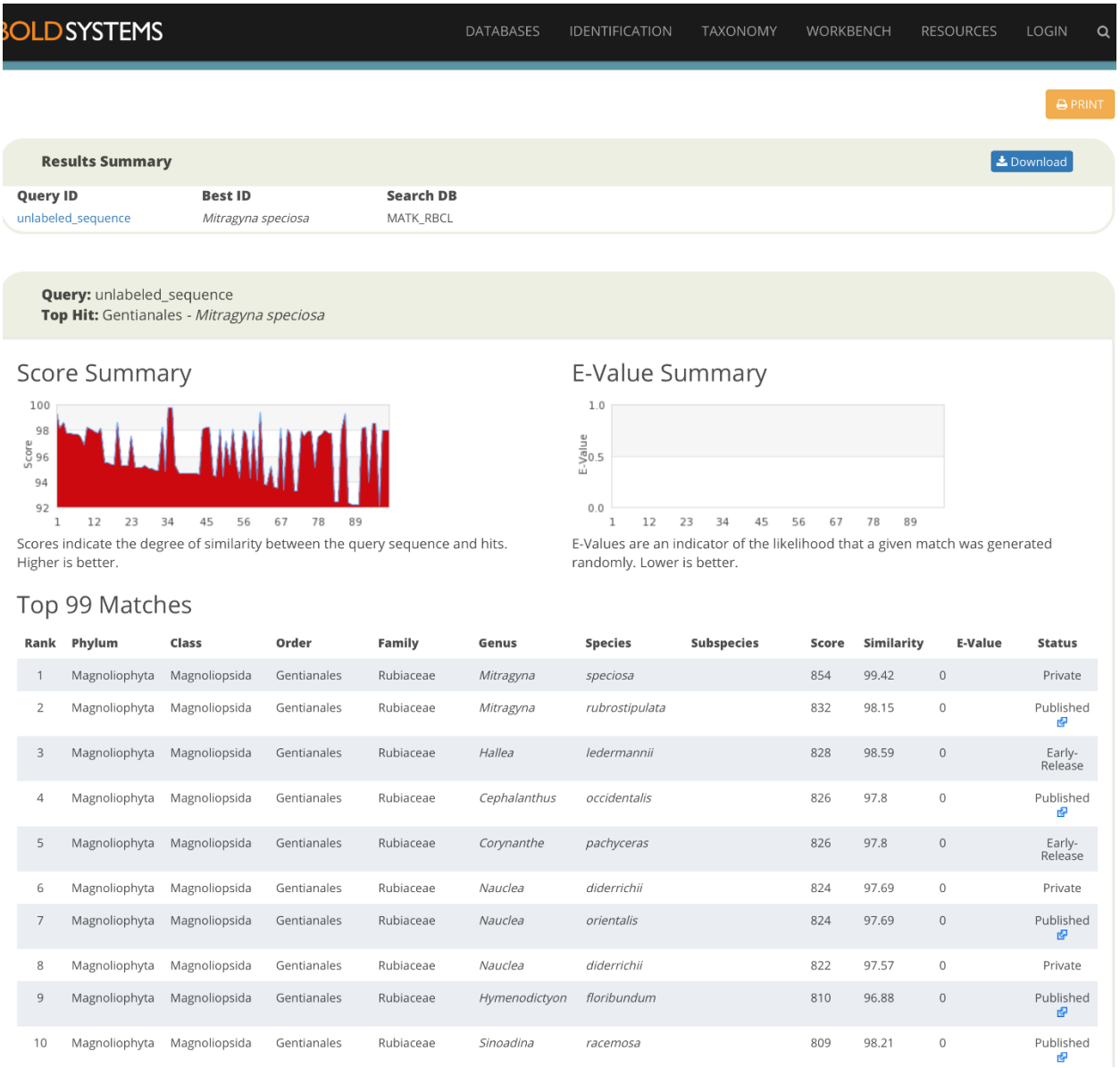

Rank	Phylum	Class	Order	Family	Genus	Species	Subspecies	Score	Similarity	E-Value	Status
1	Magnoliophyta	Magnoliopsida	Gentianales	Rubiaceae	*Mitragyna*	*speciosa*		854	99.42	0	Private
2	Magnoliophyta	Magnoliopsida	Gentianales	Rubiaceae	*Mitragyna*	*rubrostipulata*		832	98.15	0	Published
3	Magnoliophyta	Magnoliopsida	Gentianales	Rubiaceae	*Hallea*	*ledermannii*		828	98.59	0	Early-Release
4	Magnoliophyta	Magnoliopsida	Gentianales	Rubiaceae	*Cephalanthus*	*occidentalis*		826	97.8	0	Published
5	Magnoliophyta	Magnoliopsida	Gentianales	Rubiaceae	*Corynanthe*	*pachyceras*		826	97.8	0	Early-Release
6	Magnoliophyta	Magnoliopsida	Gentianales	Rubiaceae	*Nauclea*	*diderrichii*		824	97.69	0	Private
7	Magnoliophyta	Magnoliopsida	Gentianales	Rubiaceae	*Nauclea*	*orientalis*		824	97.69	0	Published
8	Magnoliophyta	Magnoliopsida	Gentianales	Rubiaceae	*Nauclea*	*diderrichii*		822	97.57	0	Private
9	Magnoliophyta	Magnoliopsida	Gentianales	Rubiaceae	*Hymenodictyon*	*floribundum*		810	96.88	0	Published
10	Magnoliophyta	Magnoliopsida	Gentianales	Rubiaceae	*Sinoadina*	*racemosa*		809	98.21	0	Published

Figure S5. Graphical overview of the BLAST results (January 2020) in BOLD database using *matK* (core locus of The Consortium for the Barcode of Life; CBOL). Sample K52 shows ≥ 99% similarity with *Mitragyna speciosa.* Only the top 10 results are shown.

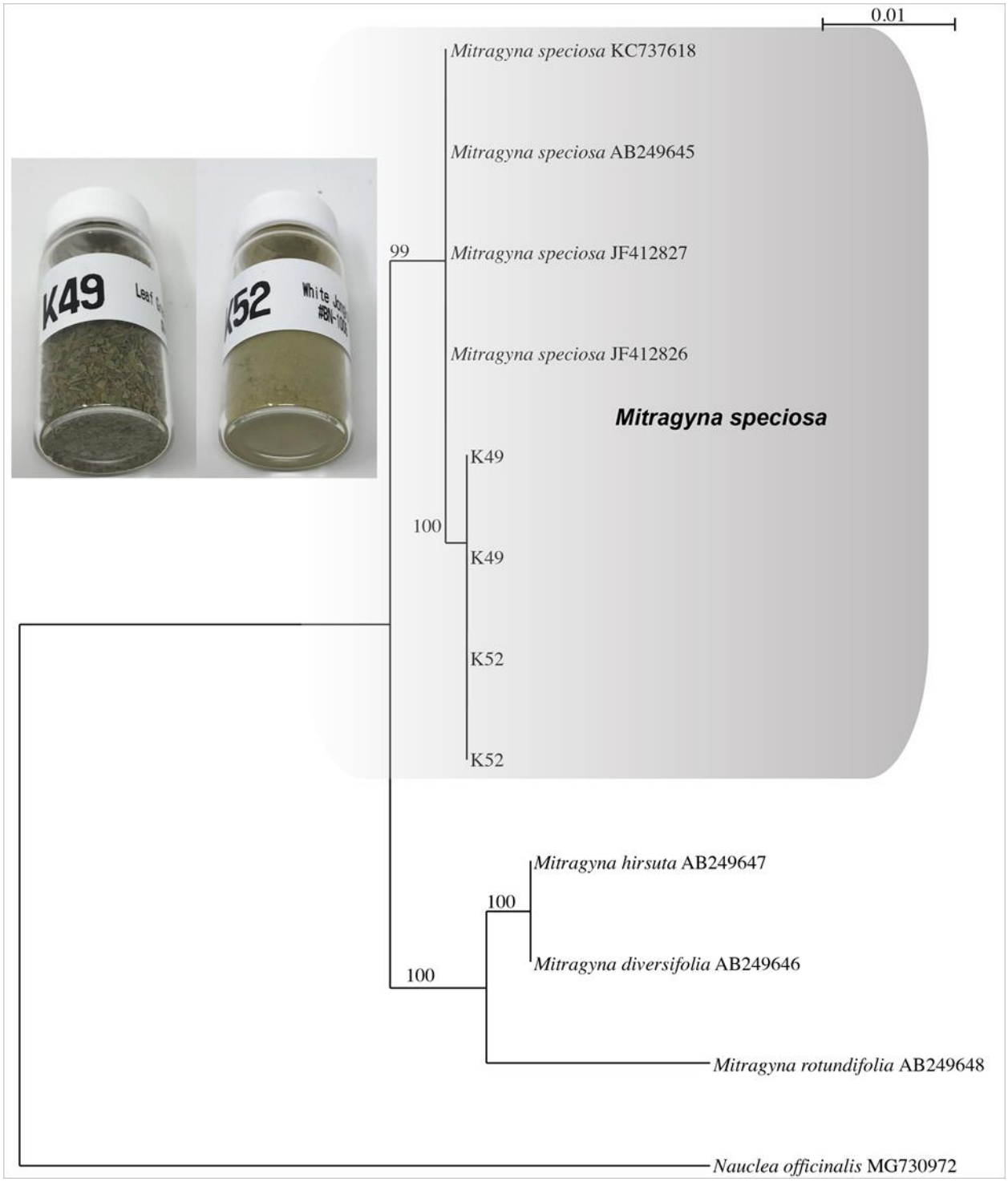

Figure S6. Phylogenetic tree (RAxML; -lnL = 1252.61) inferred from the DNA sequence data from the Internal Transcribed Spacer region (ITS; 662 bp). K49 and K52 form a strongly supported clade with published sequence data of *Mitragyna speciosa* with ≥ 99% bootstrap support. Numbers refer to RAxML bootstrap support values ≥ 70% based on 1000 replicates. Clades with samples from the present study are highlighted in gray. Bar indicates nucleotide substitutions per site. The tree was rooted to *Nauclea officinalis*. Sample vials of K49 and K52 materials are shown on the left.

Table S1. Uncorrected p-Distances from the *trnH-psbA* Region Indicating that Kratom Samples Barcoded in Our Study Have Higher Sequence Similarity with *Mitragyna speciosa*. Regions with N at the beginning and end of the nucleotide alignment were not taken into consideration for uncorrected p-distances. Comparisons were made using the listed species. *Mitragyna speciosa* MH069946; *Mitragyna speciosa* LC334417; *Mitragyna diversifolia* LC334418; *Mitragyna rotundifolia* LC334419; and *Mitragyna hirsuta* LC334420.

	K49	K52	Mitragyna_...	Mitragyna_...	Mitragyna_...	Mitragyna_...	Mitragyna_...
K49		100%	100%	100%	95%	95%	95%
K52	100%		100%	100%	95%	95%	95%
Mitragyna_speciosaM...	100%	100%		100%	95%	95%	95%
Mitragyna_speciosa_L...	100%	100%	100%		95%	95%	95%
Mitragyna_diversifolia_...	95%	95%	95%	95%		100%	100%
Mitragyna_rotundifolia...	95%	95%	95%	95%	100%		100%
Mitragyna_hirsuta_LC3...	95%	95%	95%	95%	100%	100%	

Table S2. Uncorrected p-Distances from the ITS Region Indicating that Kratom Samples Barcoded in Our Study Have Higher Sequence Similarity with *Mitragyna speciosa*. Regions with N at the beginning and end of the nucleotide alignment were not taken into consideration for uncorrected p-distances. Comparisons were made using the listed species. *Mitragyna speciosa* JF412826; *Mitragyna speciosa* JF412827; *Mitragyna speciosa* KC737618; *Mitragyna speciosa* AB249645; *Mitragyna diversifolia* AB249646; *Mitragyna hirsuta* AB249647; *Mitragyna rotundifolia* AB249648; and *Nauclea officinalis* MG730972.

	K49_1_ITS	K49_2_ITS	K52_1_ITS	K52_2_ITS	JF412826...	JF412827...	KC73761...	AB24964...	AB24964...	AB24964...	AB24964...	MG73097...
K49_1_ITS		100%	100%	100%	100%	100%	100%	100%	98%	98%	97%	92%
K49_2_ITS	100%		100%	100%	100%	100%	100%	100%	98%	98%	96%	92%
K52_1_ITS	100%	100%		100%	100%	100%	100%	100%	98%	98%	97%	92%
K52_2_ITS	100%	100%	100%		100%	100%	100%	100%	98%	98%	97%	92%
JF412826_Mitragyna_...	100%	100%	100%	100%		100%	100%	100%	98%	98%	97%	92%
JF412827_Mitragyna_...	100%	100%	100%	100%	100%		100%	100%	98%	98%	97%	92%
KC737618_Mitragyna...	100%	100%	100%	100%	100%	100%		100%	98%	98%	97%	91%
AB249645_Mitragyna...	100%	100%	100%	100%	100%	100%	100%		98%	98%	97%	91%
AB249646_Mitragyna...	98%	98%	98%	98%	98%	98%	98%	98%		100%	98%	89%
AB249647_Mitragyna...	98%	98%	98%	98%	98%	98%	98%	98%	100%		98%	89%
AB249648_Mitragyna...	97%	96%	97%	97%	97%	97%	97%	97%	98%	98%		89%
MG730972_Nauclea_...	92%	92%	92%	92%	92%	92%	91%	91%	89%	89%	89%	

Table S3. Primers and PCR Protocols for Plant Identification.

Locus	Primer	Primer Sequence 5'-3'	Direction	PCR protocol*
The chloroplast maturase K gene (*matK*)	matK-xf matK-MALP	TAATTTACGATCAATTCATTC ACAAGAAAGTCGAAGTAT	Forward Reverse	1. 98˚C – 45 sec 2. 98˚C – 10 sec 3. 54˚C – 30 sec 4. 72˚C – 40 sec 5. Repeat 2–4 for 35 cycles 6. 72˚C – 10 min 7. 4˚C on hold
The chloroplast intergenic region (*trnH-psbA*)	psbA trnH	GTTATGCATGAACGTAATGCTC CGCGCATGGTGGATTCACAATCC	Forward Reverse	1. 94˚C – 5 min 2. 94˚C – 1 min 3. 50˚C – 1 min 4. 72˚C – 2 min 5. Repeat 2–4 for 35 cycles 6. 72˚C – 7 min 7. 4˚C on hold
The internal transcribed spacer (ITS) of nuclear ribosomal DNA	ITS-u1 ITS-u4	GGAAGKARAAGTCGTAACAAGG RGTTTCTTTTCCTCCGCTTA	Forward Reverse	1. 94˚C – 4 min 2. 94˚C – 30 sec 3. 55˚C or 58˚C – 40 sec 4. 72˚C – 1 min 5. Repeat 2–4 for 34 cycles 6. 72˚C – 10 min 7. 4˚C on hold

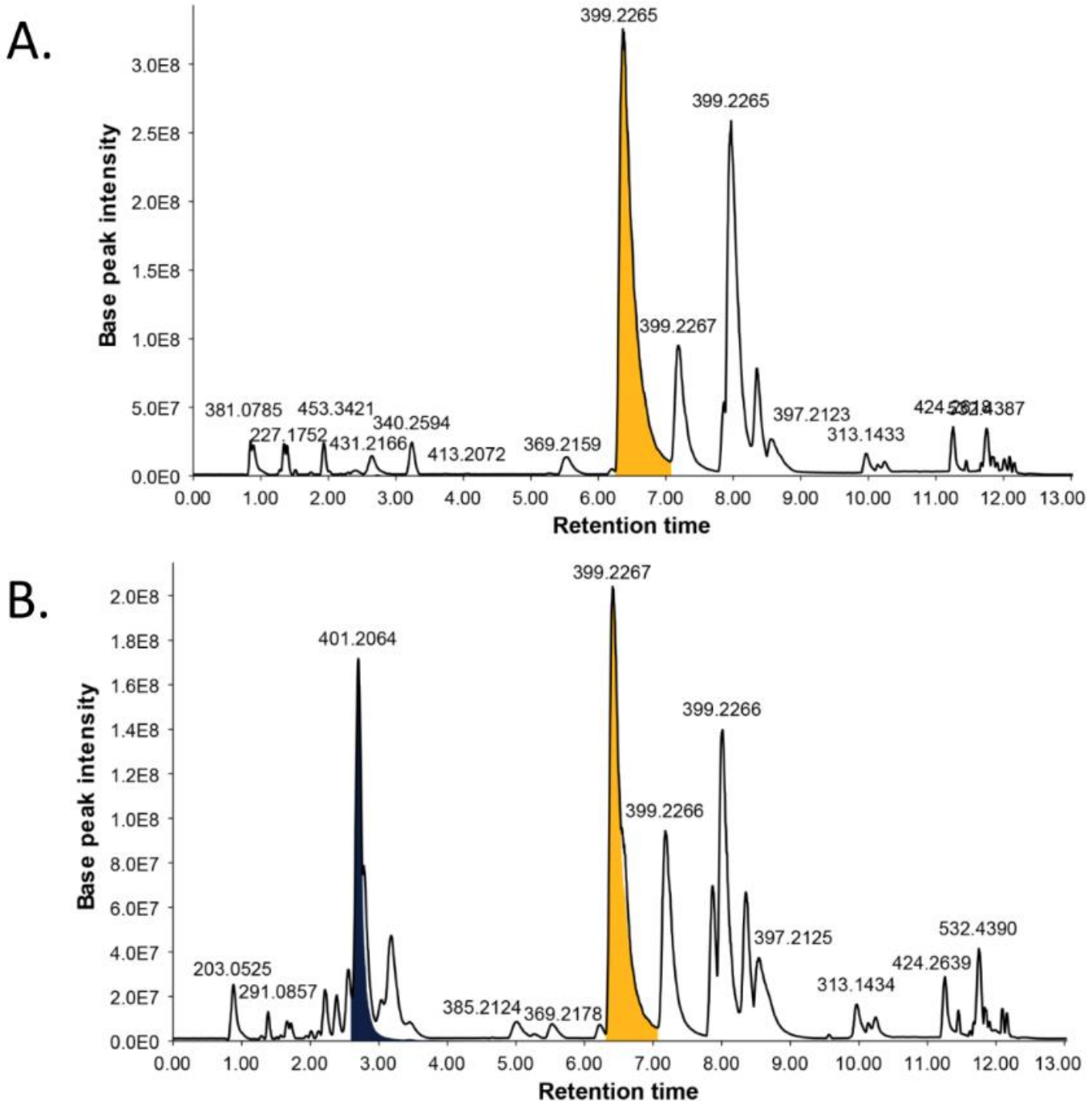

Figure S7. Chromatographic profiles of the two sources of kratom, specifically A) Green Maeng Da (K49) and B) White Jongkong (K52). The major compound present in K49 is mitragynine (**1**, yellow peak). However, in K52 speciofoline (**12**, black peak) has a much higher abundance. The chromatograms were acquired in the reverse phase using a UPLC system coupled with HRESIMS.

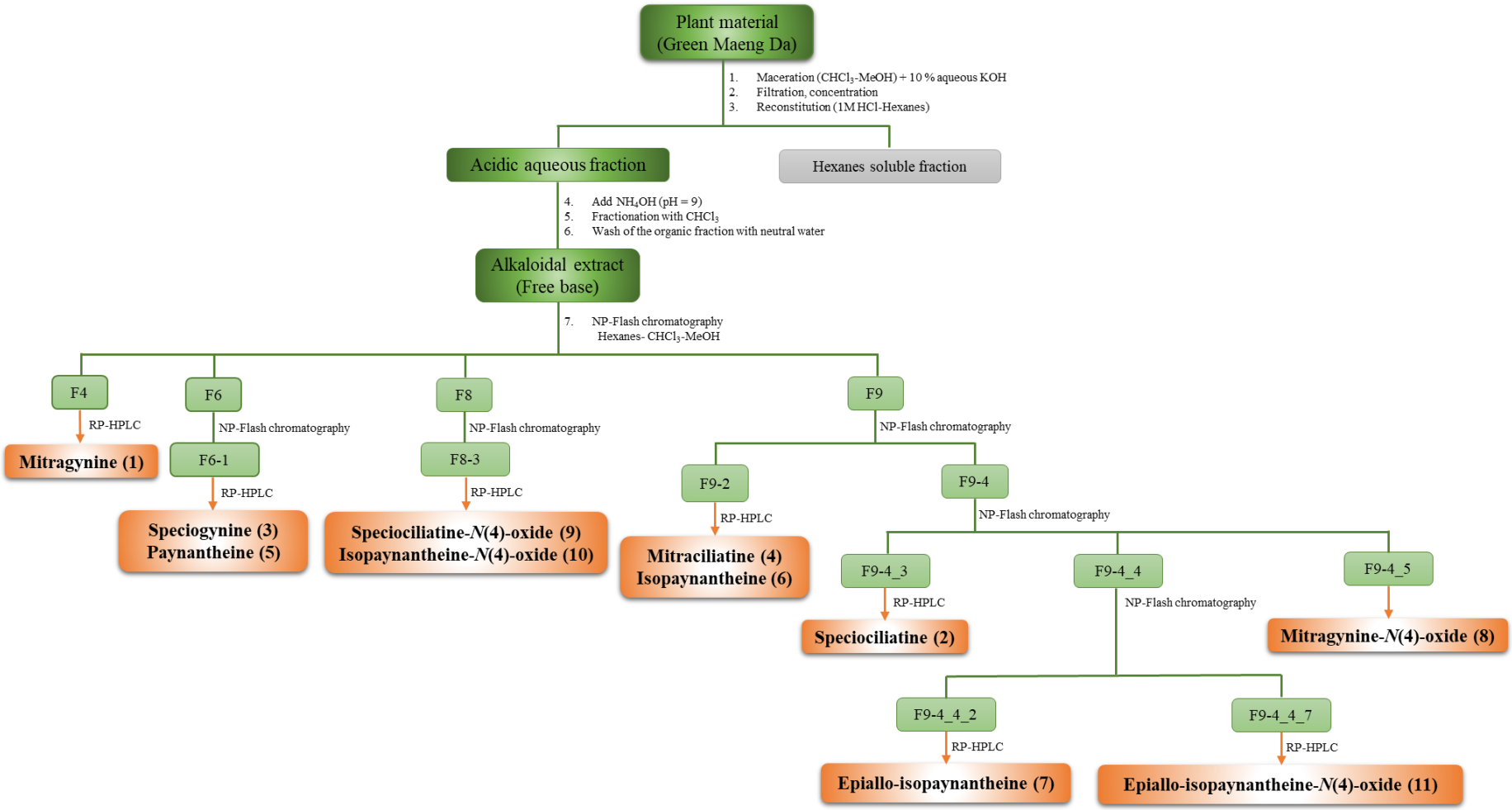

Figure S8. Workflow for the isolation of the alkaloids from the kratom product termed Green Maeng Da (i.e., sample K49).

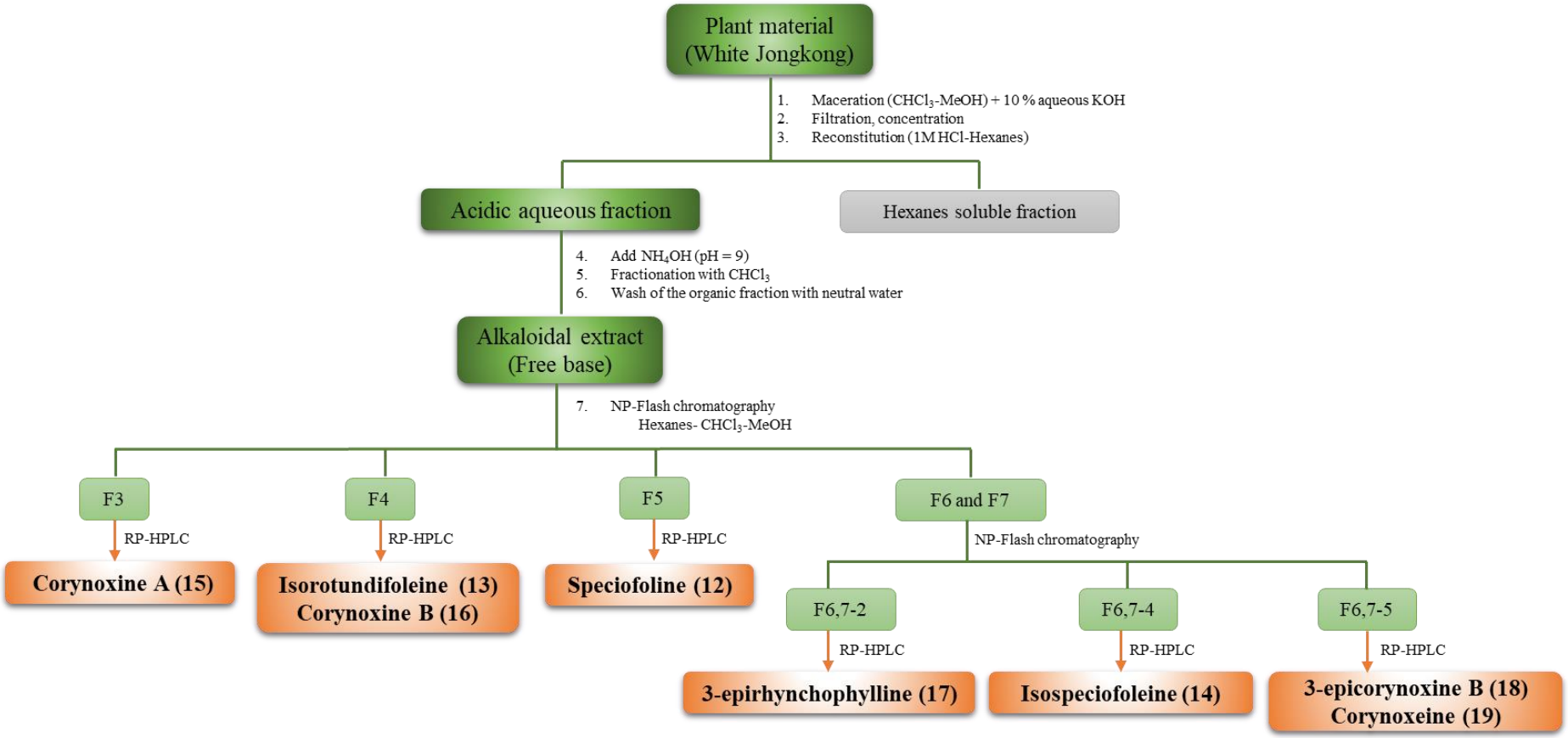

Figure S9. Workflow for the isolation of the alkaloids from the kratom product termed White Jongkong (i.e., sample K52).

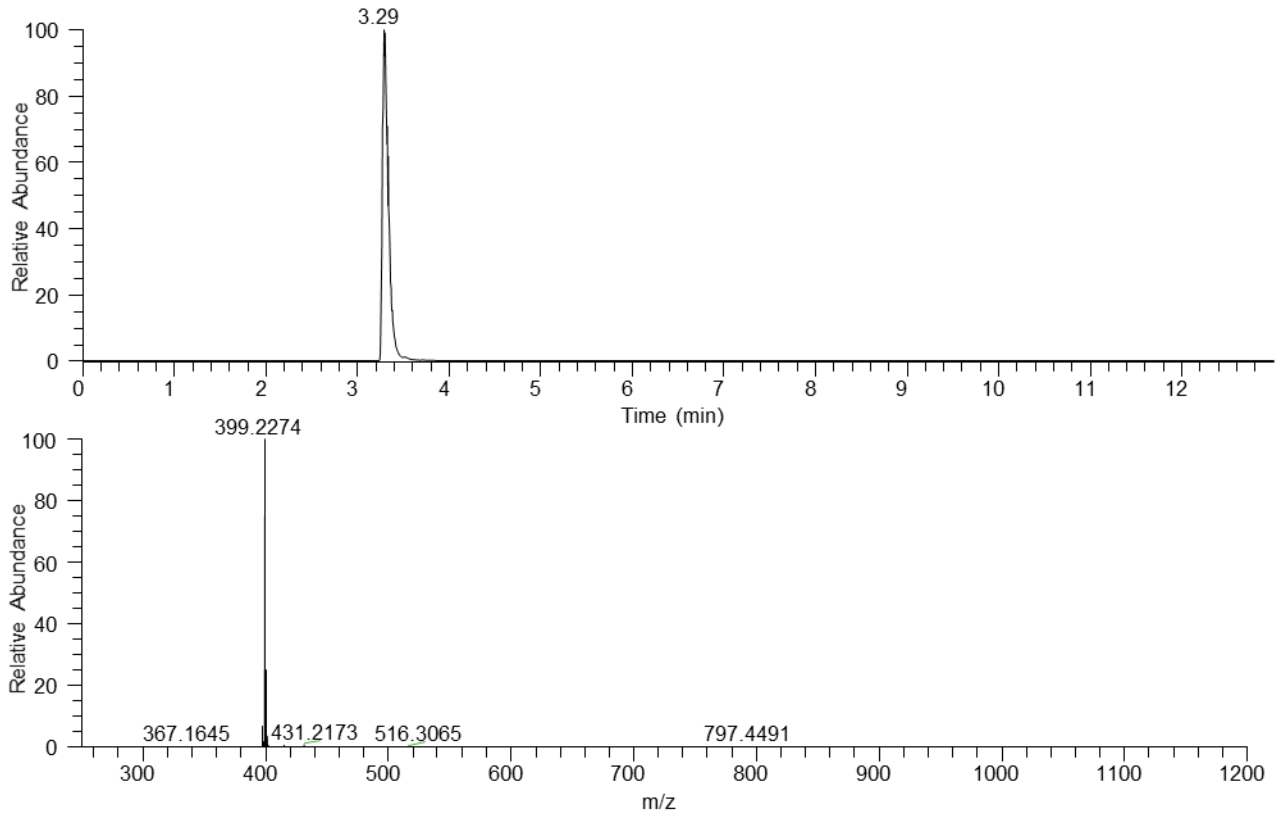

Figure S10. UPLC-HRESIMS data for mitragynine (**1**).

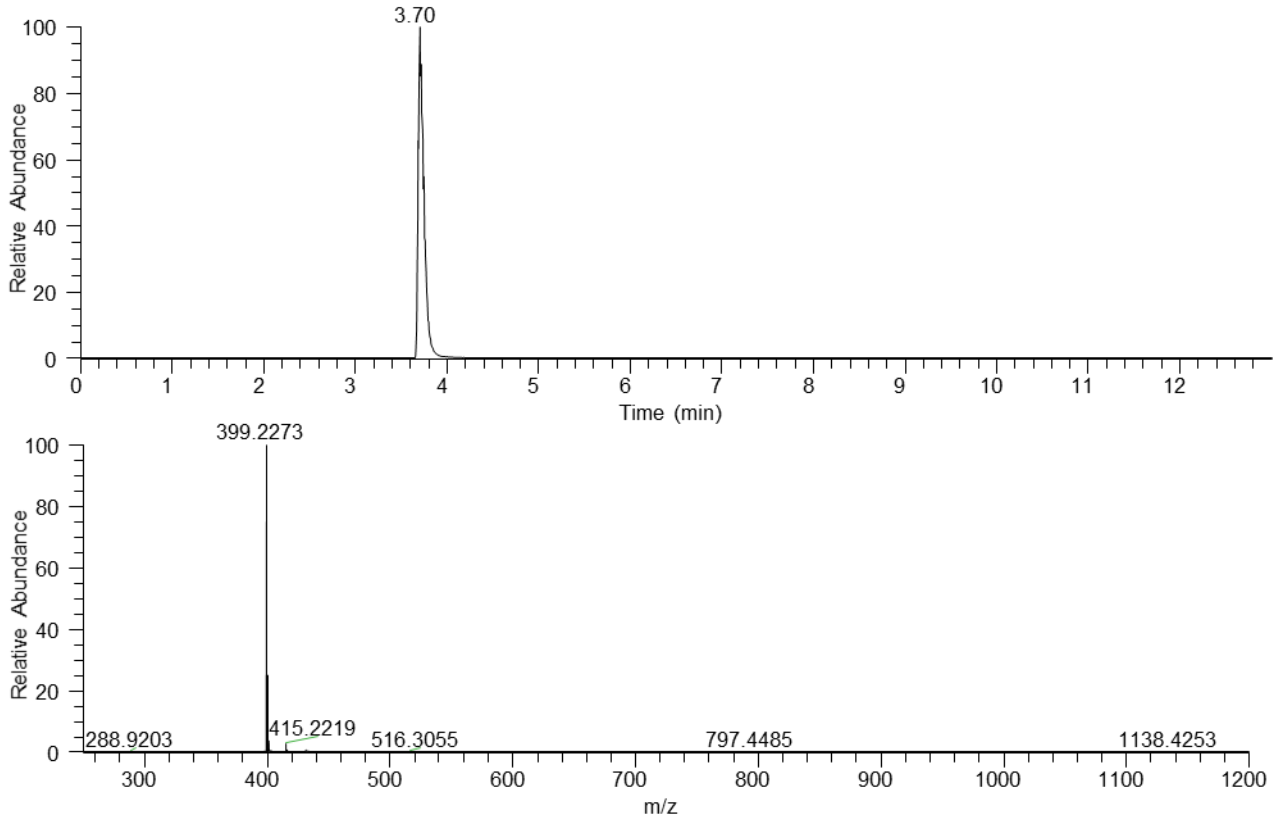

Figure S11. UPLC-HRESIMS data for speciociliatine (**2**).

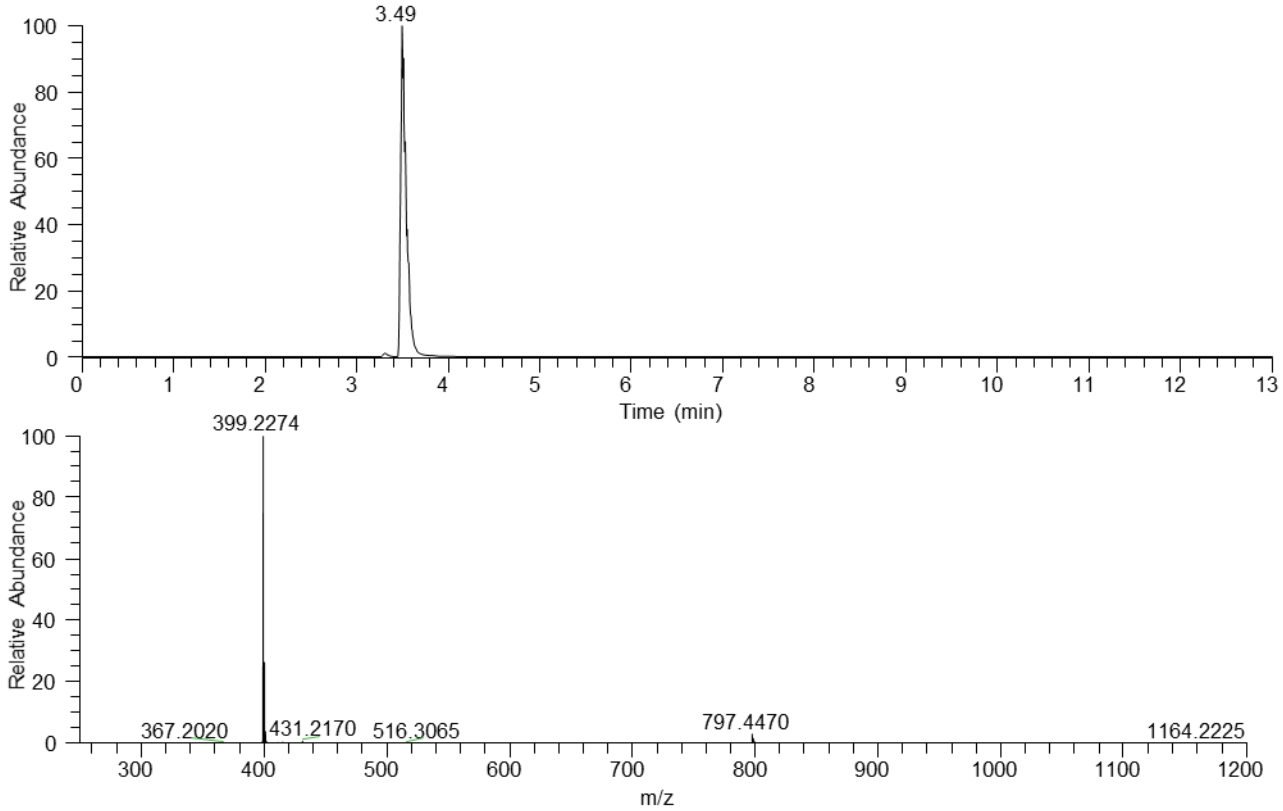

Figure S12. UPLC-HRESIMS data for speciogynine (**3**).

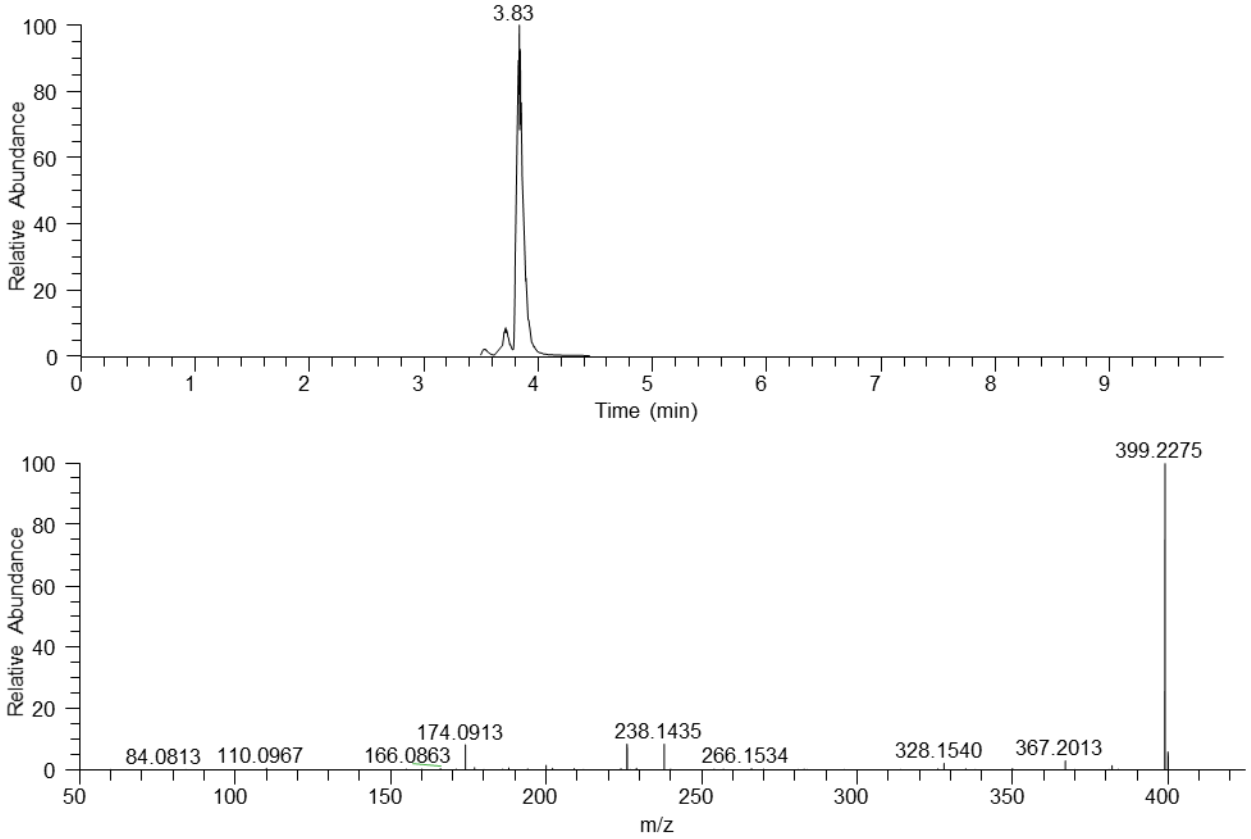

Figure S13. UPLC-HRESIMS data for mitraciliatine (**4**).

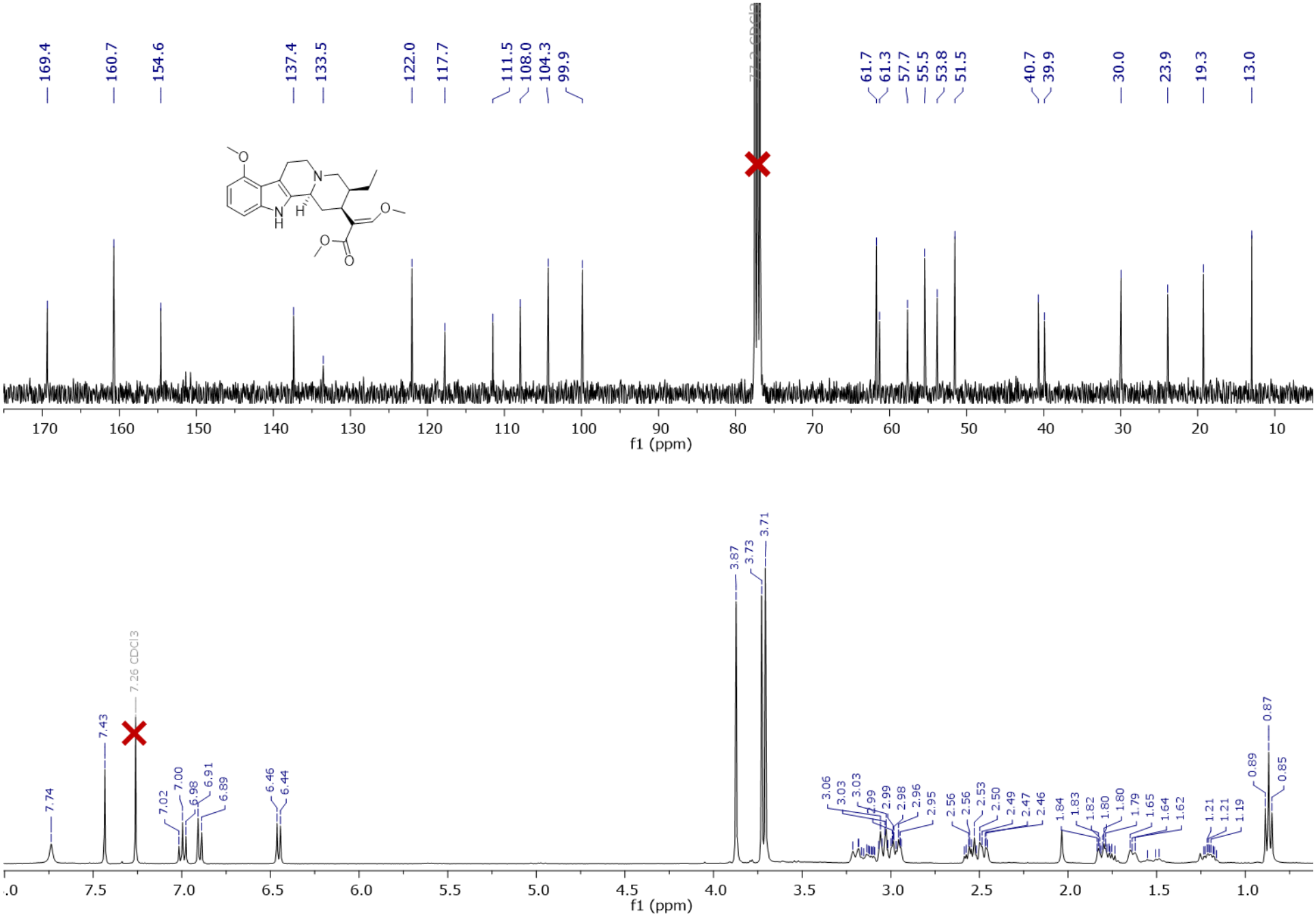

Figure S14. ^{1}H and ^{13}C NMR spectra for mitragynine (**1**) ($CDCl_3$, 400 MHz and 100 MHz, respectively).

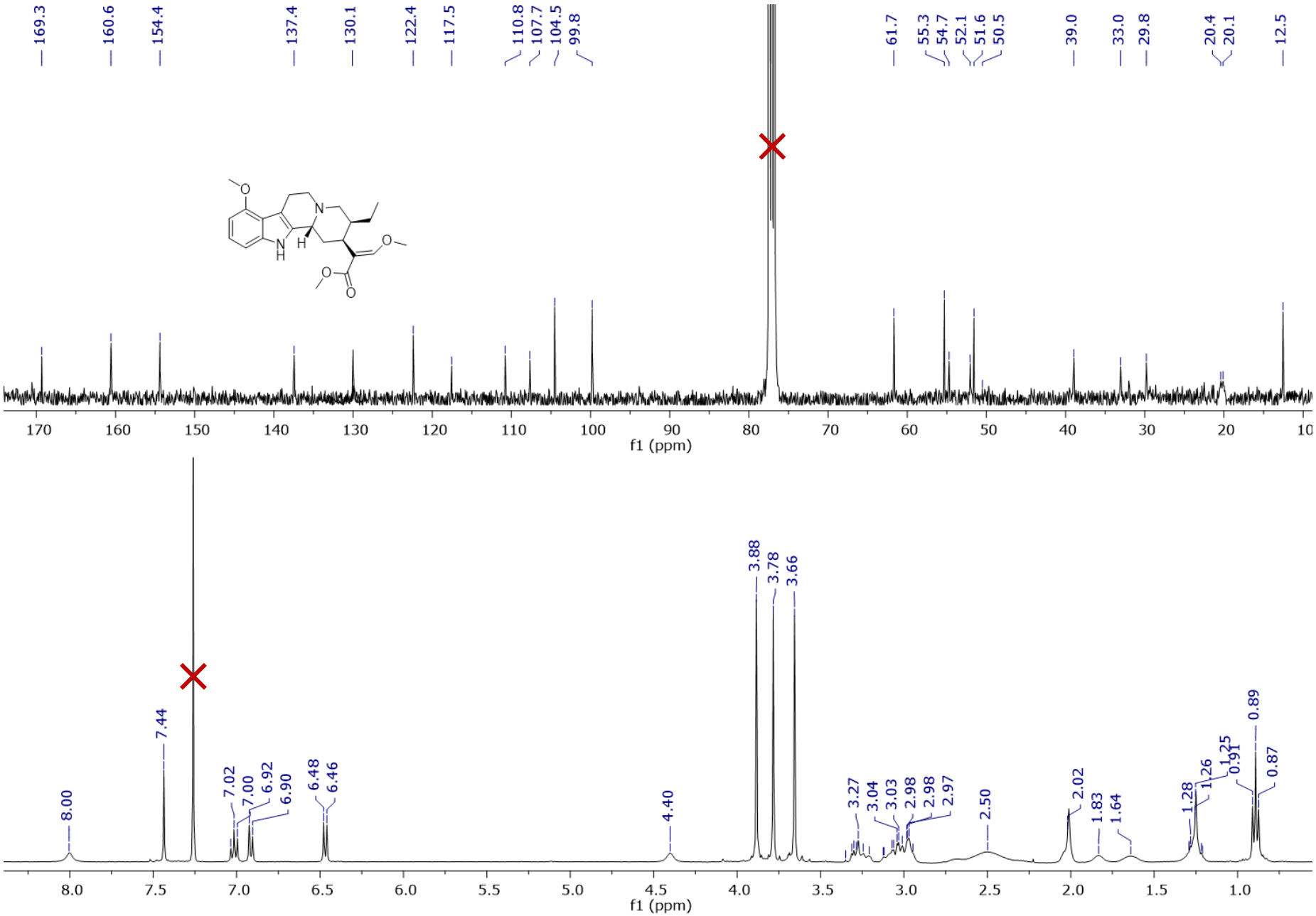

Figure S15. ^{1}H and ^{13}C NMR spectra for speciociliatine (**2**) ($CDCl_3$, 400 MHz and 100 MHz, respectively).

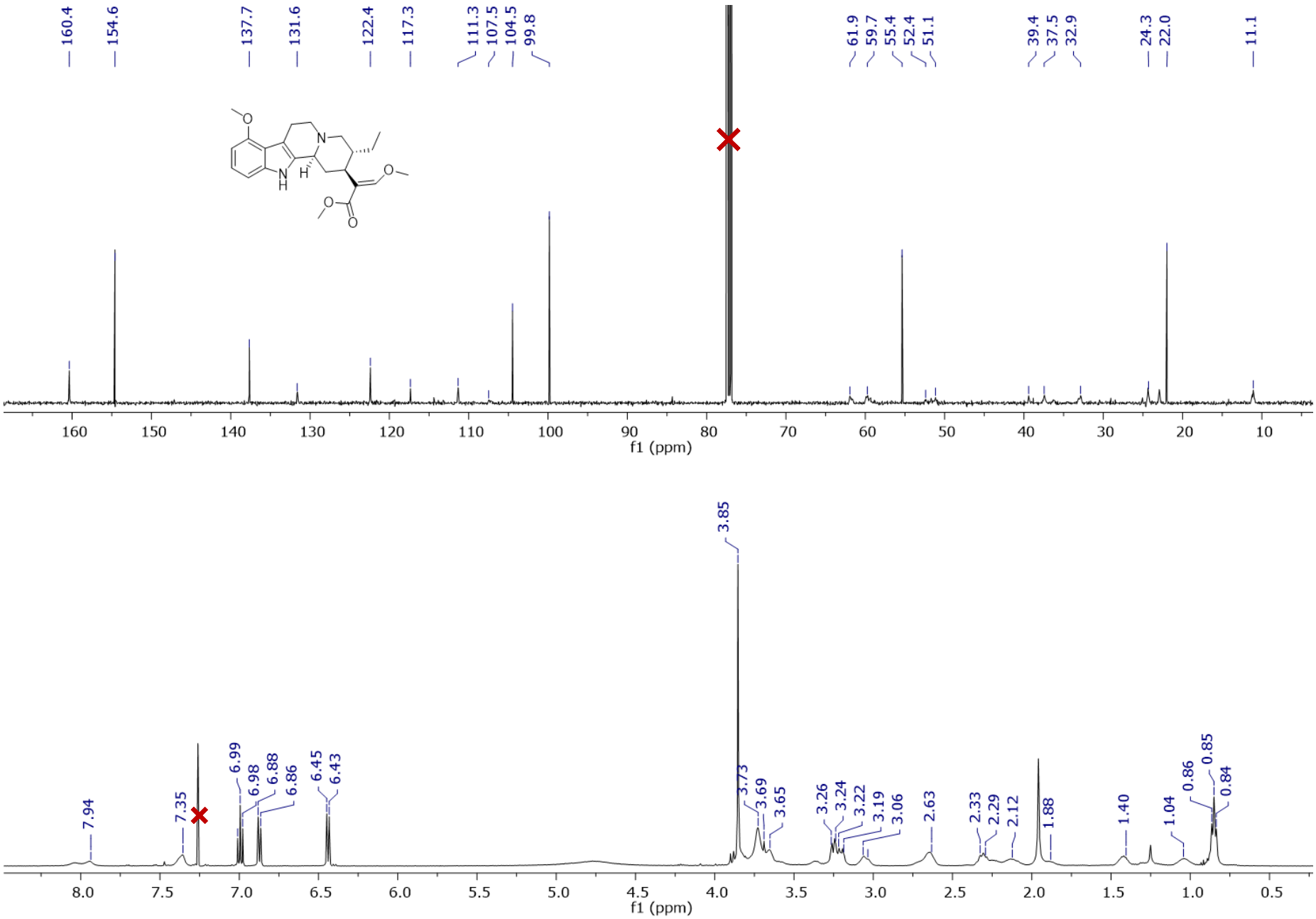

Figure S16. ^{1}H and ^{13}C NMR spectra for speciogynine (**3**) ($CDCl_3$, 400 MHz and 100 MHz, respectively).

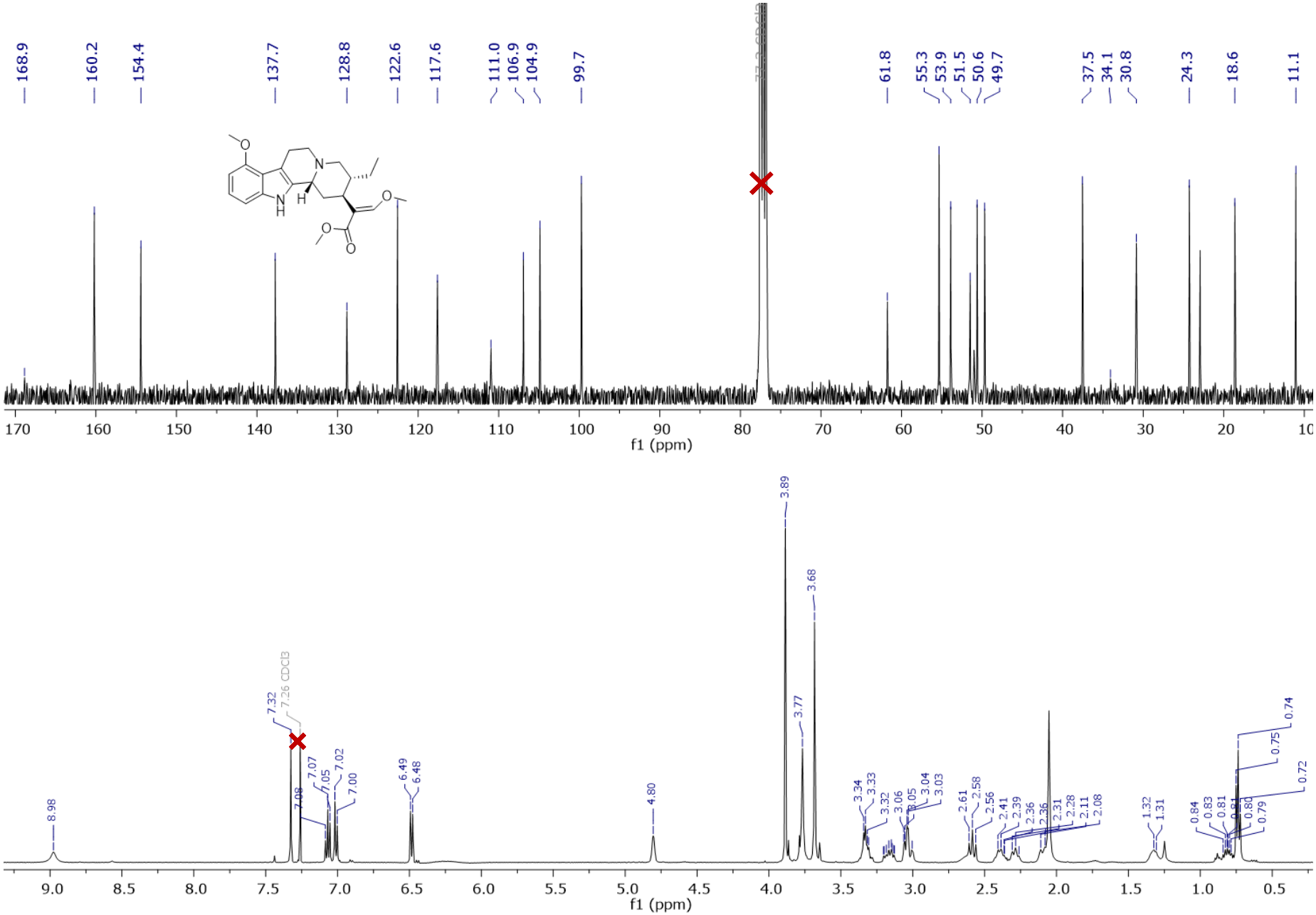

Figure S17. ^{1}H and ^{13}C NMR spectra for mitraciliatine (**4**) ($CDCl_3$, 400 MHz and 100 MHz, respectively).

Table S4. Comparison of NMR Data for Compounds 1-4 ($CDCl_3$, 100 MHz and 400 MHz).

			mitragynine (**1**)			speciociliatine (**2**)			speciogynine (**3**)			mitraciliatine (**4**)
position	δ_C	type	δ_H (*J* in Hz)	δ_C	type	δ_H (*J* in Hz)	δ_C	type	δ_H (*J* in Hz)	δ_C	type	δ_H (*J* in Hz)
2	133.5	C		130.1	C		131.6	C		128.8	C	
3	61.3	CH	3.20, d (8.4)	54.7	CH	4.40, bs	61.9	CH	3.21, m	53.9	CH	4.80, s
5	53.8	CH_2	2.97, m	52.1	CH_2	3.23, m	52.4[a]	CH_2	3.20, m	50.6	CH_2	3.32, m
			2.55, m			3.04, m			2.68, m			
6	23.9	CH_2	3.11, m	20.4	CH_2	3.31, m	22.0	CH_2	3.19, m	18.6	CH_2	3.20, m
			2.97, m			2.89, m			3.06, m			3.02, m
7	108.0	C		107.7	C		107.5[a]	C		106.9	C	
8	117.7	C		117.5	C		117.3	C		117.6	C	
9	154.6	C		154.4	C		154.6	C		154.4	C	
10	99.9	CH	6.45, d (7.7)	99.8	CH	6.47, d (7.7)	99.8	CH	6.44, d (7.8)	99.7	CH	6.49, d (7.6)
11	122.0	CH	7.00, t (7.9)	122.4	CH	7.02, t (8.0)	122.4	CH	6.99, t (7.9)	122.6	CH	7.07, t (7.9)
12	104.3	CH	6.90, d (8.1)	104.5	CH	6.91, d (8.1)	104.5	CH	6.87, d (8.0)	104.9	CH	7.01, d (8.0)
13	137.4	C		137.4	C		137.7	C		137.7	C	
14	30.0	CH_2	2.55, m	29.8	CH_2	2.50, m	32.9	CH_2	2.17, m	30.8	CH_2	2.60, t (11.5)
			1.81, m			2.02, m			1.95, m			2.10, bd (11.4)
15	39.9	CH	3.06, m	33.0	CH	2.97, m	39.4	CH	2.63, m	34.1	CH	2.28, m
16	111.5	C		110.8	C		111.3	C		111.0	C	
17	160.7	CH	7.43, s	160.6	CH	7.44, s	160.4	CH	7.35, bs	160.2	CH	7.32, s
18	13.0	CH_3	0.87, t (7.3)	12.5	CH_3	0.89, t (7.9)	11.1	CH_3	0.85, t (7.2)	11.1	CH_3	0.74, t (7.0)
19	19.3	CH_2	1.75, m	20.1	CH_2	1.64, m	24.3	CH_2	1.40, m	24.3	CH_2	1.32, m
			1.19, qd (7.4, 2.7)			1.25, m			1.04, m			0.84, m
20	40.7	CH	1.64, dt (11.5, 2.6)	39.0	CH	1.83, m	37.5	CH	2.31, m	37.5	CH	2.40, m
21	57.7	CH_2	3.00, m	50.5	CH_2	3.27, m	59.7	CH_2	3.26, m	49.7	CH_2	3.05, m
			2.44, m			2.89, m			2.21, m			2.57, m
22	169.4	C		169.3	C		170.2[a]	C		168.9	C	
9-OCH_3	55.5	CH_3	3.87, s	55.3	CH_3	3.88, s	55.4	CH_3	3.85, s	55.3	CH_3	3.89, s
17-OCH_3	61.7	CH_3	3.73, s	61.7	CH_3	3.78, s	61.9	CH_3	3.72, s	61.8	CH_3	3.77, s
22-OCH_3	51.5	CH_3	3.71, s	51.6	CH_3	3.66, s	51.1	CH_3	3.72, s	51.5	CH_3	3.68, s
NH			7.74, bs			8.00, bs			7.94, bs			8.98, bs

[a]Signals observed by 2D experiments

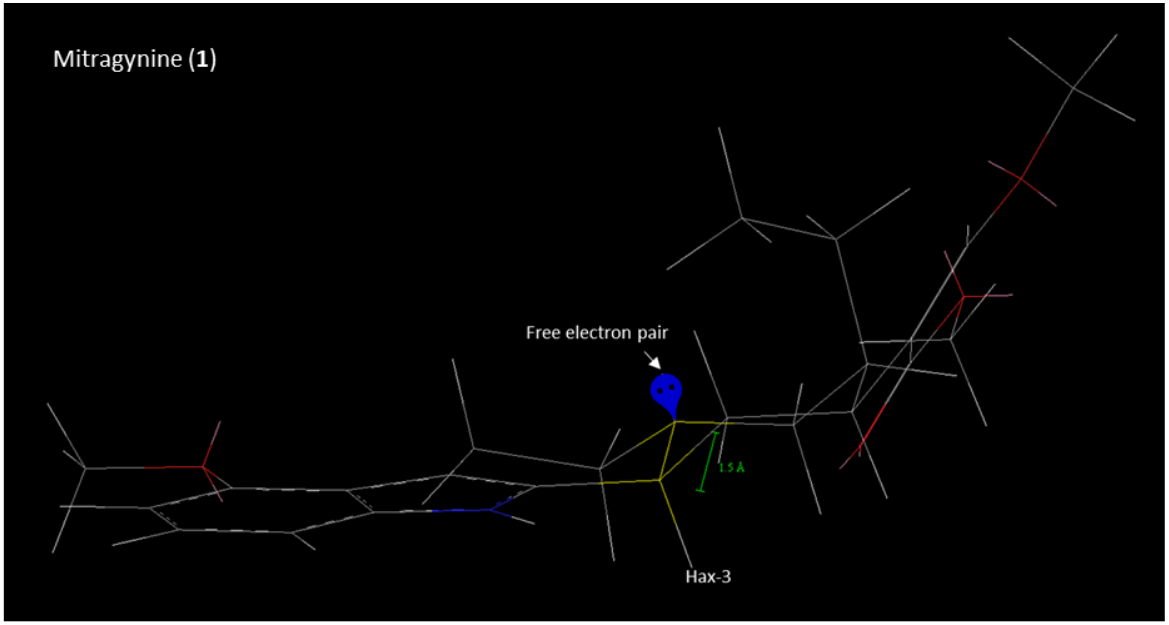

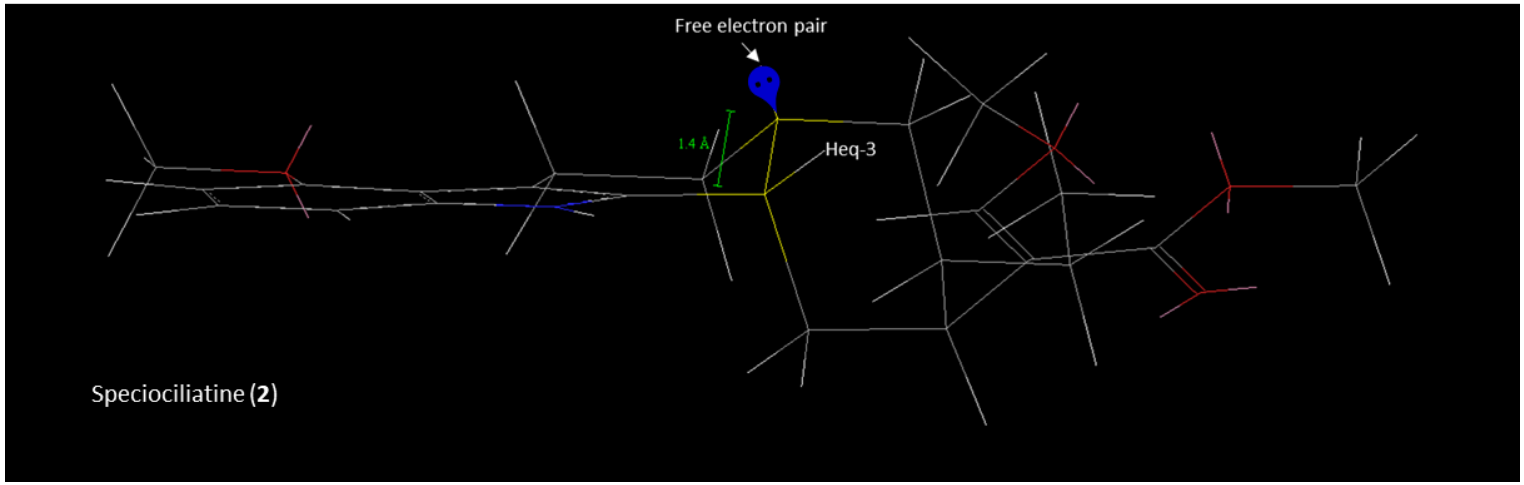

Figure S18. Representation for the different orientations of H-3 with respect to the nitrogen non-bonding electron pair for the most stable conformation of mitragynine (**1**) and speciociliatine (**2**).

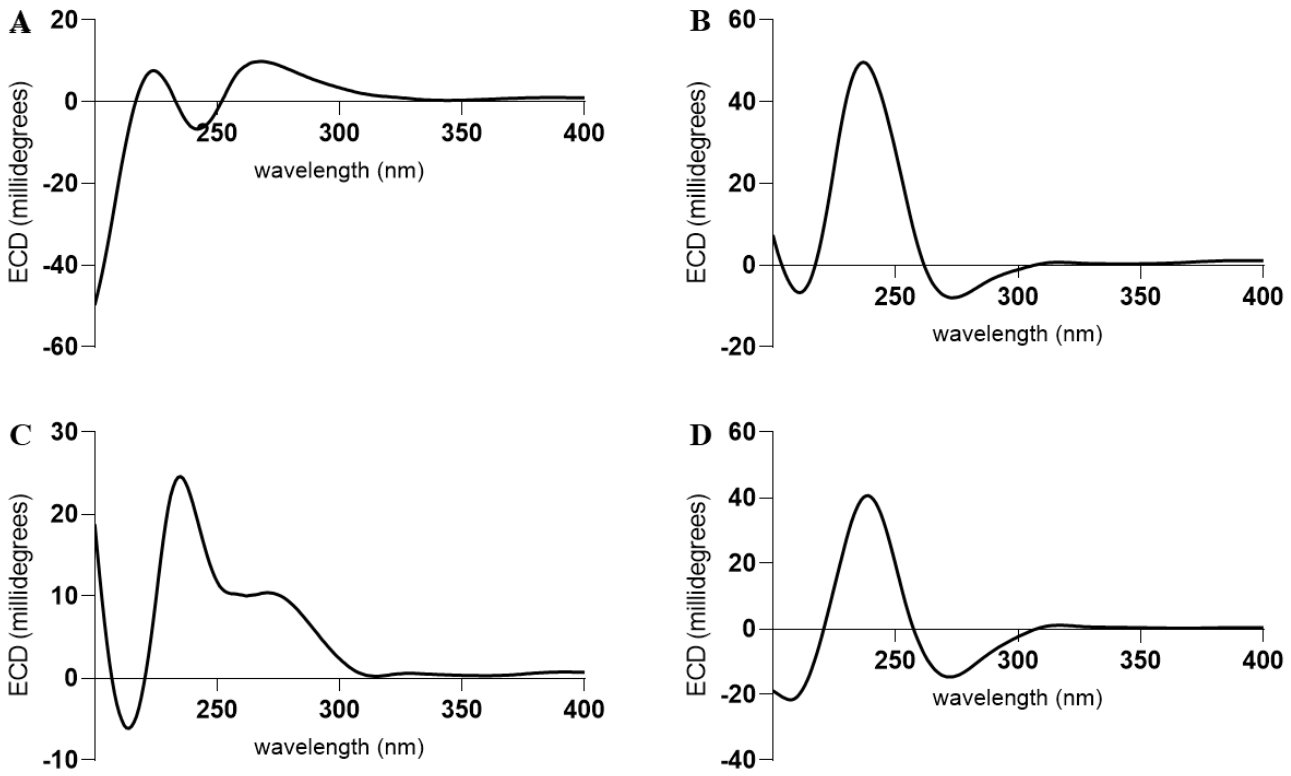

Figure S19. Comparison of the ECD spectra acquired in CH_3OH for A) mitragynine (**1**), B) speciociliatine (**2**), C) speciogynine (**3**), and D) mitraciliatine (**4**).

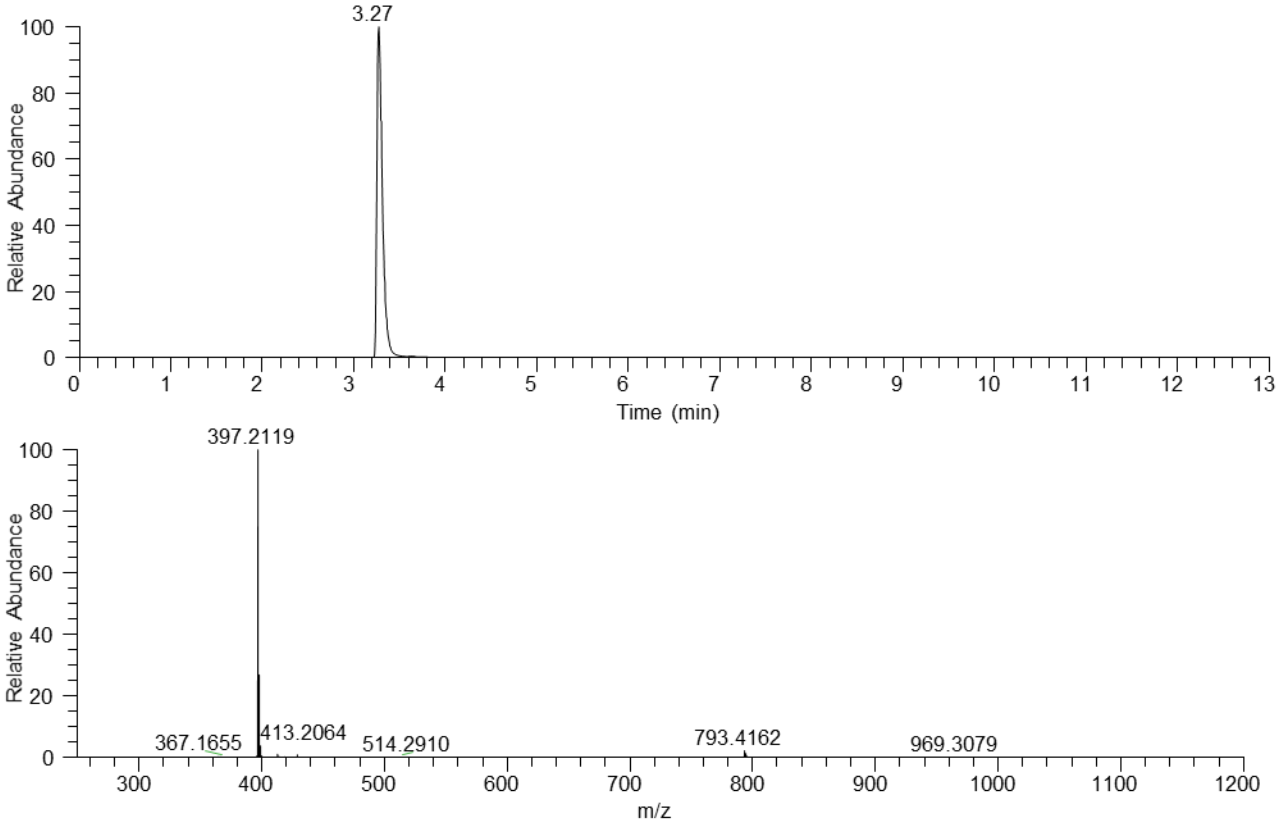

Figure S20. UPLC-HRESIMS data for paynantheine (**5**).

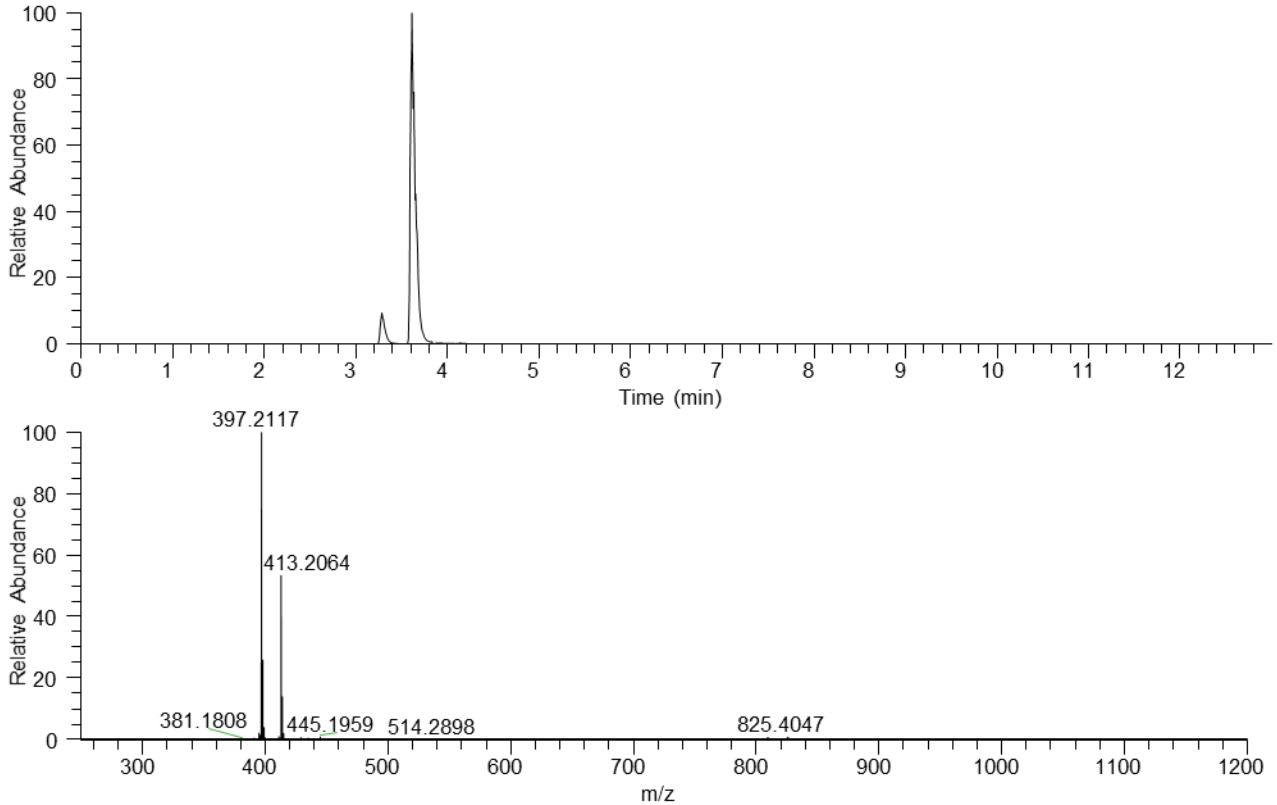

Figure S21. UPLC-HRESIMS data for isopaynantheine (**6**).

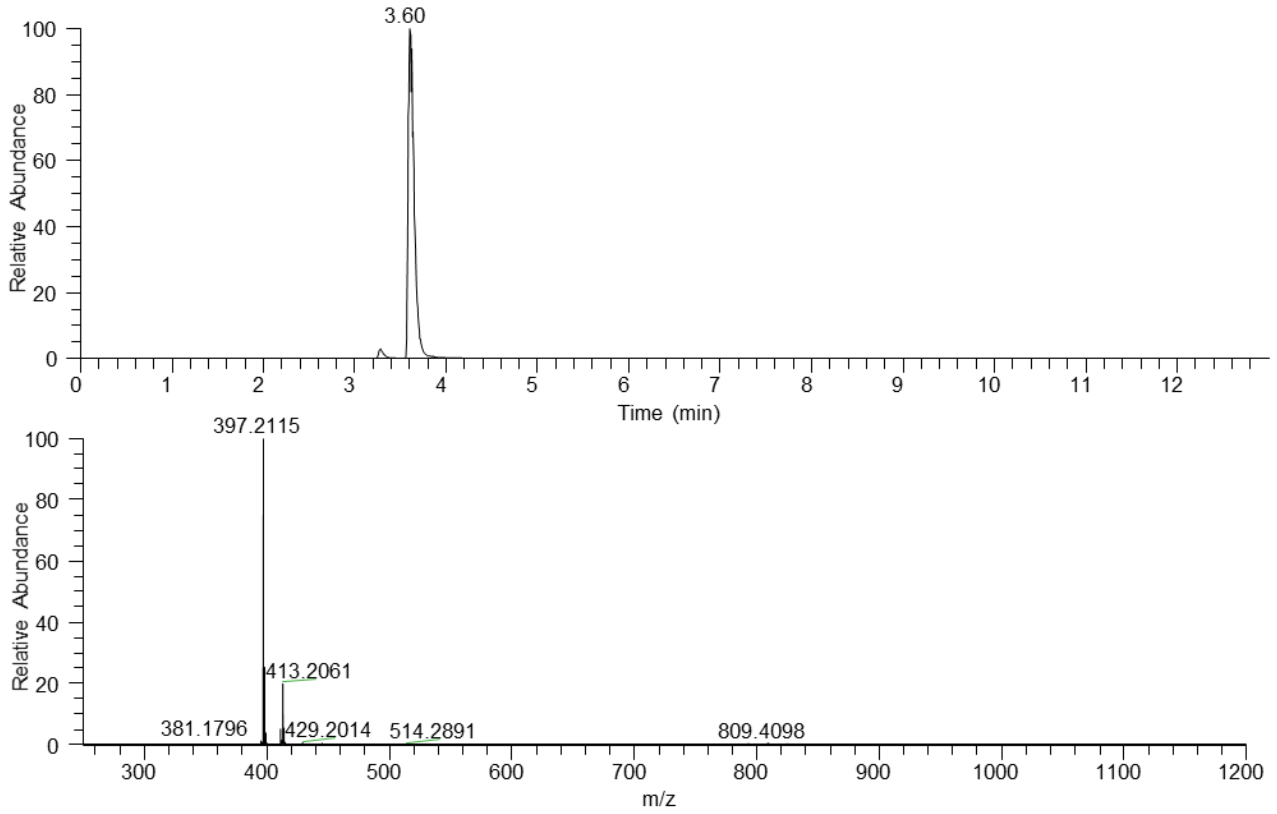

Figure S22. UPLC-HRESIMS data for epiallo-isopaynantheine (**7**).

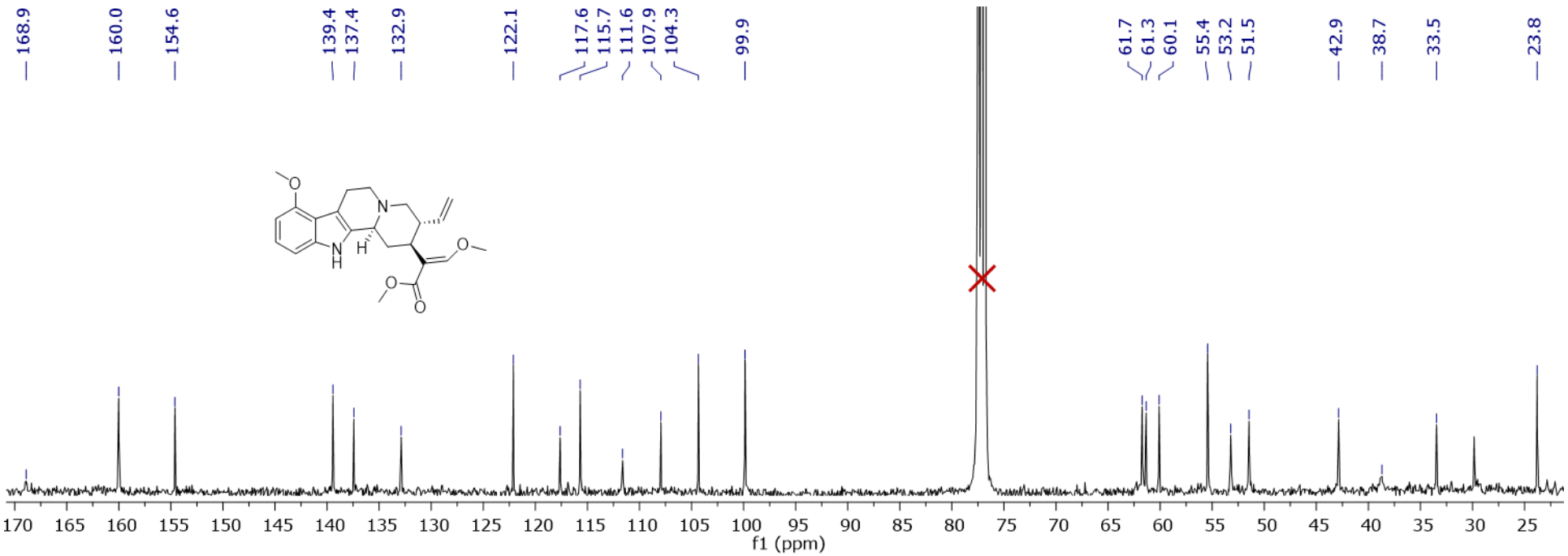

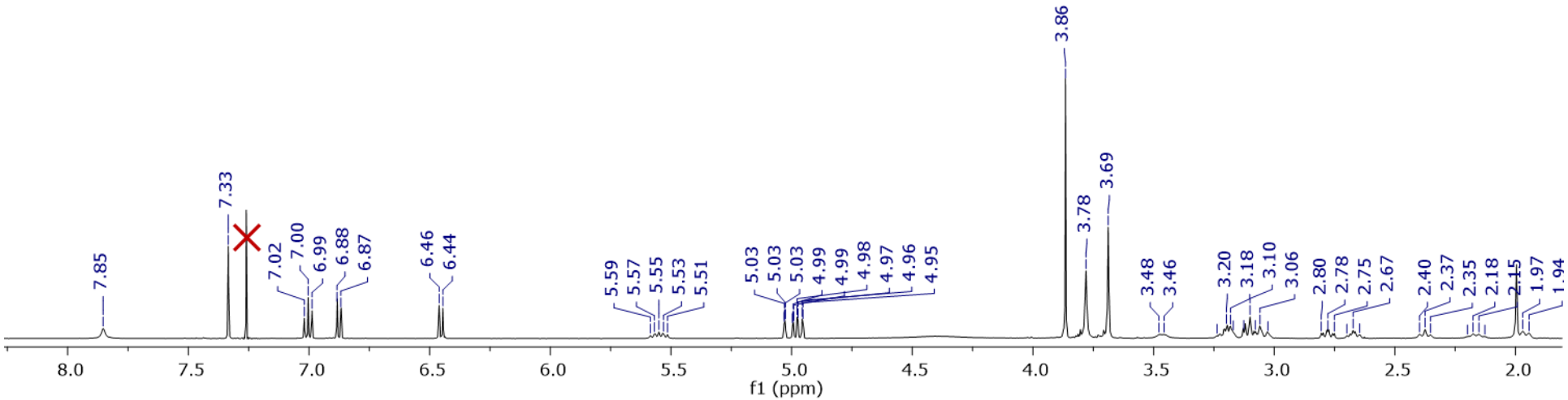

Figure S23. ^{1}H and ^{13}C NMR spectra for paynantheine (**5**) ($CDCl_3$, 400 MHz and 100 MHz, respectively).

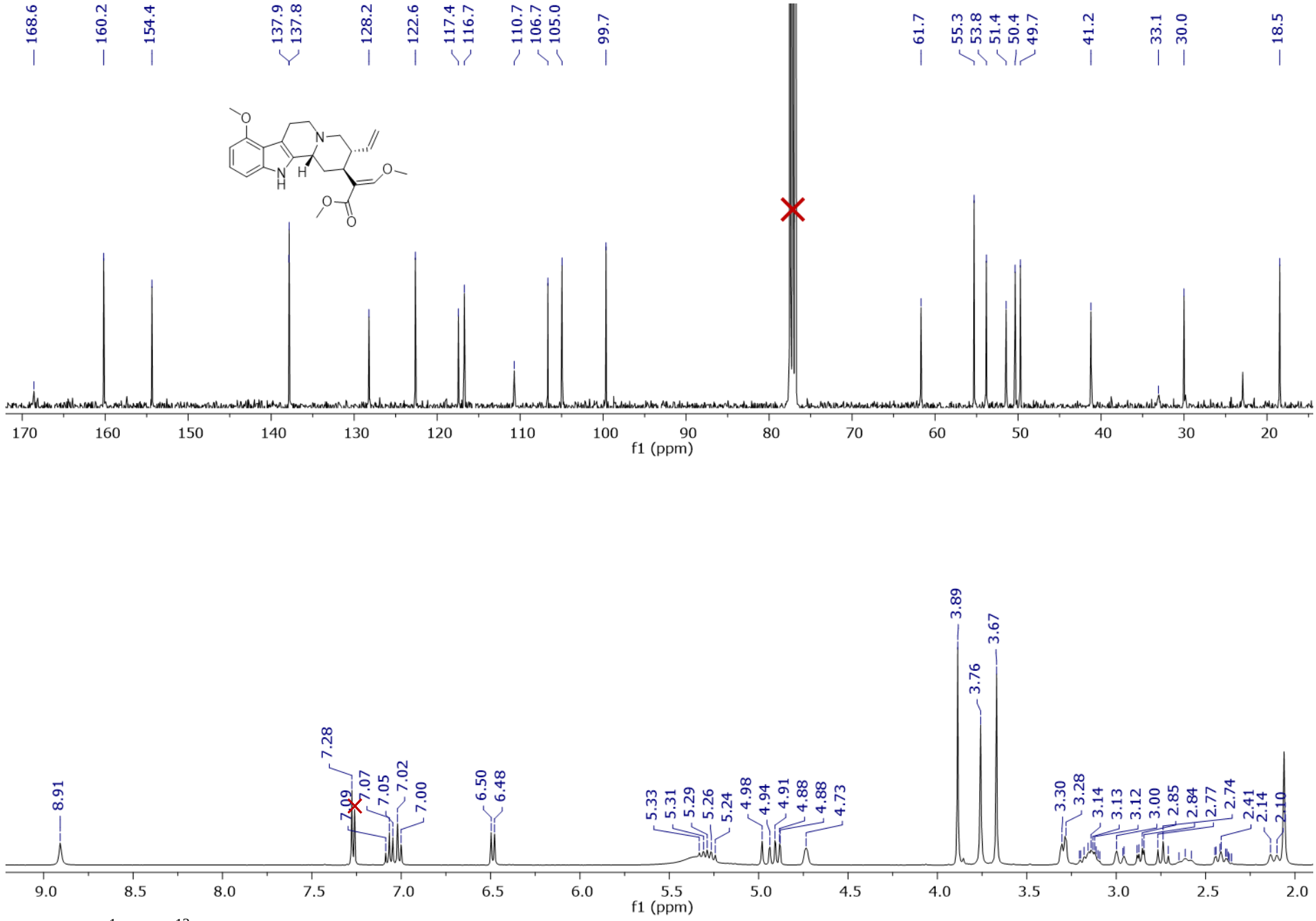

Figure S24. ^{1}H and ^{13}C NMR spectra for isopaynantheine (**6**) ($CDCl_3$, 400 MHz and 100 MHz, respectively).

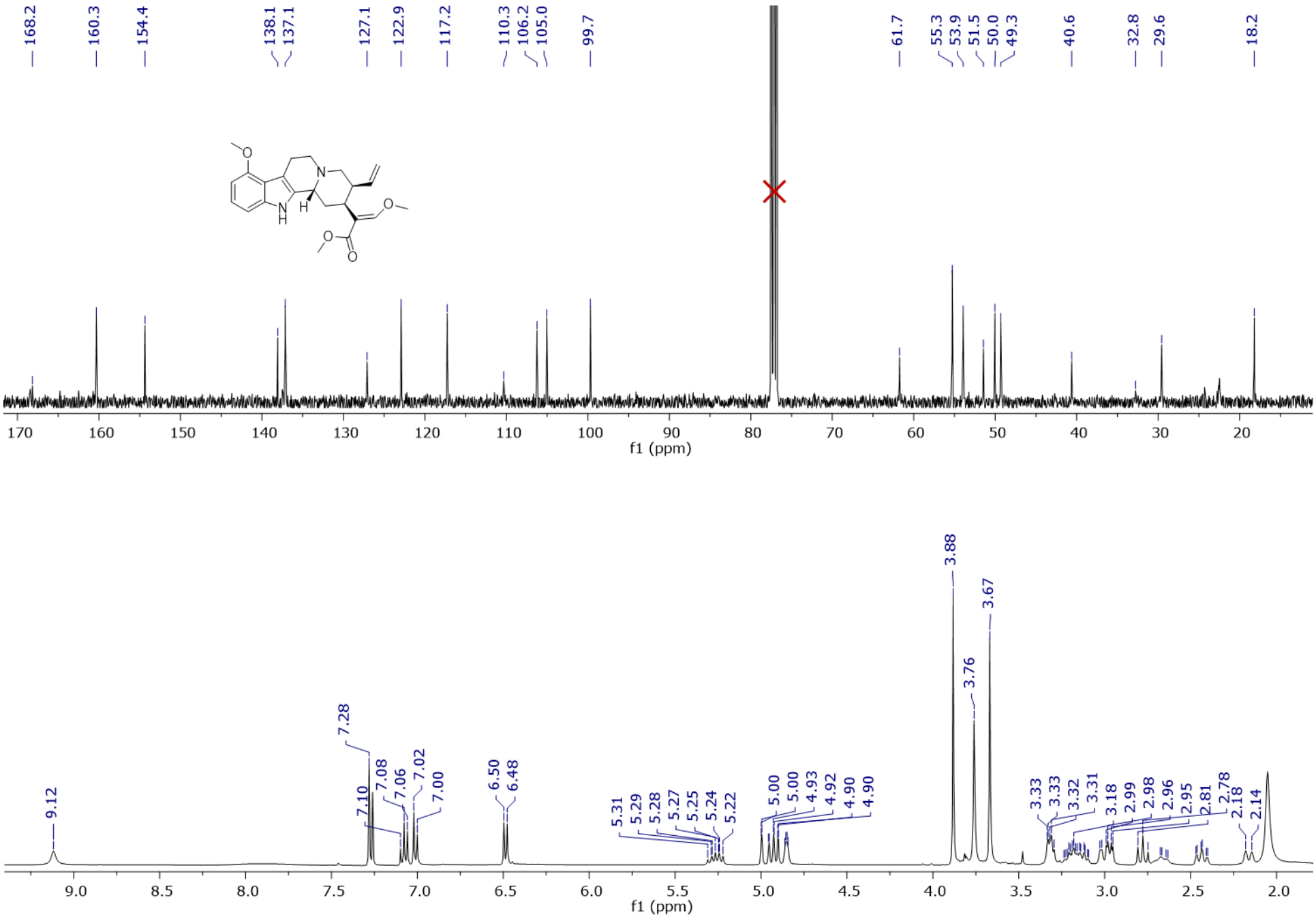

Figure S25. ^{1}H and ^{13}C NMR spectra for epiallo-isopaynantheine (**7**) ($CDCl_3$, 400 MHz and 100 MHz, respectively).

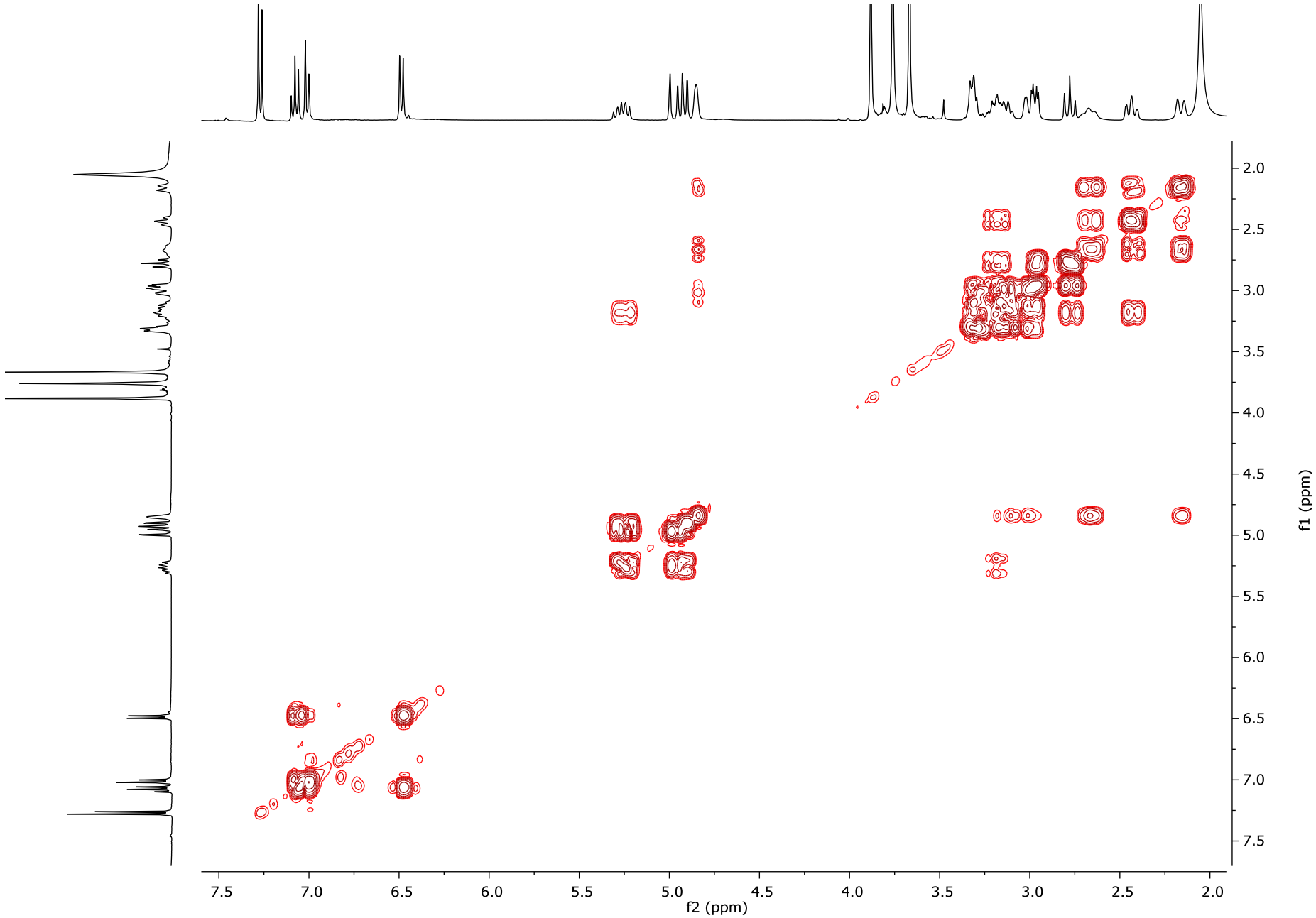

Figure S26. COSY spectrum for epiallo-isopaynantheine (**7**) ($CDCl_3$, 400 MHz).

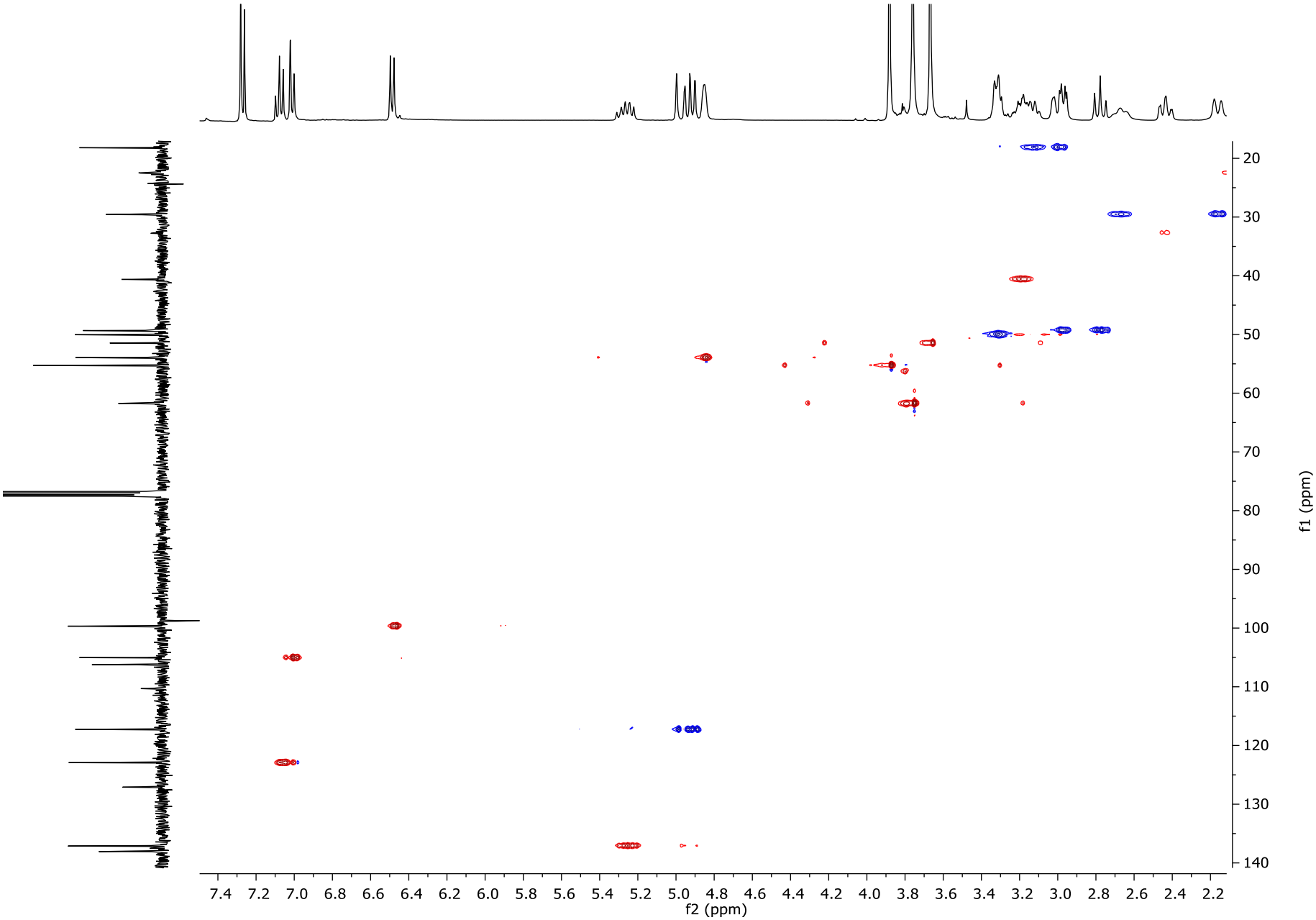

Figure S27. HSQC spectrum for epiallo-isopaynantheine (**7**) ($CDCl_3$, 400 MHz).

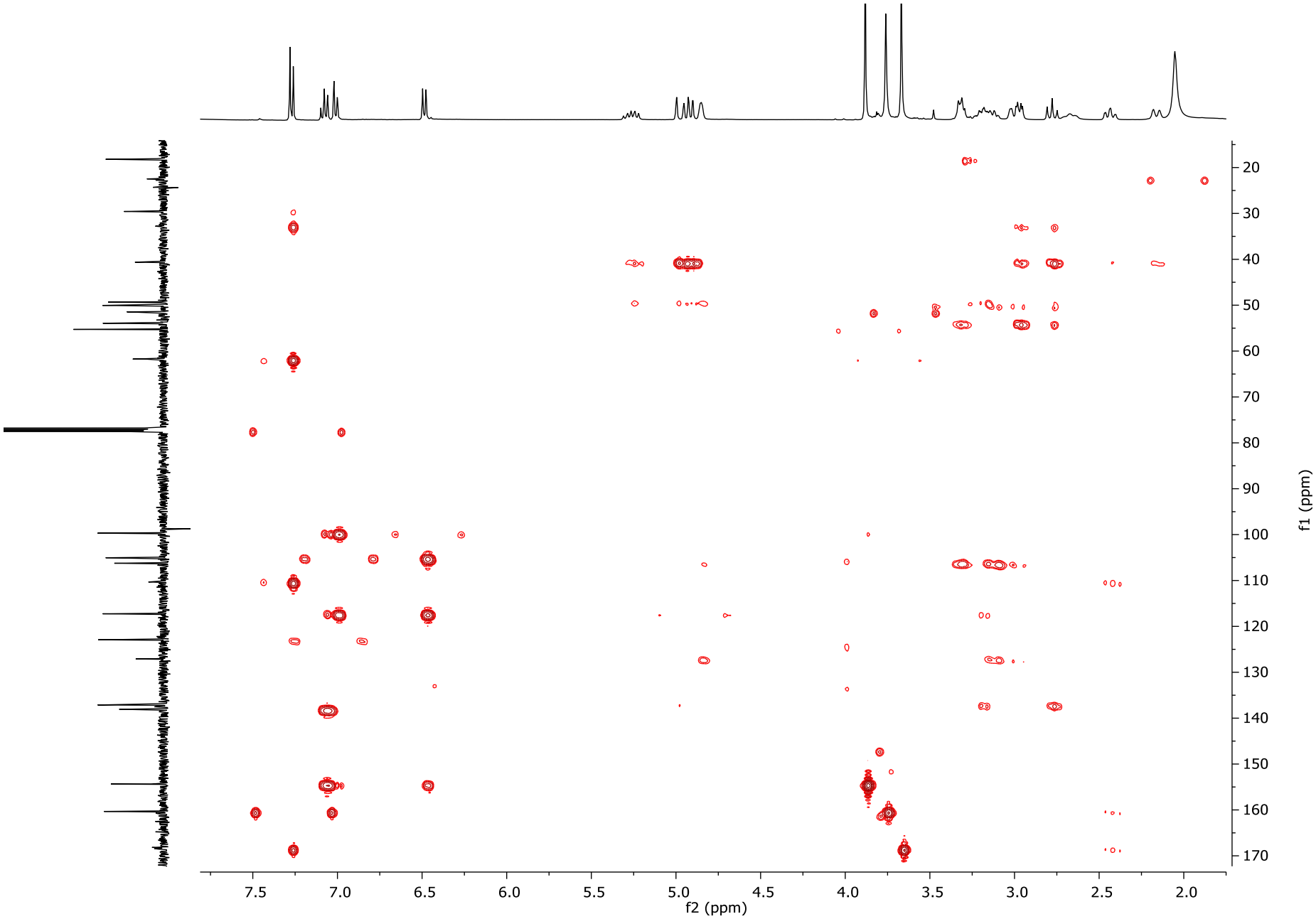

Figure S28. HMBC spectrum for epiallo-isopaynantheine (**7**) ($CDCl_3$, 400 MHz).

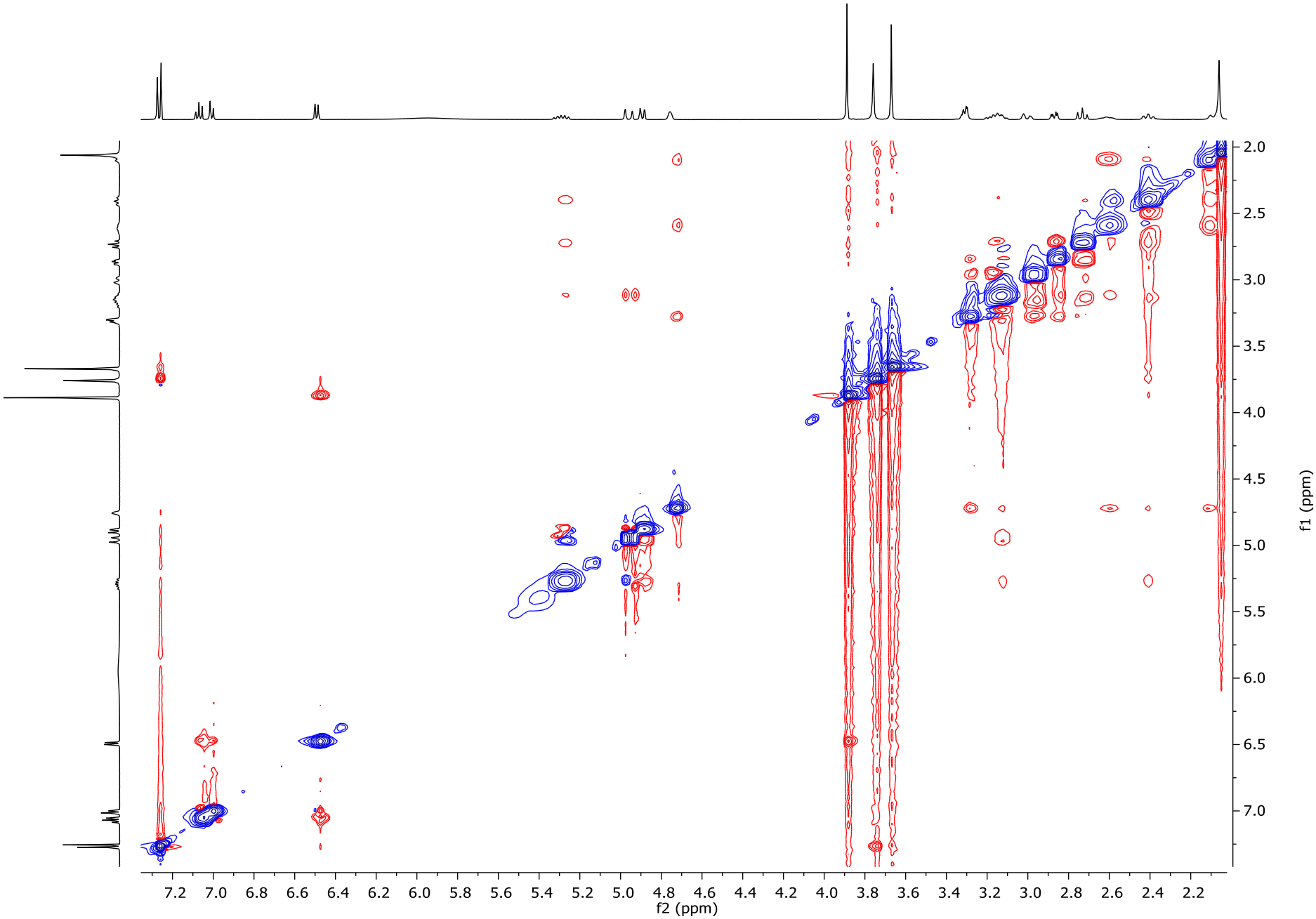

Figure S29. NOESY spectrum for isopaynantheine (**6**) ($CDCl_3$, 400 MHz).

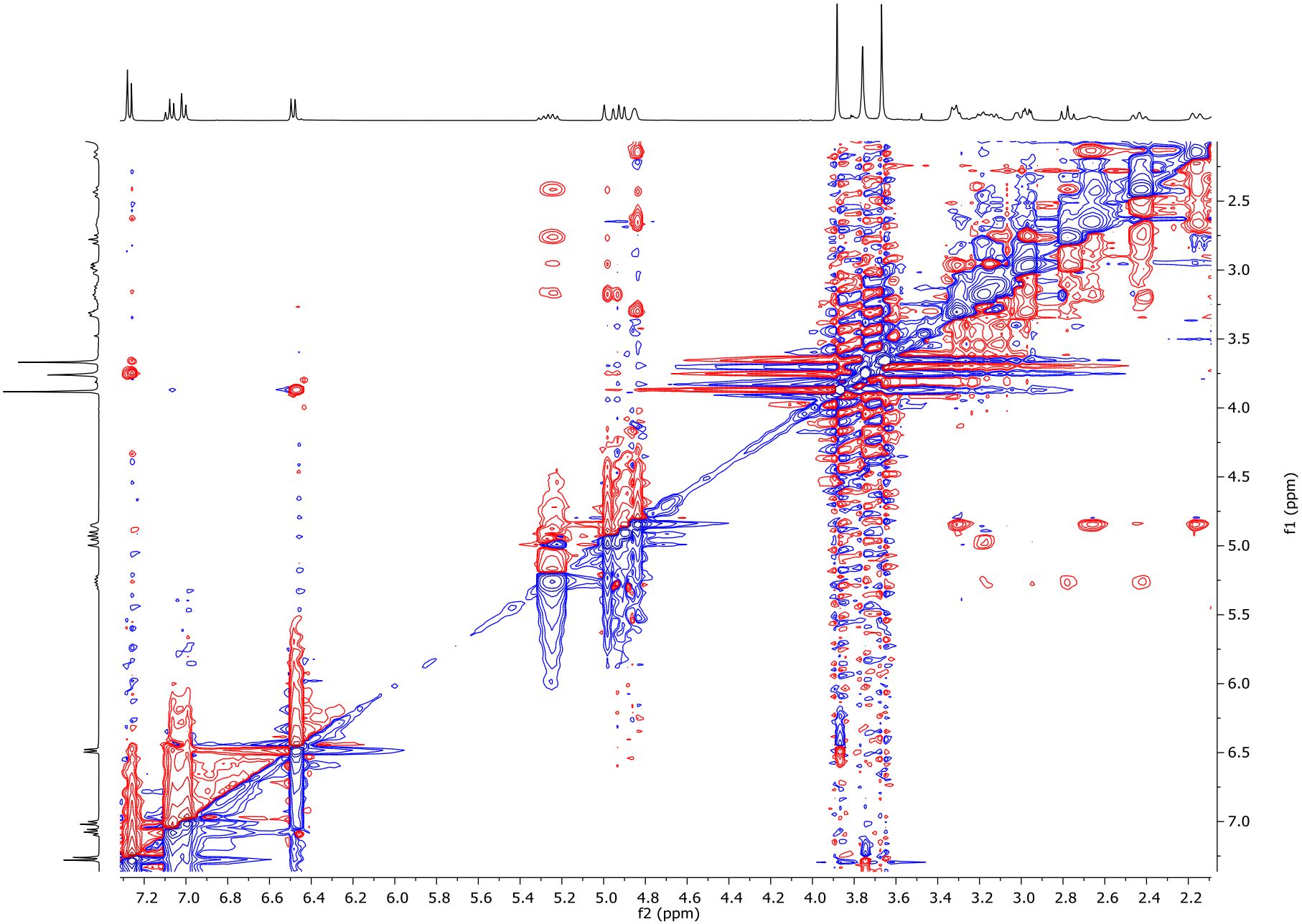

Figure S30. NOESY spectrum for epiallo-isopaynantheine (**7**) ($CDCl_3$, 400 MHz).

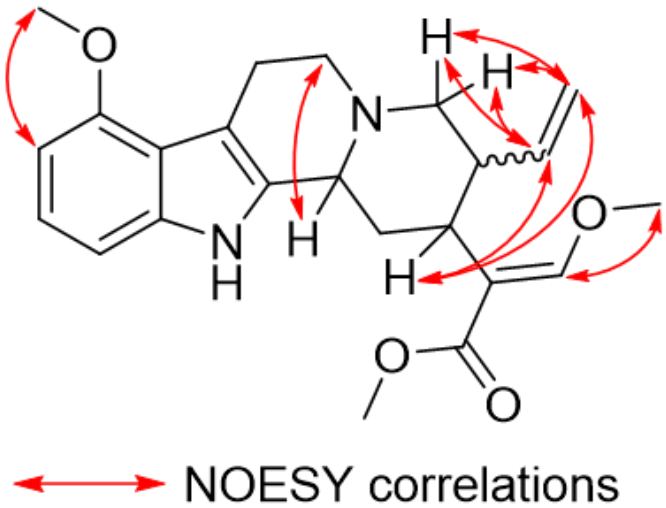

Compound	Distances (Å)	
	$H_{15} \rightarrow H_{18}$	$H_{15} \rightarrow H_{19}$
Isopaynantheine (**6**)	2.6	4.6
Epiallo-isopaynantheine (**7**)	3.6	2.8

Figure S31. Observed NOESY correlations for compounds **6** and **7**, and the distances for the key positions in the diastereoisomers.

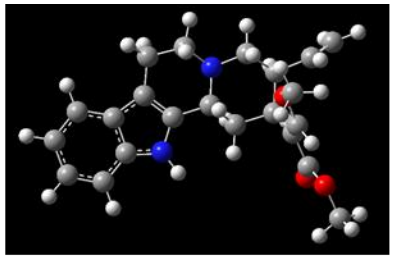

7a (ΔG 0.000 kcal/mol; P = 23.33%)

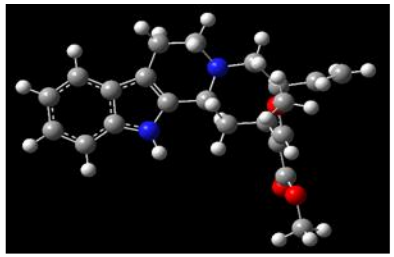

7b (ΔG 0.003 kcal/mol; P = 23.23%)

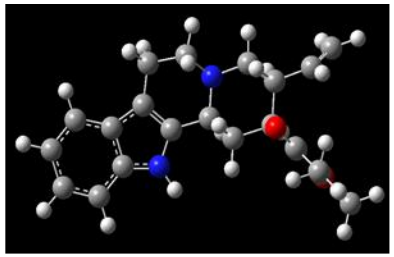

7c (ΔG 0.366 kcal/mol; P = 12.56%)

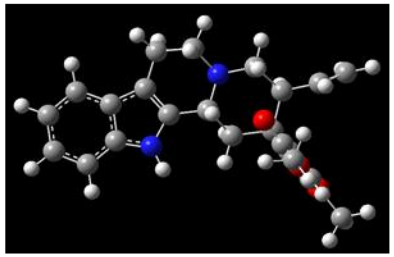

7d (ΔG 0.336 kcal/mol; P = 12.56%)

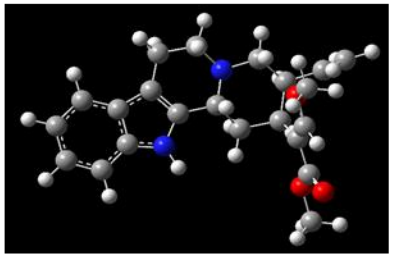

7e (ΔG 0.470 kcal/mol; P = 10.53%)

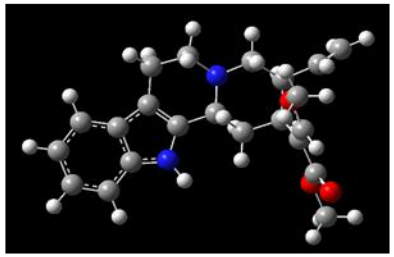

7f (ΔG 0.470 kcal/mol; P = 10.53%)

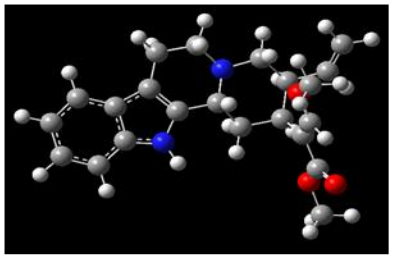

7g (ΔG 1.293 kcal/mol; P = 2.63%)

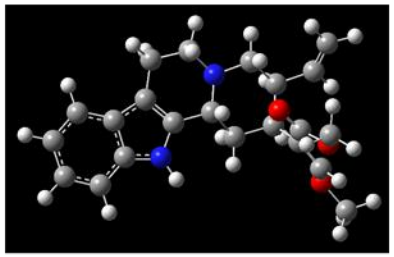

7h (ΔG 1.364 kcal/mol; P = 2.33%)

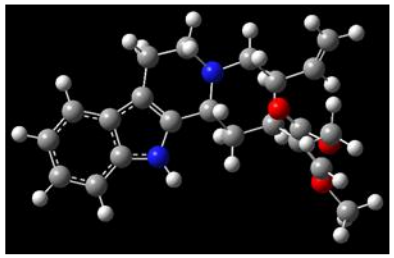

7i (ΔG 1.373 kcal/mol; P = 2.29%)

Figure S32. Nine conformers for the prediction of the ECD spectrum for **7**. The Boltzmann distributions are expressed as a percentage of population (P); the number of excited states considered for the calculation was n = 30.

Table S5. Comparison of NMR Data for Compounds 5-7 ($CDCl_3$, 100 MHz and 400 MHz)

	paynantheine (**5**)			isopaynantheine (**6**)			epiallo-isopaynantheine (**7**)		
Position	δ_C	type	δ_H (*J* in Hz)	δ_C	type	δ_H (*J* in Hz)	δ_C	type	δ_H (*J* in Hz)
2	132.9	C		128.2	C		127.1	C	
3	60.1	CH	3.20, m	53.8	CH	4.73, bs	53.9	CH	4.85, bs
5	53.2	CH_2	3.47, m	50.4	CH_2	3.29, m	50.0	CH_2	3.32, m
			2.67, m						
6	23.8	CH_2	3.18, m	18.5	CH_2	3.18, m	18.2	CH_2	3.10, m
			2.80, m			3.00, m			3.02, m
7	107.9	C		106.7	C		106.2	C	
8	117.6	C		117.4	C		117.2	C	
9	154.6	C		154.4	C		154.4	C	
10	99.9	CH	6.45, d (7.8)	99.7	CH	6.49, d (7.6)	99.7	CH	6.49, d (7.8)
11	122.1	CH	7.00, t (7.9)	122.6	CH	7.07, t (7.9)	122.9	CH	7.08, t (7.9)
12	104.3	CH	6.88, d (8.0)	105.0	CH	7.02, d (8.1)	105.0	CH	7.01, d (8.1)
13	137.4	CH		137.8	CH		138.1	CH	
14	33.5	CH_2	2.16, dd (12.5, 12.00)	30.0	CH_2	2.61, t (14.0)	29.6	CH_2	2.65, m
			1.96, d (13.2)			2.11, d (14.3)			2.16, d (14.5)
15	38.7	CH	2.78, td (11.8, 3.7)	33.1	CH	2.40, td (12.8, 3.1)	32.8	CH	2.44, td (12.1, 3.0)
16	111.6	C		110.7	C		110.3	C	
17	160.0	CH	7.33, s	160.2	CH	7.28, s	160.3	CH	7.28, s
18	115.7	CH_2	5.01, dd (17.3, 2.0)	116.7	CH_2	4.96, dd (17.2, 1.8)	117.2	CH_2	4.98, dd (17.3, 1.7)
			4.96, dd (10.4, 2.1)			4.89, dd (10.2, 1.8)			4.91, dd (10.3, 1.8)
19	139.4	CH	5.55, dt (17.9, 9.3)	137.9	CH	5.29, ddd (18.0, 10.3, 8.3)	137.1	CH	5.27, ddd (18.0, 10.3, 8.3)
20	42.9	CH	3.08, m	41.2	CH	3.13, m	40.6	CH	3.19, m
21	61.3	CH_2	3.03, m	49.7	CH_2	2.86, dd (11.6, 3.9)	49.3	CH_2	2.97, dd (11.7, 3.8)
			2.37, m			2.74, t (11.6)			2.78, t (11.8)
22	168.9	C		168.6	C		168.2	C	
9-OCH_3	55.4	CH_3	3.86, s	55.3	CH_3	3.89, s	55.3	CH_3	3.88, s
17-OCH_3	61.7	CH_3	3.78, s	61.7	CH_3	3.76, s	61.7	CH_3	3.76, s
22-OCH_3	51.5	CH_3	3.69, s	51.4	CH_3	3.67, s	51.5	CH_3	3.67, s
NH			7.85, s			8.91, s			9.12, s

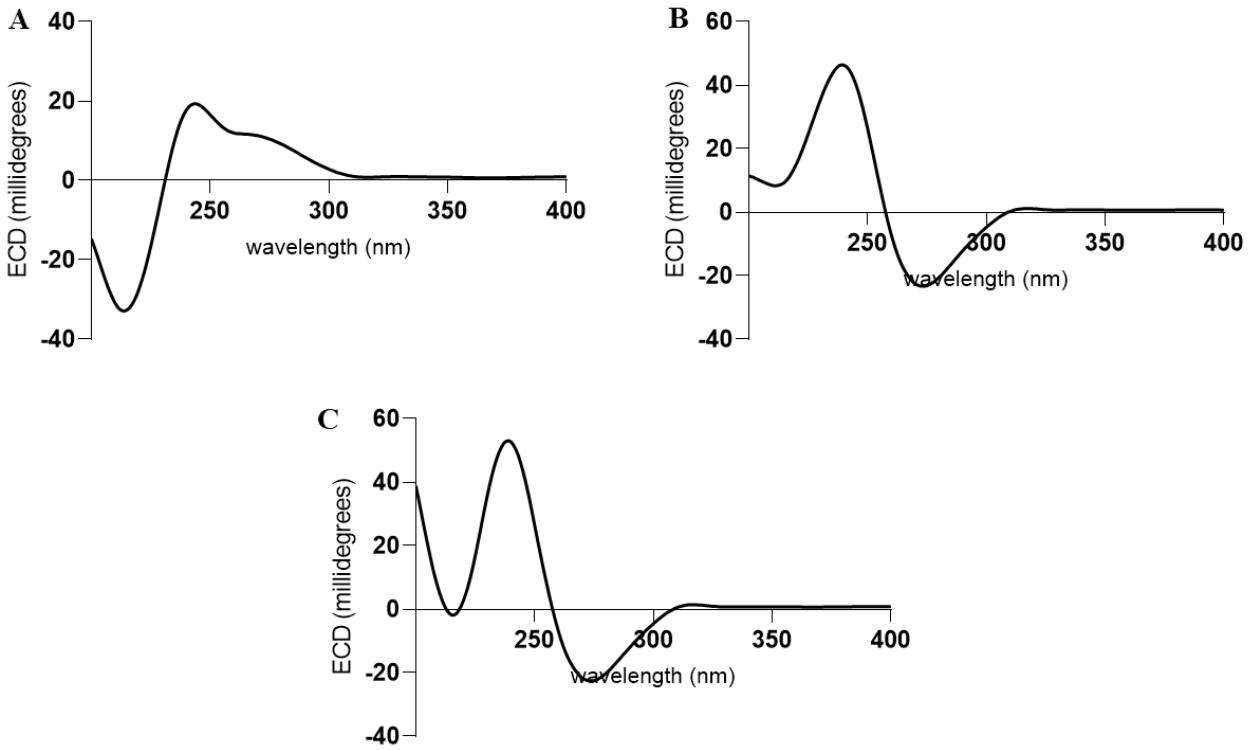

Figure S33. Comparison of the ECD spectra acquired in CH_3OH for A) paynantheine (**5**), B) isopaynantheine (**6**), and C) epiallo-isopaynantheine (**7**).

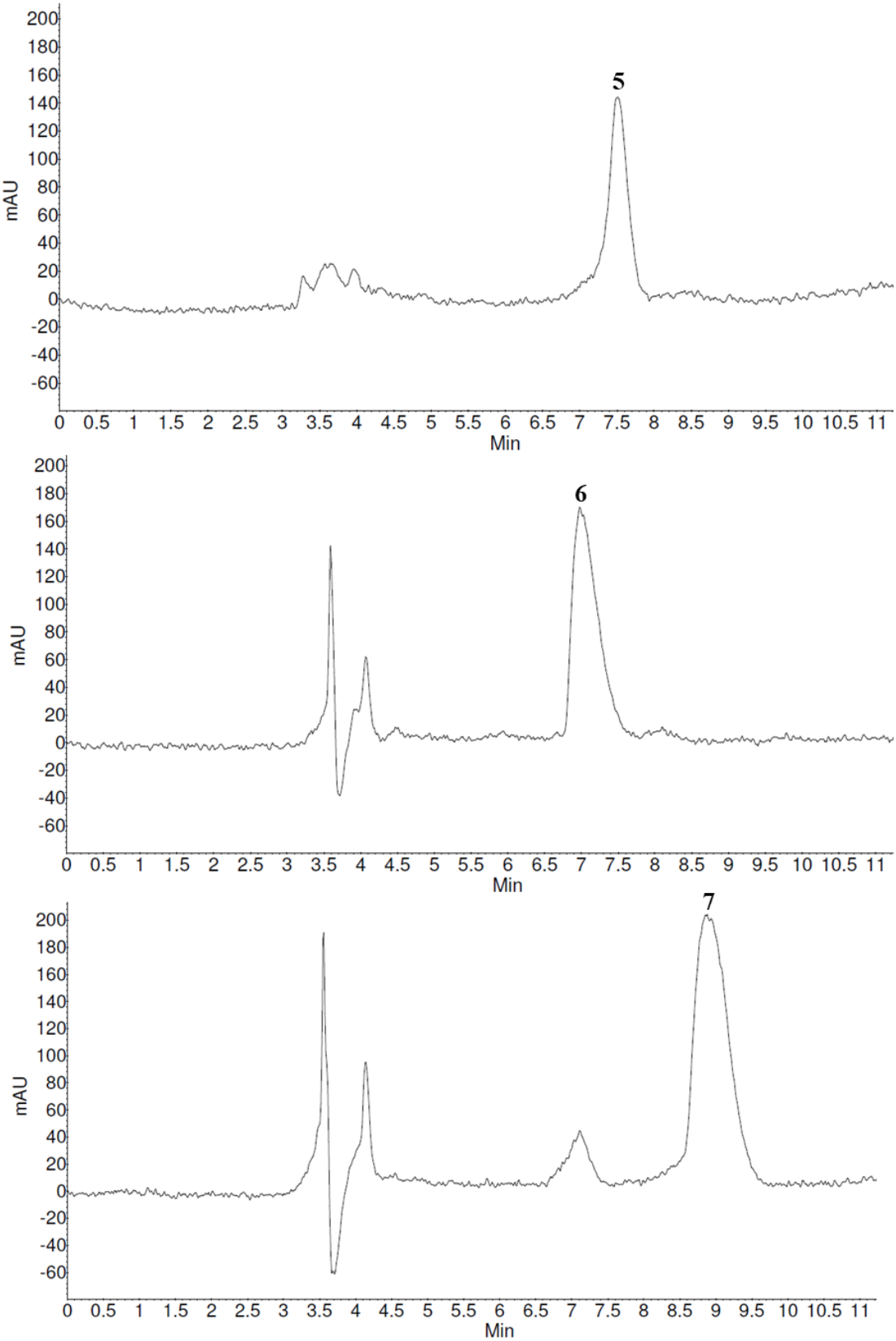

Figure S34. NP-HPLC chromatograms for compounds **5**, **6**, and **7**. These data were acquired using a Luna Silica column (Phenomenex, 250 x 4.6 mm) via isocratic conditions using a mixture of $CHCl_3$-MeOH (95:5) with a flow rate of 1 mL/min and UV set at 250 nm.

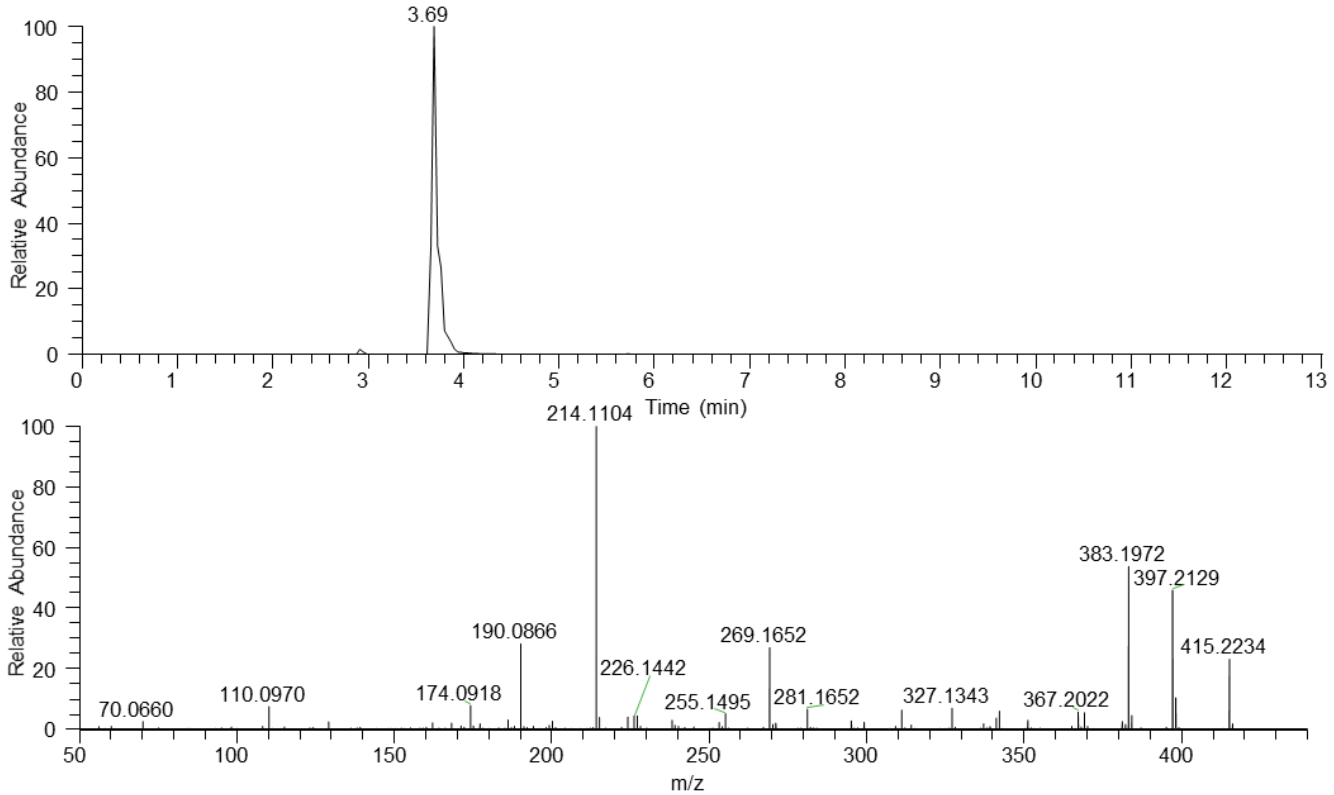

Figure S35. UPLC-HRESIMS data for mitragynine-*N*(4)-oxide (**8**).

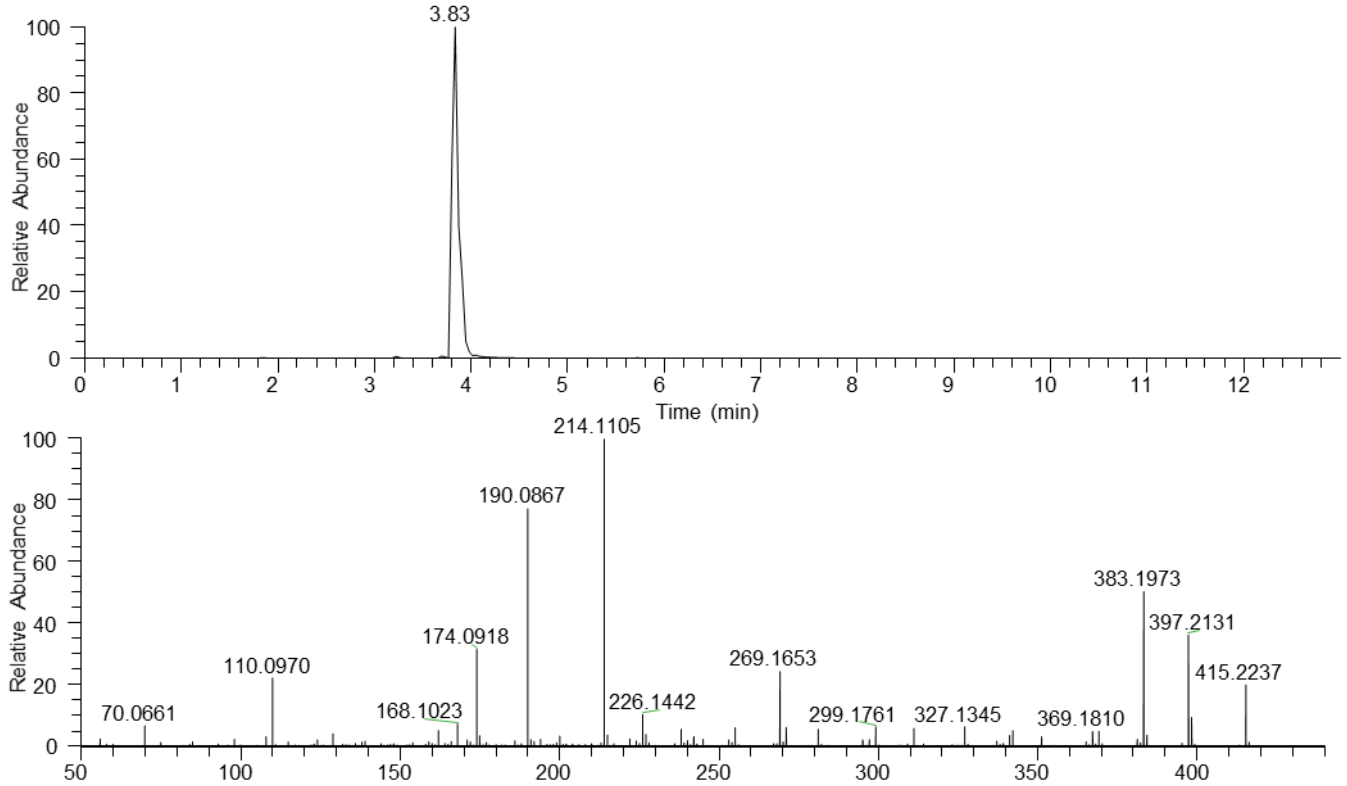

Figure S36. UPLC-HRESIMS data for speciociliatine-*N*(4)-oxide (**9**).

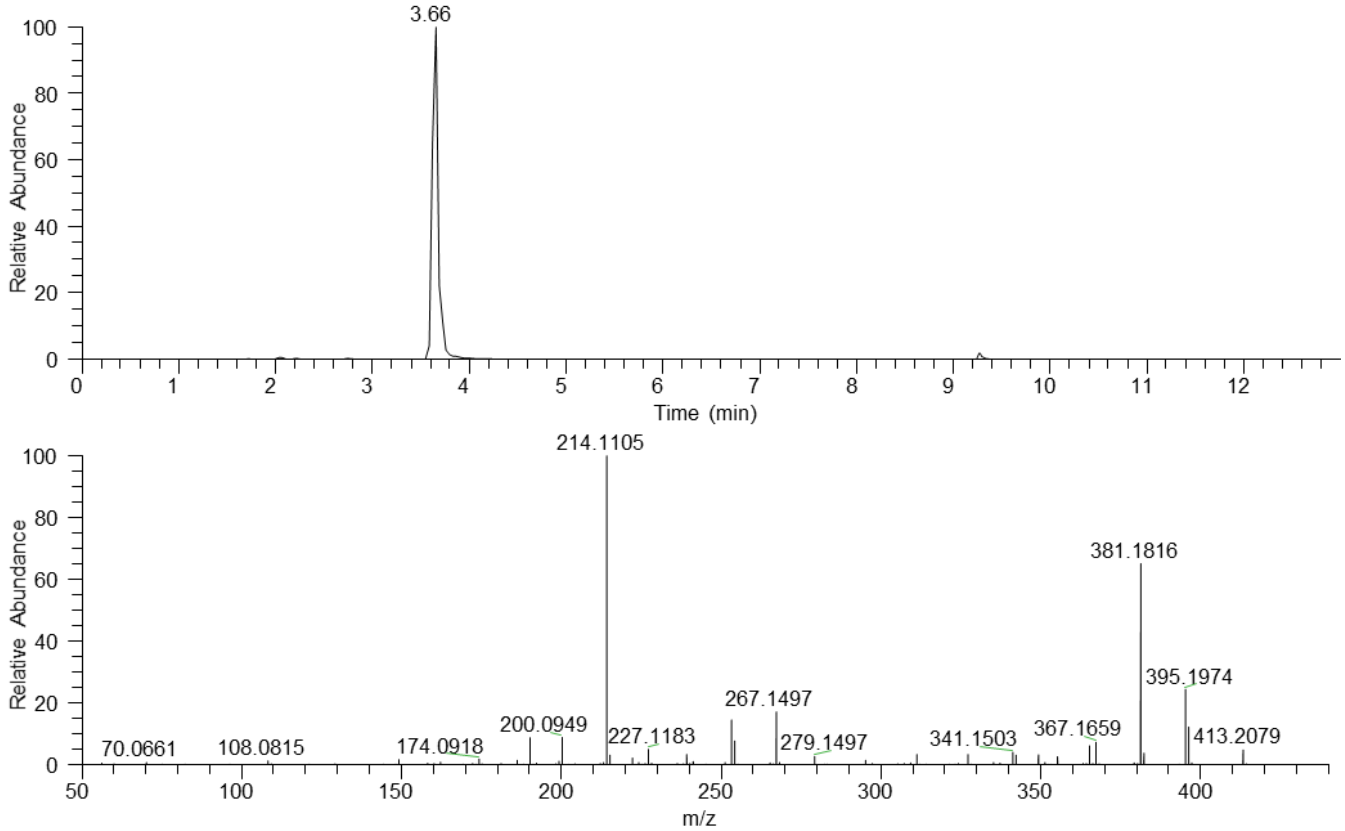

Figure S37. UPLC-HRESIMS data for isopaynantheine-*N*(4)-oxide (**10**).

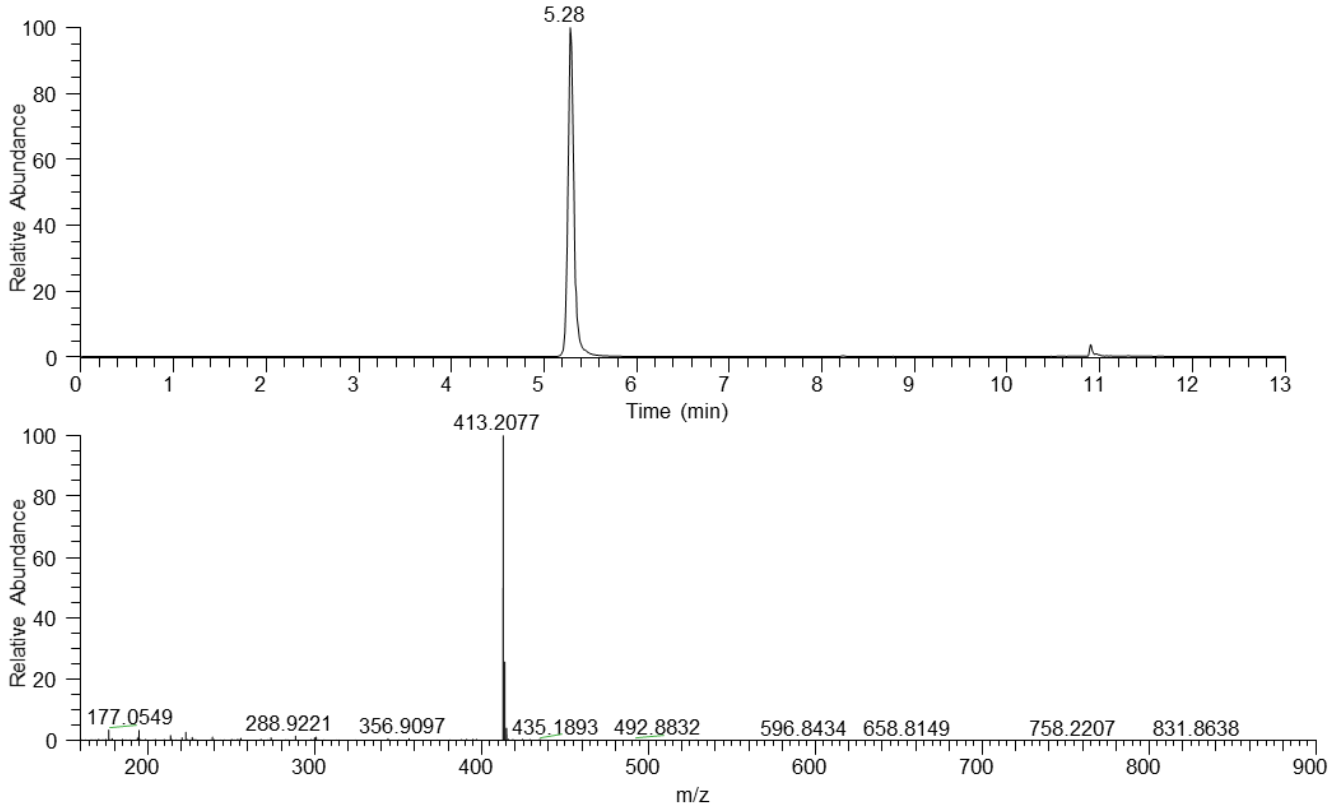

Figure S38. UPLC-HRESIMS data for epiallo-isopaynantheine-*N*(4)-oxide (**11**)

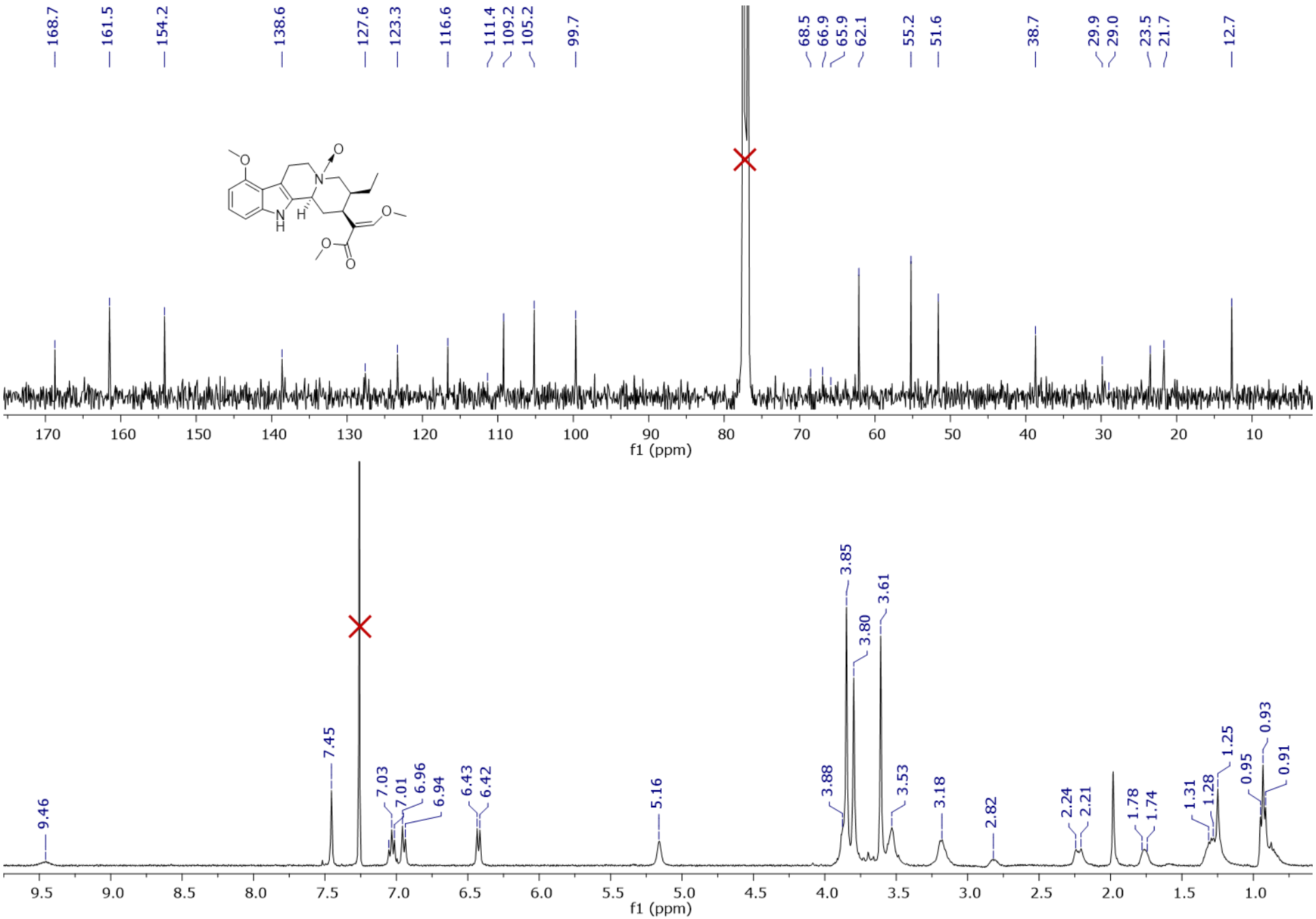

Figure S39. ^{1}H and ^{13}C NMR spectra for mitragynine-*N*(4)-oxide (**8**) ($CDCl_3$, 400 MHz and 100 MHz, respectively).

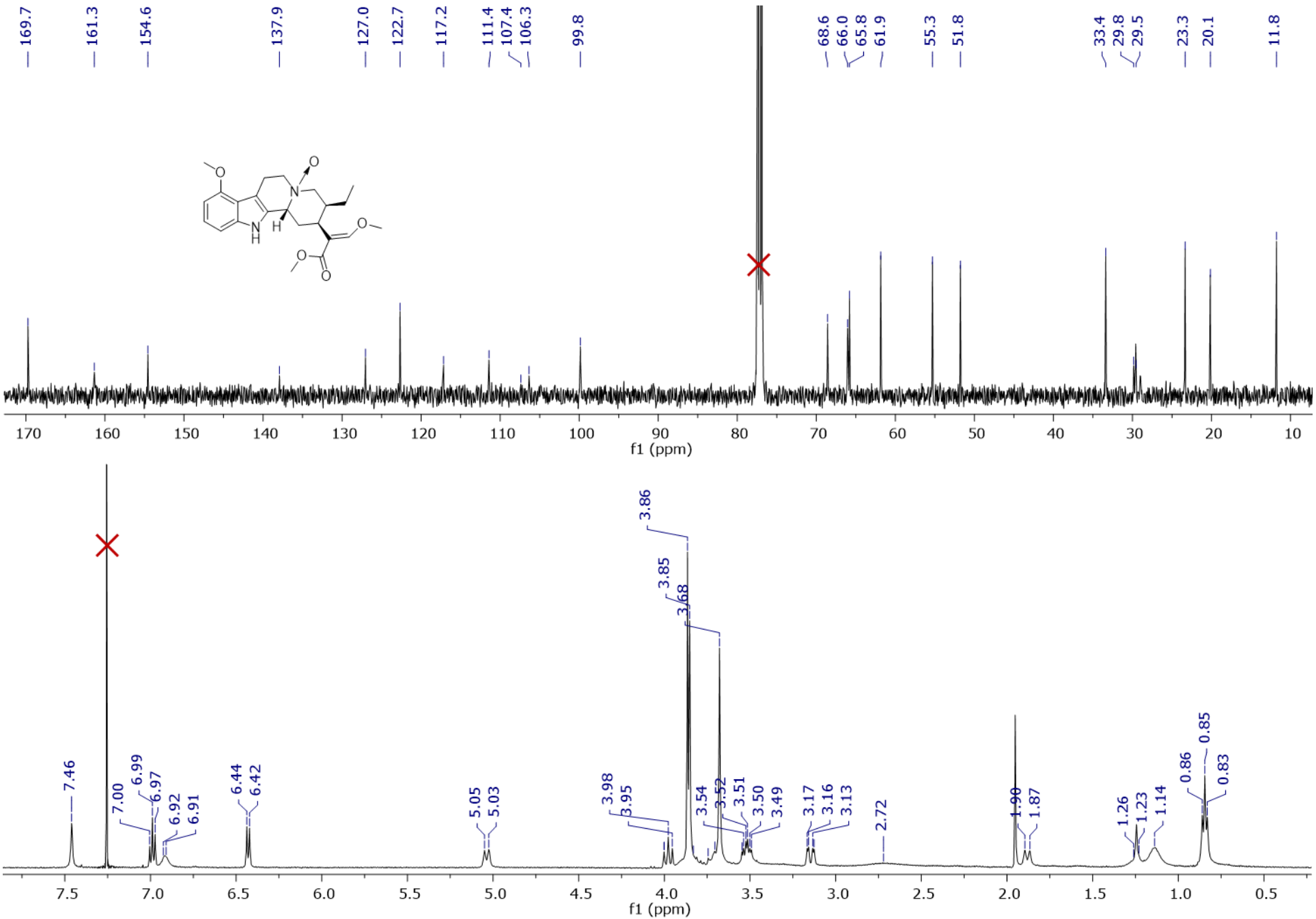

Figure S40. ^{1}H and ^{13}C NMR spectra for speciociliatine-*N*(4)-oxide (**9**) ($CDCl_3$, 400 MHz and 100 MHz, respectively).

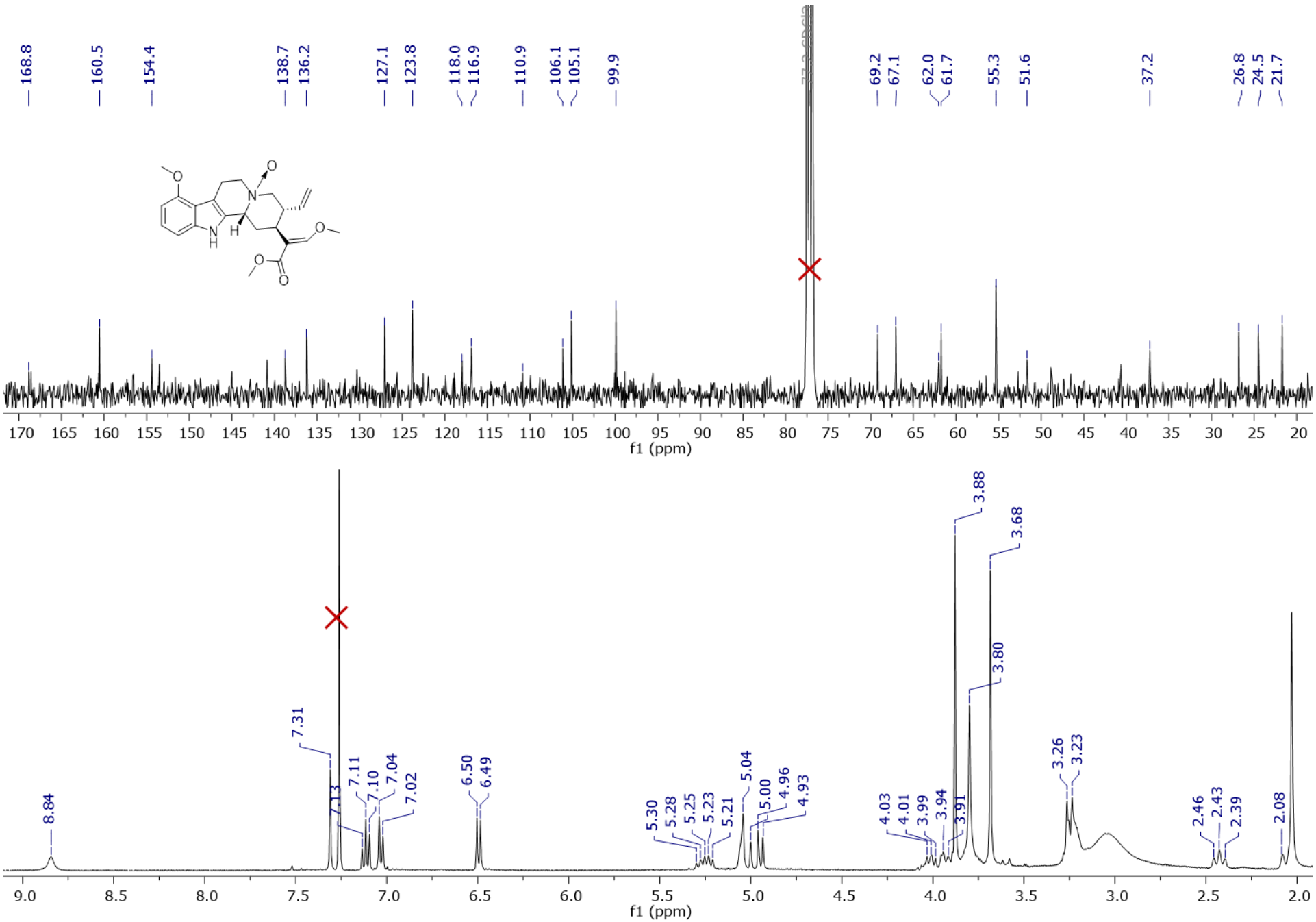

Figure S41. ^{1}H and ^{13}C NMR spectra for isopaynantheine-*N*(4)-oxide (**10**) ($CDCl_3$, 400 MHz and 100 MHz, respectively).

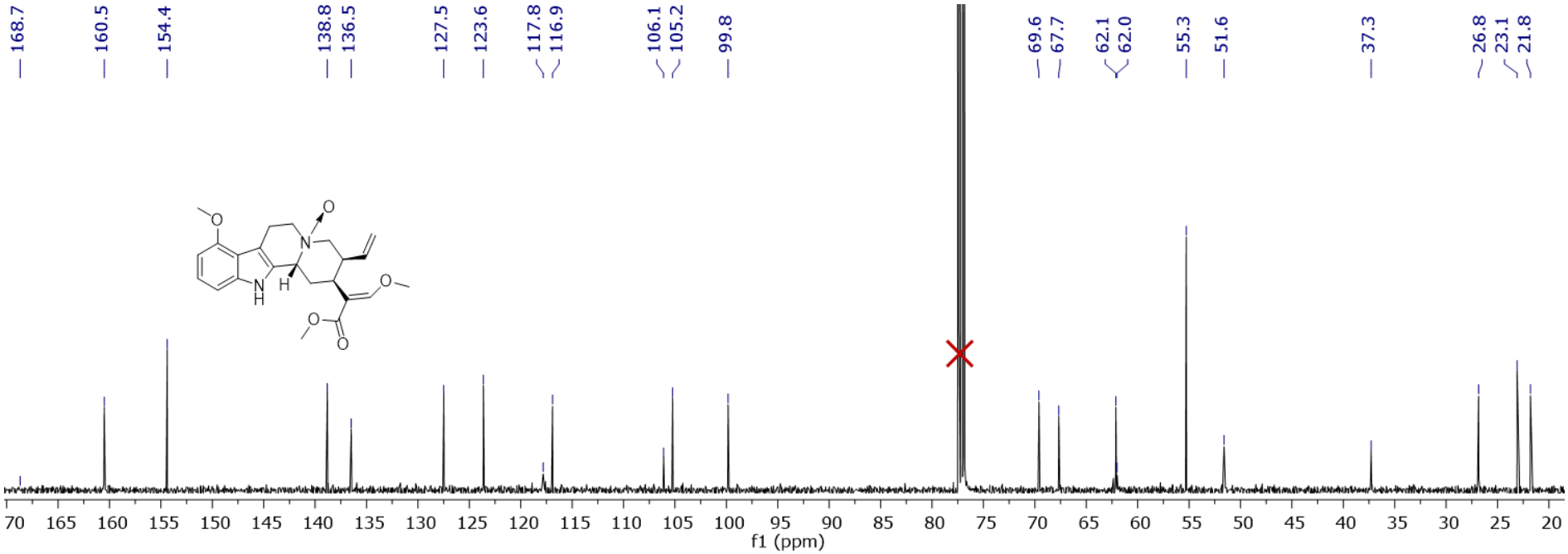

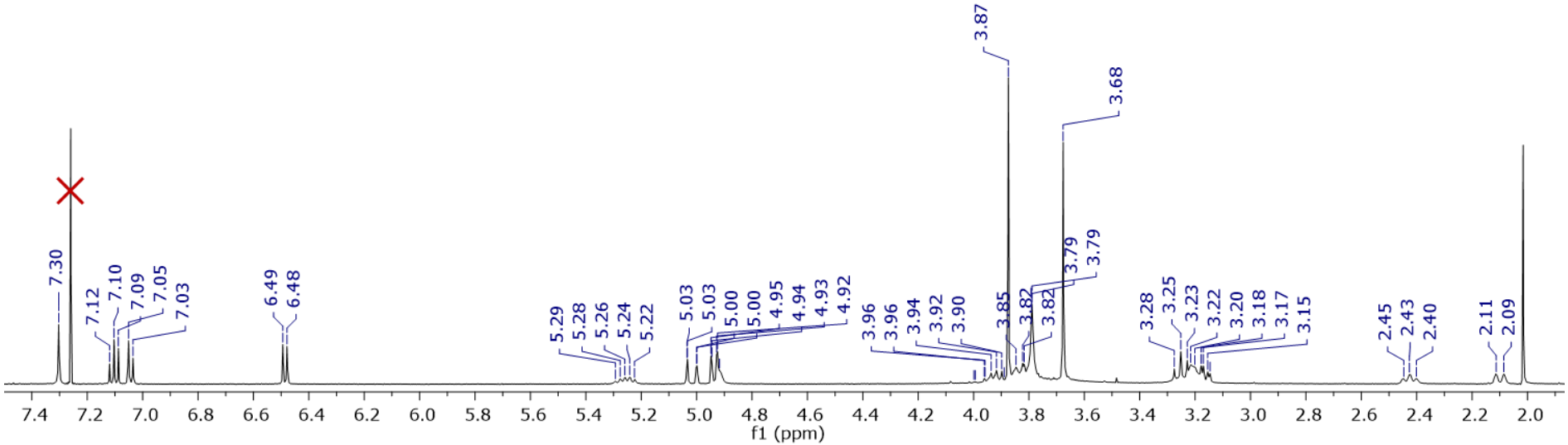

Figure S42. ^{1}H and ^{13}C NMR spectra for epiallo-isopaynantheine-*N*(4)-oxide (**11**) ($CDCl_3$, 400 MHz and 100 MHz, respectively).

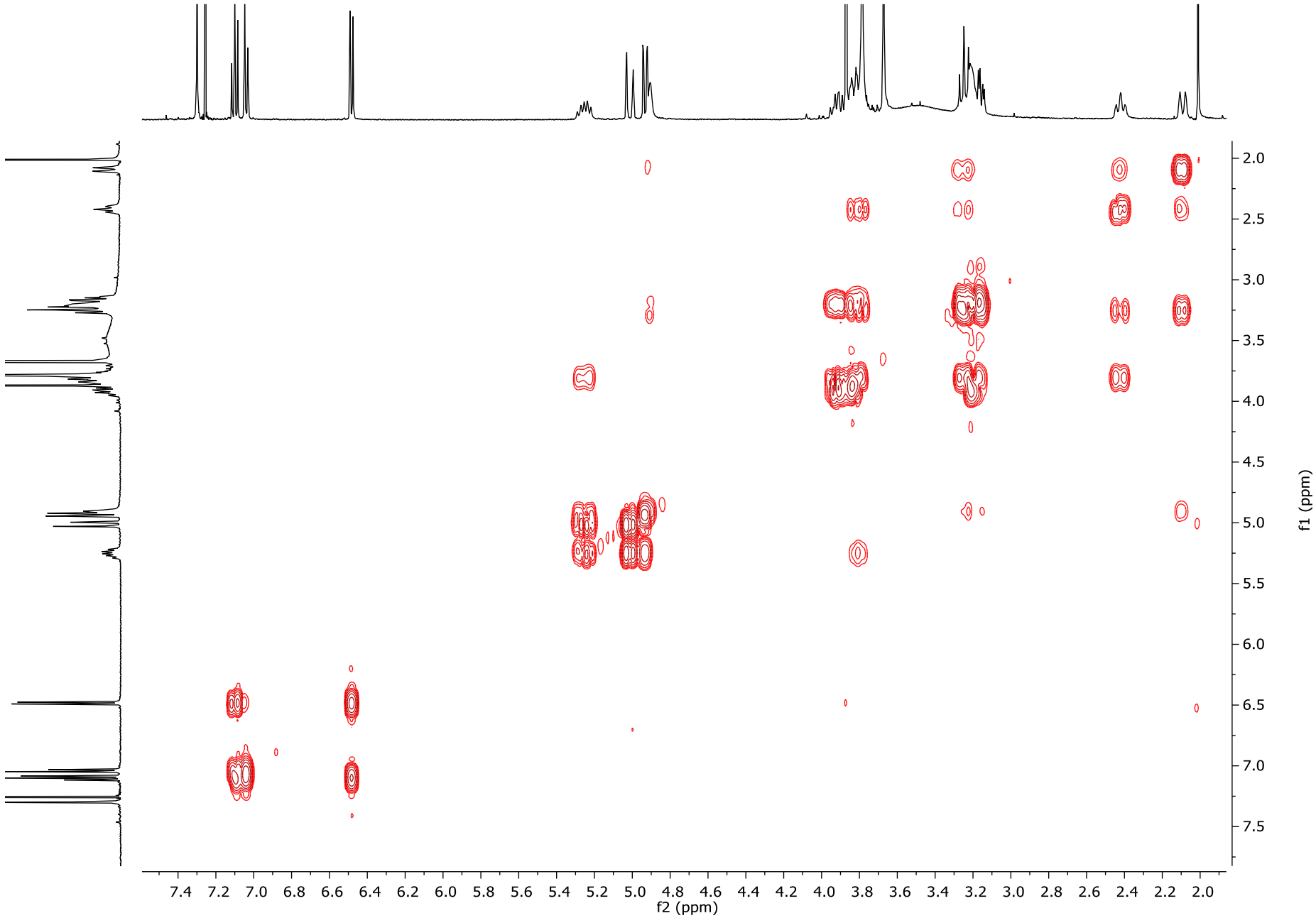

Figure S43. COSY spectrum for epiallo-isopaynantheine-*N*(4)-oxide (**11**) ($CDCl_3$, 400 MHz).

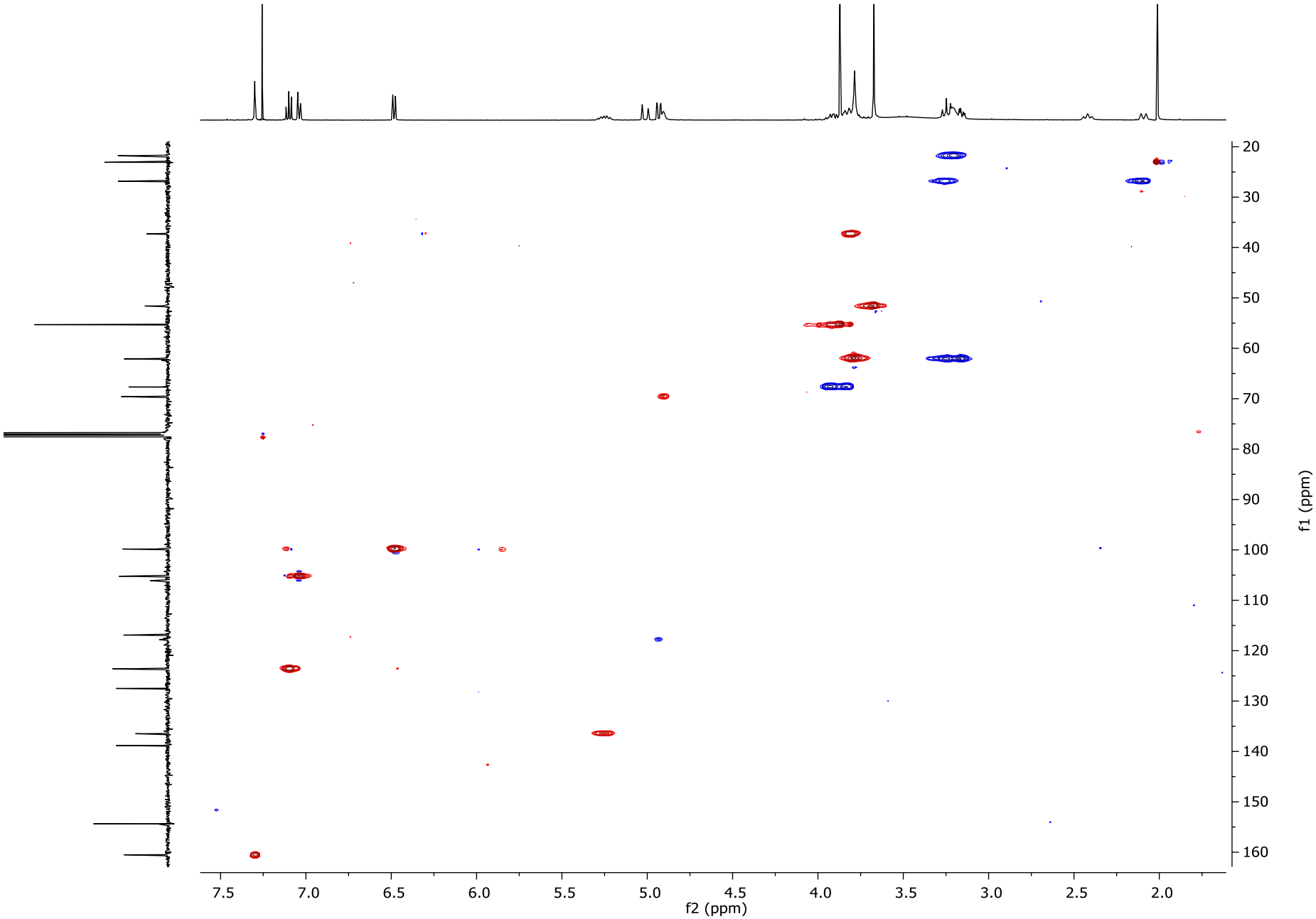

Figure S44. HSQC spectrum for epiallo-isopaynantheine-*N*(4)-oxide (**11**) ($CDCl_3$, 400 MHz).

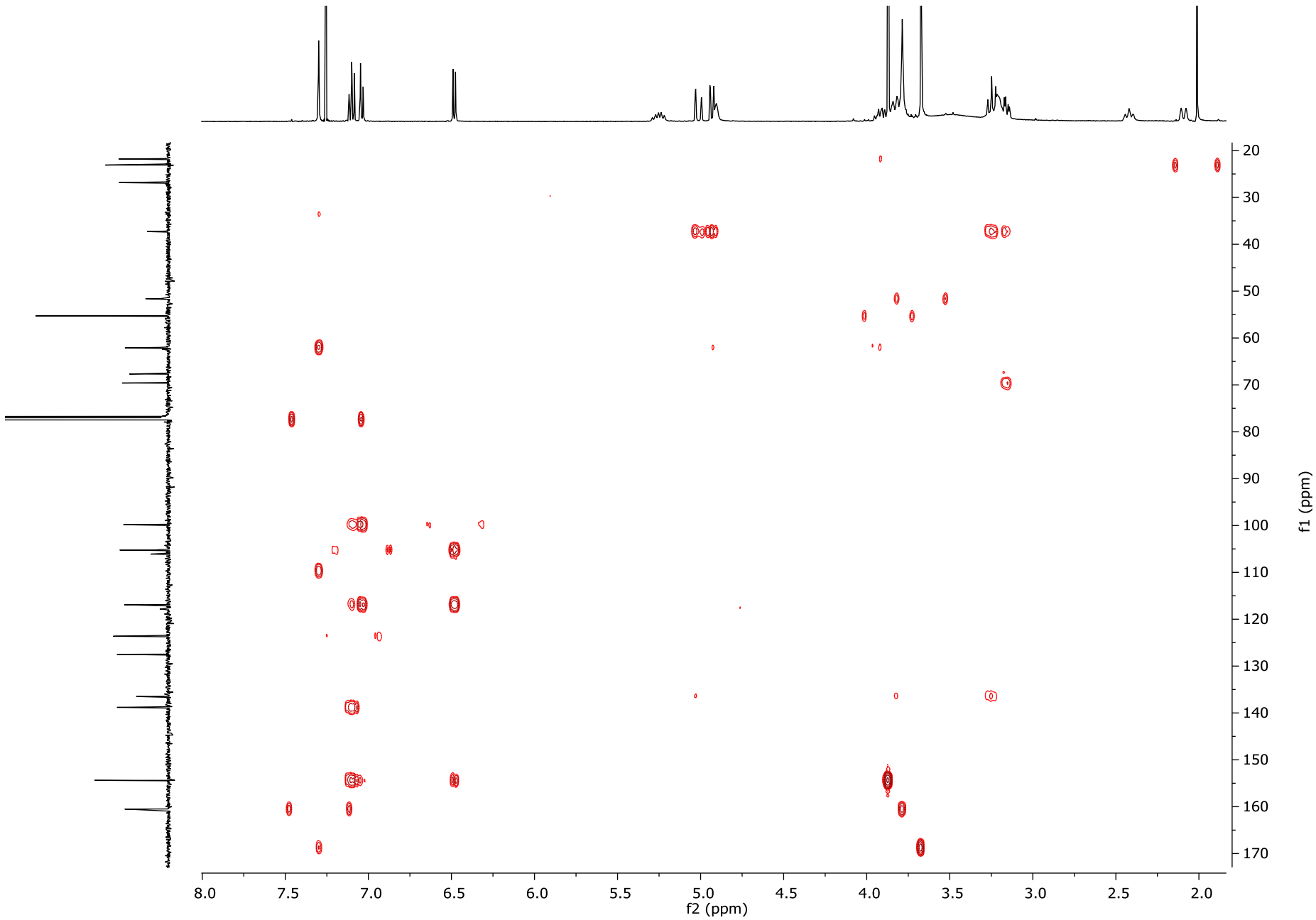

Figure S45. HMBC spectrum for epiallo-isopaynantheine-*N*(4)-oxide (**11**) ($CDCl_3$, 400 MHz).

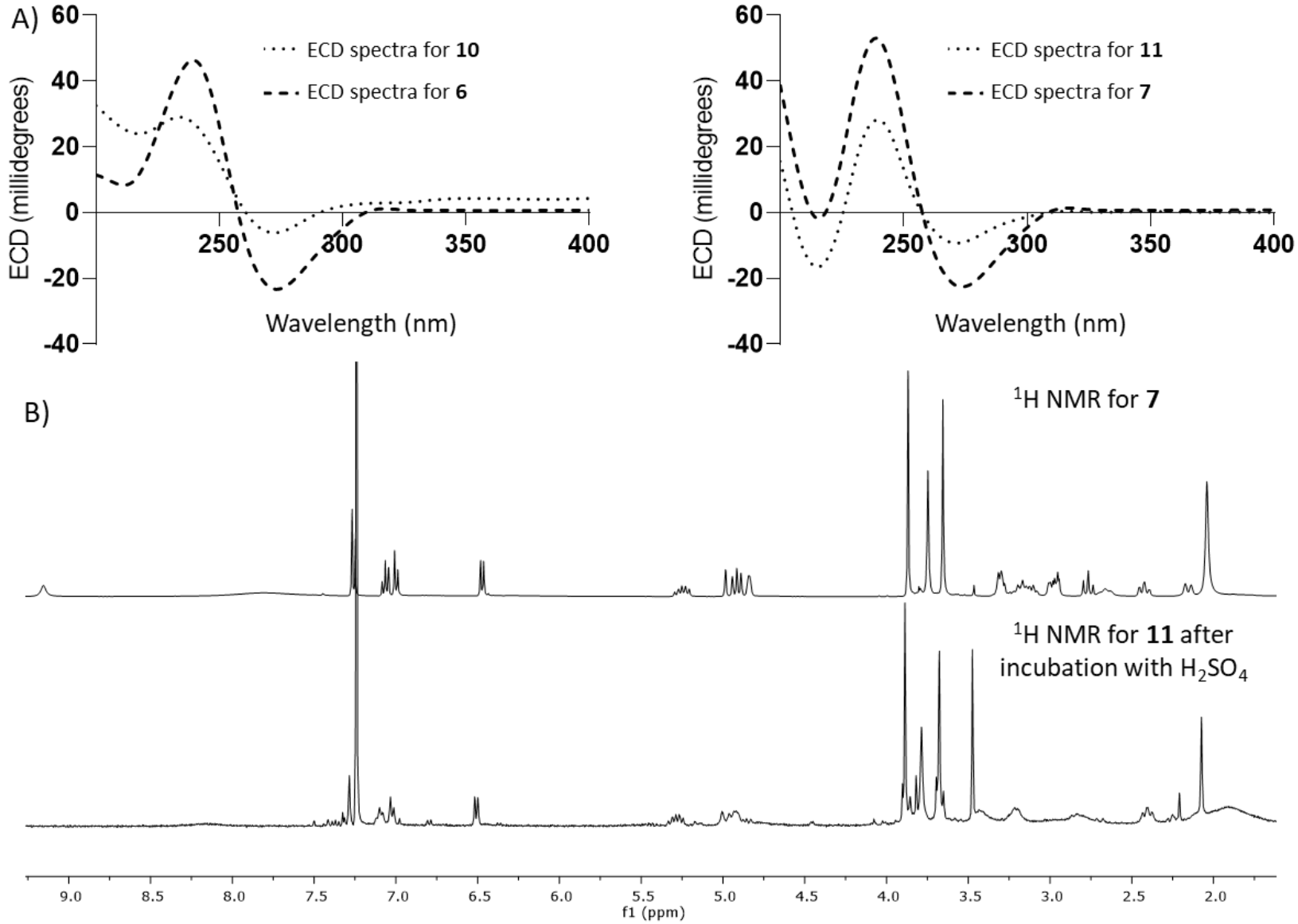

Figure S46. A) Comparison of the ECD spectra for *N*-oxides (**10** and **11**), and indole alkaloids (**6** and **7**); B) Comparison of the ^{1}H NMR of **7**, and that of **11** after incubation with sulfuric acid.

Table S6. Comparison of NMR Data for Compounds 8-11 ($CDCl_3$, 100 MHz and 400 MHz)

	mitragynine-*N*(4)-oxide (**8**)			speciociliatine-*N*(4)-oxide (**9**)			isopaynantheine-*N*(4)-oxide (**10**)			epiallo-isopaynantheine-*N*(4)-oxide (**11**)		
position	δ_C	type	δ_H (*J* in Hz)	δ_C	type	δ_H (*J* in Hz)	δ_C	type	δ_H (*J* in Hz)	δ_C	type	δ_H (*J* in Hz)
2	127.6	C		127.0	C		127.1	C		127.5	C	
3	66.9	CH	5.16, s	66.0	CH	5.04, d (12.5)	69.2	CH	5.04, bs	69.6	CH	4.91, bs
5	65.9	CH_2	3.88, m	65.8	CH_2	3.98, m	67.1	CH_2	3.81,m	67.7	CH_2	3.94, m
						3.51, td (11.7, 4.7)						3.83, m
6	21.7	CH_2	3.18, m	20.1	CH_2	3.15, dd (16.7, 4.5)	21.7	CH_2	3.25, m	21.8	CH_2	3.20, m
7	109.2	C		107.4	C		106.1	C		106.1	C	
8	116.6	C		117.2	C		116.9	C		116.9	C	
9	154.2	C		154.6	C		154.4	C		154.4	C	
10	99.7	CH	6.43, d (7.7)	99.8	CH	6.43, d (7.7)	99.9	CH	6.49, d (7.8)	99.8	CH	6.48 d (7.7
11	123.3	CH	7.03, t (7.9)	122.7	CH	6.99, t (7.9)	123.8	CH	7.11, t (7.9)	123.6	CH	7.10, t (7.9)
12	105.2	CH	6.95, d (8.1)	106.3	CH	6.92, bs	105.1	CH	7.03, d (8.2)	105.2	CH	7.04, d (8.1)
13	138.6	C	-	137.9	C	-	138.7	C	-	138.8	C	
14	29.0	CH_2	2.23, d (15.0)	29.5	CH_2	1.25, m	26.8	CH_2	2.08, m	26.8	CH_2	2.10, d (13.8)
15	29.9	CH_2	2.82, bs	29.8	CH_2	1.88, d (14.7)	24.5	CH_2	2.43, t (12.3)	23.1	CH_2	2.42 t (11.4)
16	111.4	C	-	111.4	C	-	110.9	C	-	109.1[a]	C	
17	161.5	CH	7.45, s	161.3	CH	7.46, s	160.5	CH	7.31, s	160.5	CH	7.30, s
18	12.7	CH_3	0.93, t (7.2)	11.8	CH_3	0.85, t (7.4)	118.0	CH_2	5.02, dd (17.5, 1.0)	117.8	CH_2	5.02, d (17.2)
									4.95, dd (10.2, 1.7)			4.94, dd (10.3, 1.6)
19	23.5	CH_2	1.31, m	23.3	CH_2	1.14, m	136.2	CH	5.25, dt (17.5, 9.3)	136.5	CH	5.26, dt (17.5, 8.6)
			1.28, m									
20	38.7	CH	1.76, bs	33.4	CH	2.72, bs	37.2	CH	3.85, m	37.3	CH	3.81, m
21	68.5	CH_2	3.53, m	68.6	CH_2	3.72, m	61.7	CH_2	3.25, m	62.1	CH_2	3.25, t (11.7)
									3.10, m			3.17, m
22	168.7	C		169.7	C		168.8	C		168.7	C	
9-OCH_3	55.2	CH_3	3.85, s	55.3	CH_3	3.86, s	55.3	CH_3	3.88, s	55.3	CH_3	3.87, s
17-OCH_3	62.1	CH_3	3.80, s	61.9	CH_3	3.85, s	62.0	CH_3	3.80, s	62.0	CH_3	3.79, s
22-OCH_3	51.6	CH_3	3.61, s	51.8	CH_3	3.68, s	51.6	CH_3	3.68, s	51.6	CH_3	3.68, s
NH			9.46, s			-			8.84, s			-

[a]Signal observed by HMBC

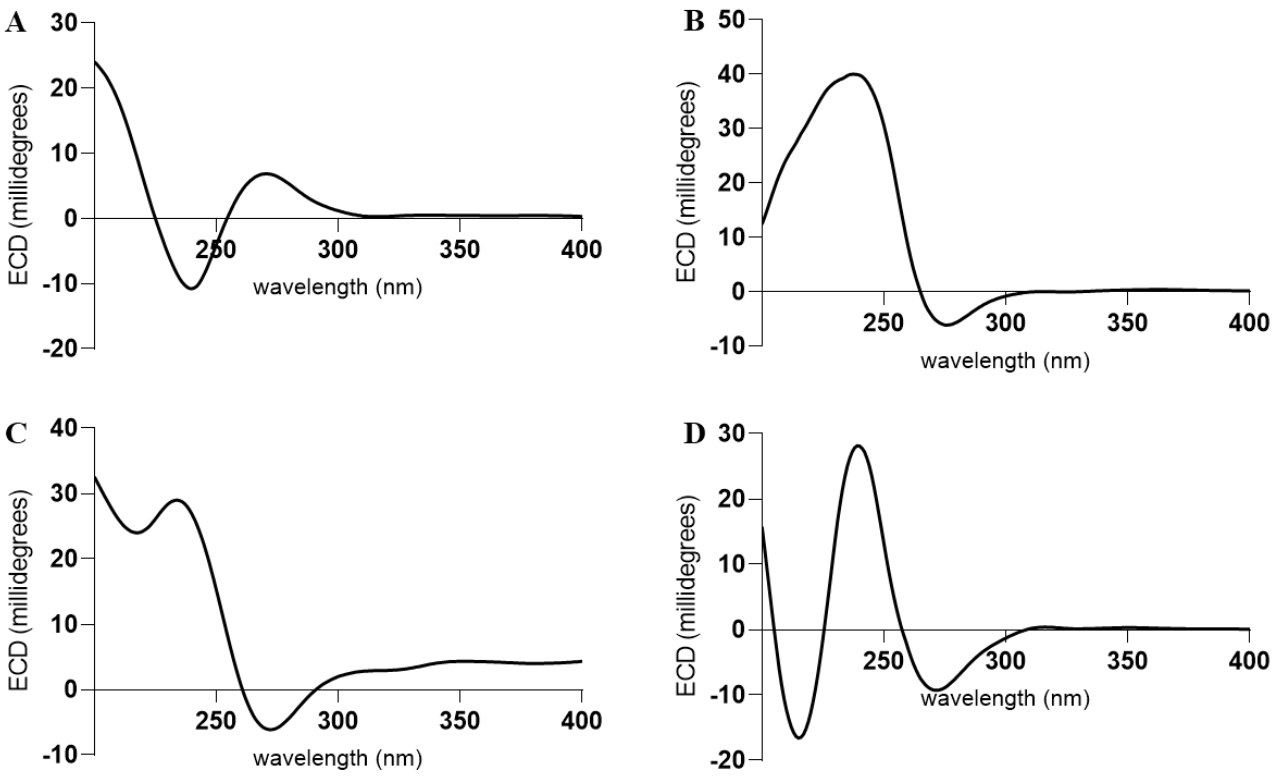

Figure S47. Comparison of the ECD spectra acquired in CH_3OH for A) mitragynine-*N*(4)-oxide (**8**), B) speciociliatine-*N*(4)-oxide (**9**), C) isopaynantheine-*N*(4)-oxide (**10**), and D) epiallo-isopaynantheine-*N*(4)-oxide (**11**).

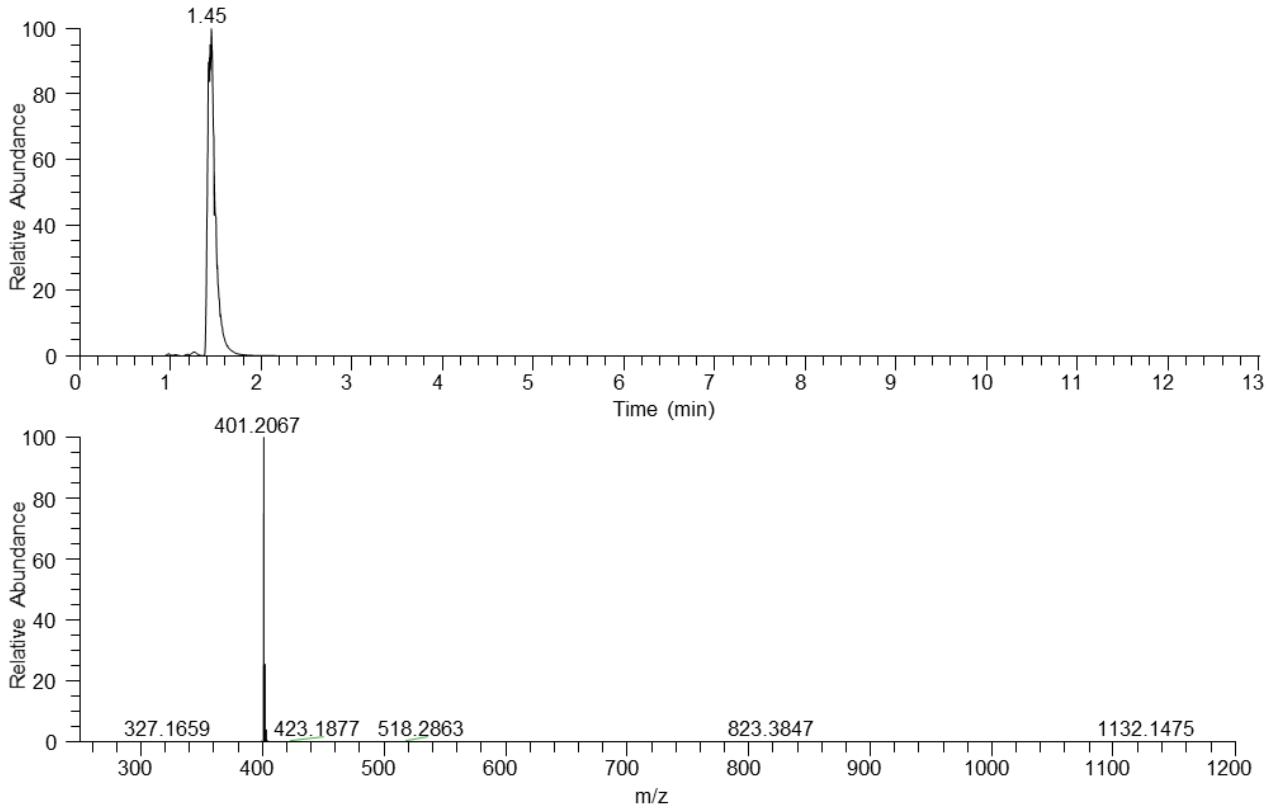

Figure S48. UPLC-HRESIMS data for speciofoline (**12**).

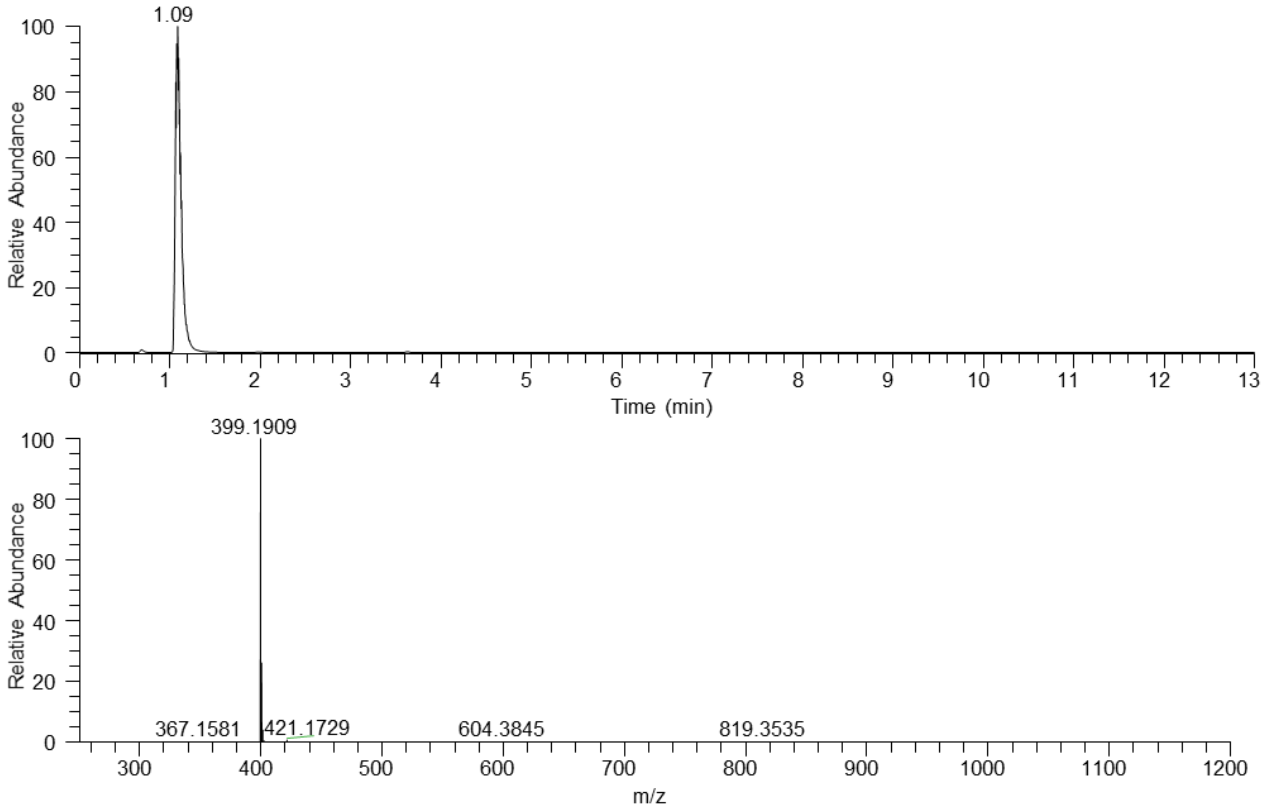

Figure S49. UPLC-HRESIMS data for isorotundifoleine (**13**).

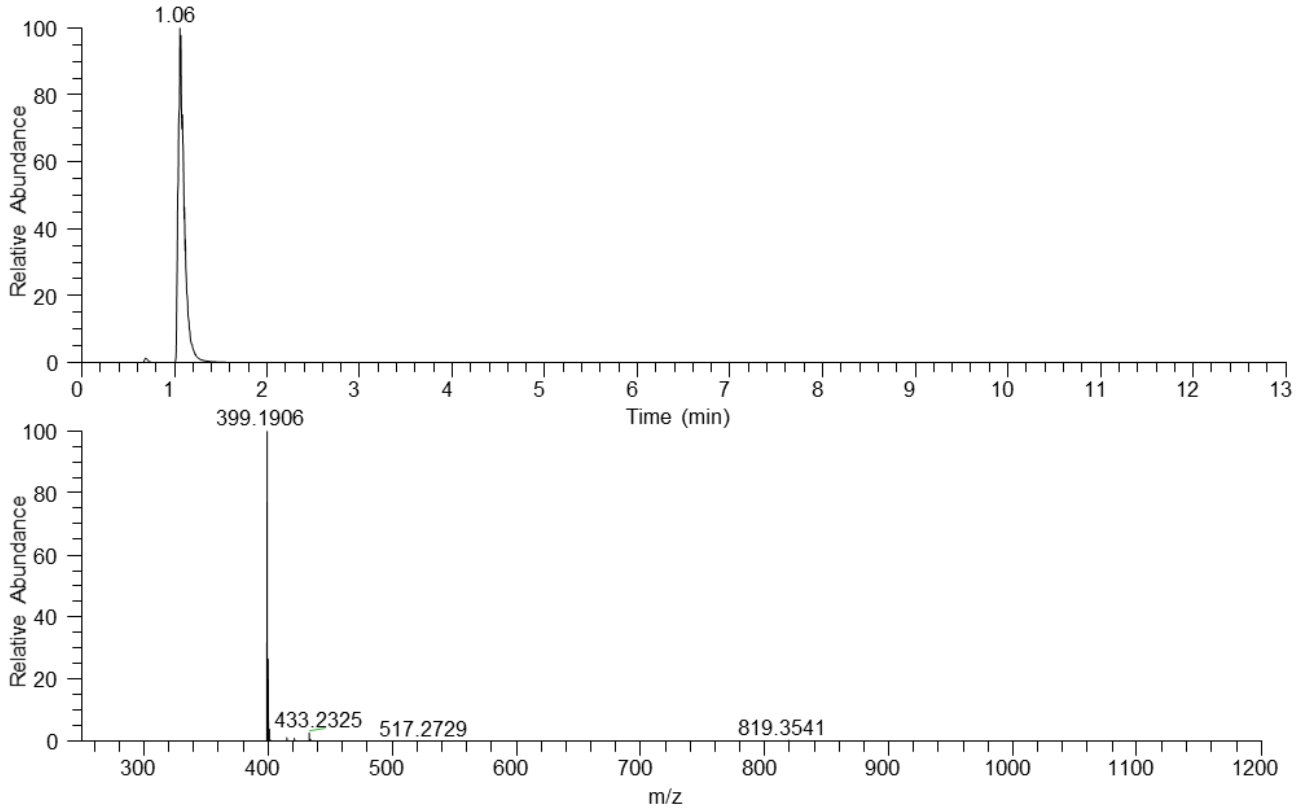

Figure S50. UPLC-HRESIMS data for isospeciofoleine (**14**).

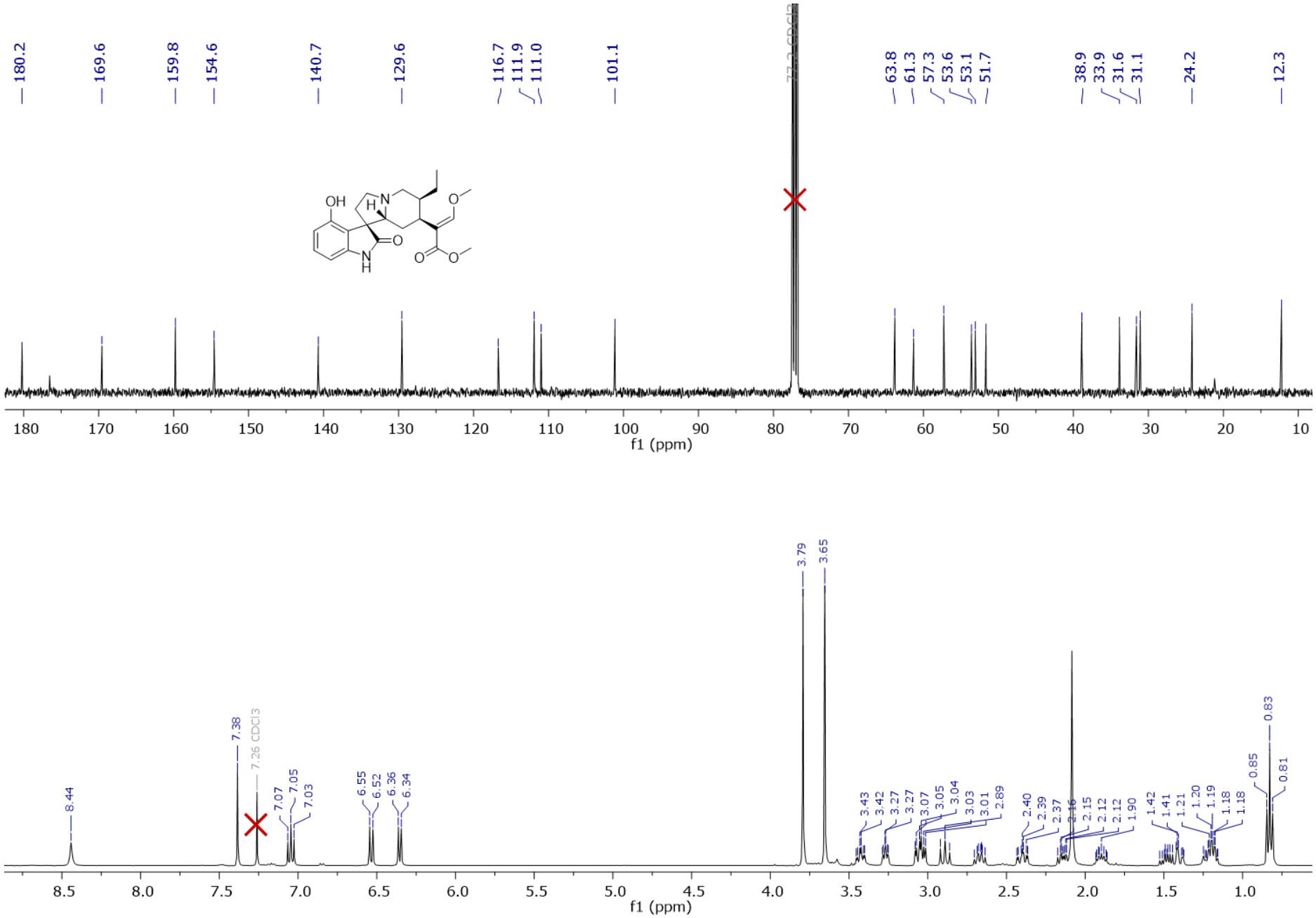

Figure S51. ^{1}H and ^{13}C NMR spectra for speciofoline (**12**) ($CDCl_3$, 400 MHz and 100 MHz, respectively).

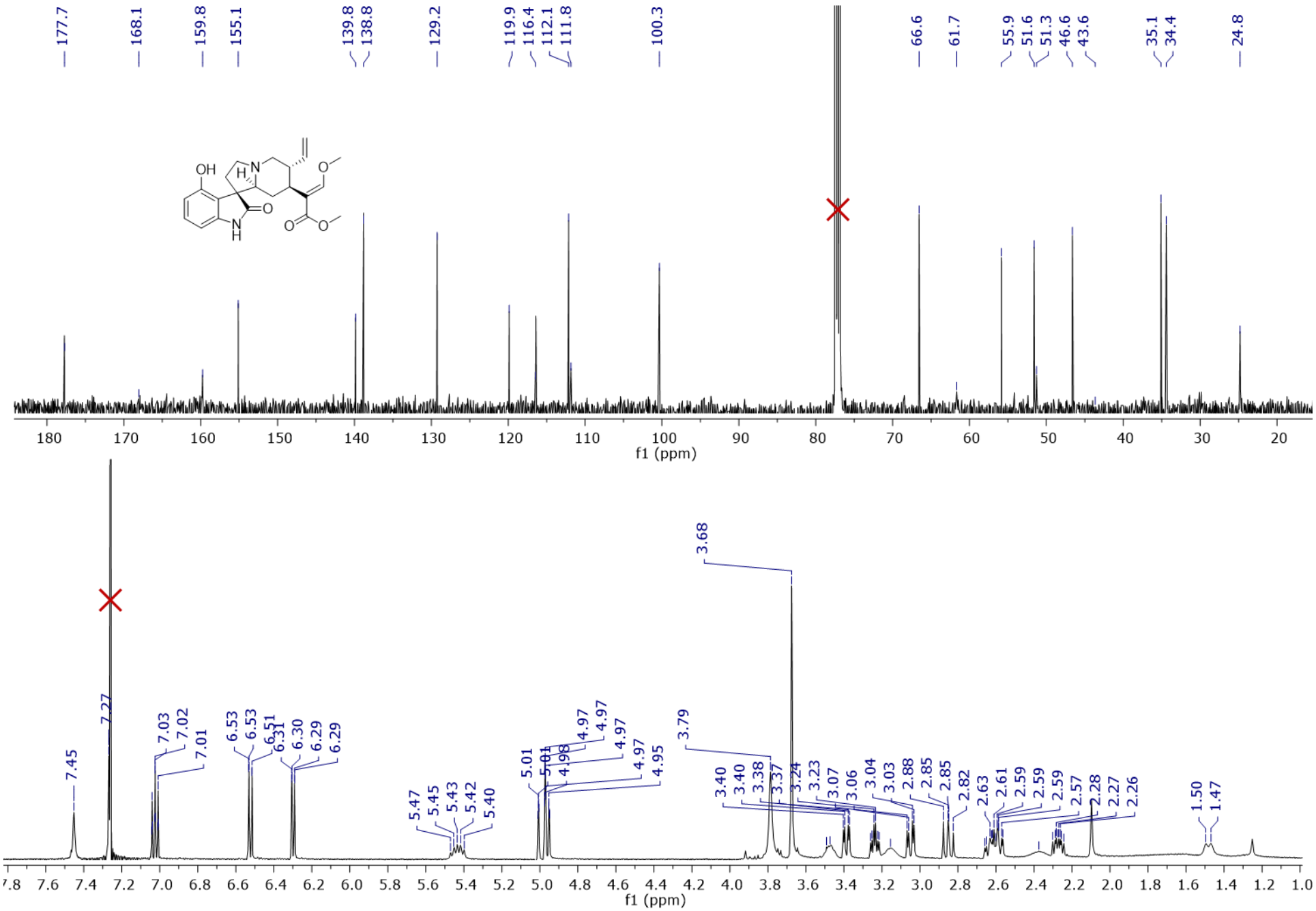

Figure S52. ^{1}H and ^{13}C NMR spectra for isorotundifoleine (**13**) ($CDCl_3$, 500 MHz and 125 MHz, respectively).

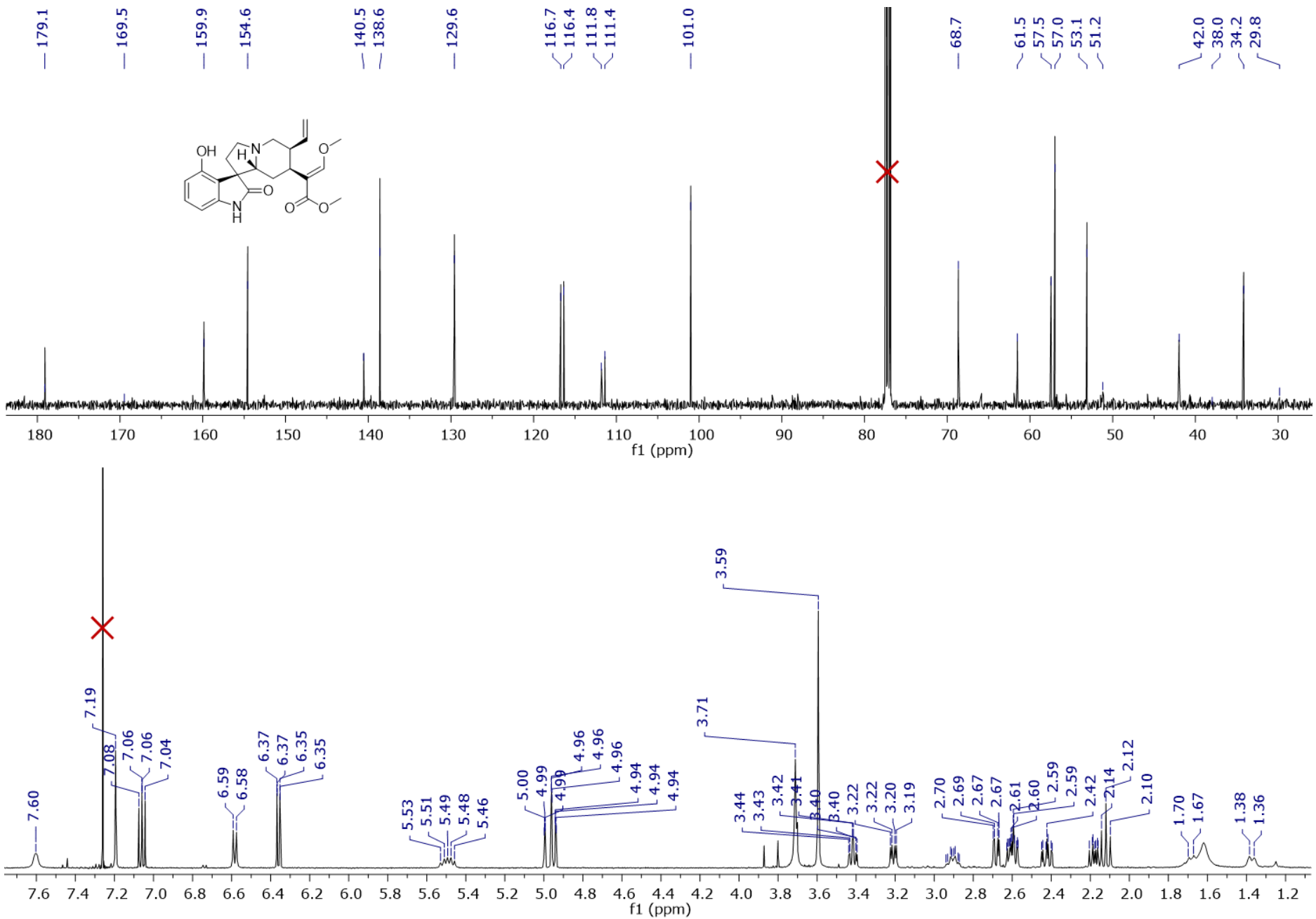

Figure S53. ^{1}H and ^{13}C NMR spectra for isospeciofoleine (**14**) ($CDCl_3$, 500 MHz and 125 MHz, respectively).

Table S7. Comparison of NMR Data for Compounds 12-14 ($CDCl_3$, 125 MHz and 500 MHz)

	speciofoline (**12**)			isorotundifoleine (**13**)			isospeciofoleine (**14**)		
Position	δ_C	type	δ_H (*J* in Hz)	δ_C	type	δ_H (*J* in Hz)	δ_C	type	δ_H (*J* in Hz)
2	180.2	C		177.7	C		179.1	C	
3	63.8	CH	3.06, dd (11.7, 3.6)	66.6	CH	3.39, dd (12.5, 3.6)	68.7	CH	2.68, dd (11.6, 3.2)
5	53.1	CH_2	3.43, td (9.2, 3.2)	46.6	CH_2	3.48, m	53.1	CH_2	3.42, td (9.2, 3.1)
			2.67, m			3.24, td (9.4, 4.1)			2.60, m
6	33.9	CH_2	2.40, ddd (13.8, 10.9, 3.3)	34.4	CH_2	2.61, m	34.2	CH_2	2.42, ddd (13.7, 10.7, 3.1)
			2.14, m			2.27, ddd (13.5, 9.3, 6.6)			2.18, m
7	57.3	C		55.9	C		57.5	C	
8	116.7	C		119.9	C		116.7	C	
9	154.6	C		155.1	C		154.6	C	
10	111.9	CH	6.35, d (7.6)	112.1	CH	6.30, dd (7.6, 0.8)	111.4	CH	6.36, dd (7.6, 0.7)
11	129.6	CH	7.05, t (8.0)	129.2	CH	7.02, dd (8.3, 7.7)	129.6	CH	7.06, dd (8.3, 7.7)
12	101.1	CH	6.53, d (8.3)	100.3	CH	6.52, dd (8.5, 0.8)	101.0	CH	6.58, d (8.3)
13	140.7	C		139.8	C		140.5	C	
14	31.6	CH_2	1.49, ddd (13.7, 12.1, 6.5)	24.8	CH_2	2.38, m	29.8	CH_2	1.68, d (13.4)
			1.40, m			1.48, d (14.0)			1.37, d (11.8)
15	31.1	CH	3.27, t (5.7)	43.6	CH	2.61, m	38.0	CH	2.60, m
16	111.0	C		111.8	C		111.8	C	
17	159.8	CH	7.38, s	159.8	CH	7.27, s	159.9	CH	7.19, s
18	12.3	CH_3	0.83, d (7.4)	116.4	CH_2	5.01, m	116.4	CH_2	4.97, m
						4.96, m			4.95, m
19	24.2	CH_2	1.21, dqd (14.0, 6.8, 2.8)	138.8	CH	5.43, dt (18.7, 9.1)	138.6	CH	5.49, dt (17.3, 9.5)
20	38.9	CH	1.90, dp (12.3, 7.1)	35.1	CH	3.16, m	42.0	CH	2.90, m
21	53.6	CH_2	3.06, dd (11.7, 3.6)	51.6	CH_2	3.05, dd (14.0, 4.2)	57.0	CH_2	3.21, dd (11.2, 3.9)
			2.89, t (11.6)			2.85, dd (13.8, 12.2)			2.12, t (11.3)
22	169.6	C		168.1	C		169.5	C	
17-OCH_3	61.3	CH_3	3.79, s	61.7	CH_3	3.79, s	61.5	CH_3	3.71, s
22-OCH_3	51.7	CH_3	3.65, s	51.3	CH_3	3.68, s	51.2	CH_3	3.59, s
NH			8.44, s			7.45,s			7.60, s

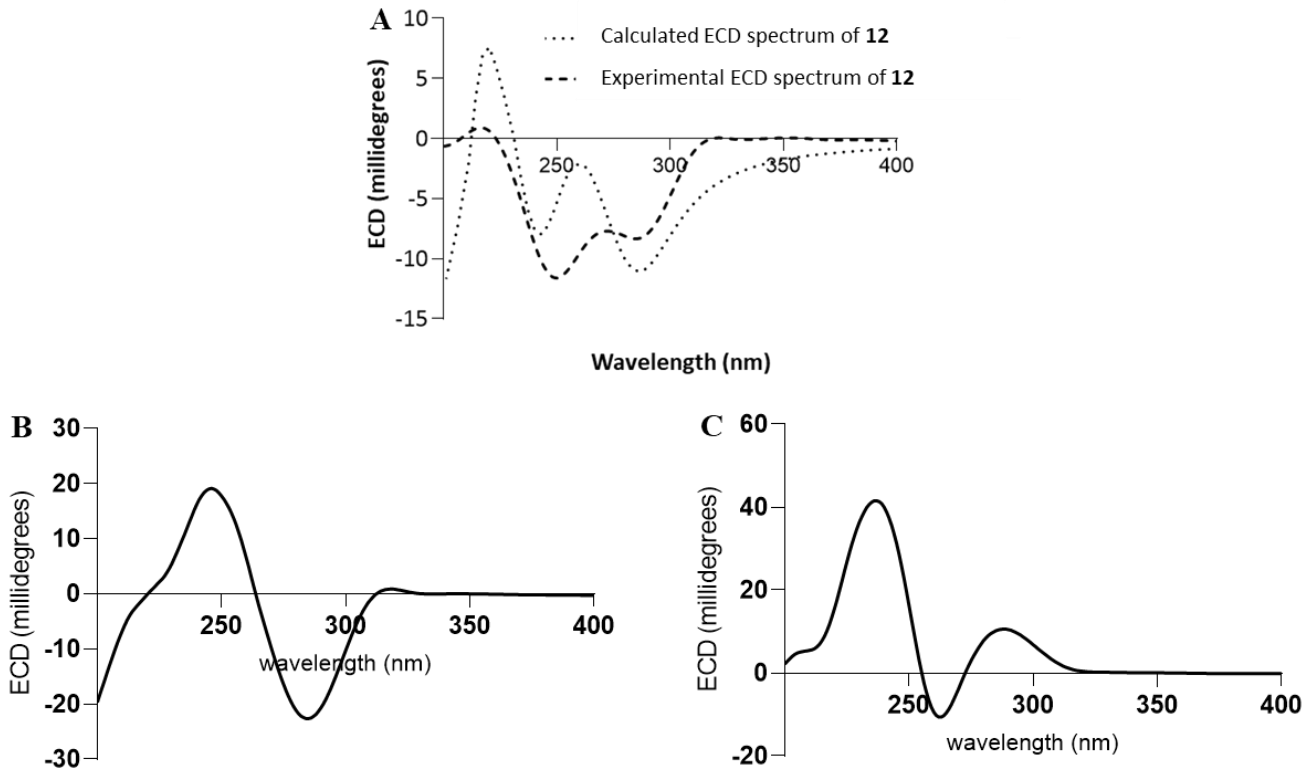

Figure S54. Comparison of the ECD spectra acquired in CH_3OH for A) speciofoline (**12**), B) isorotundifoleine (**13**), and C) isospeciofoleine (**14**).

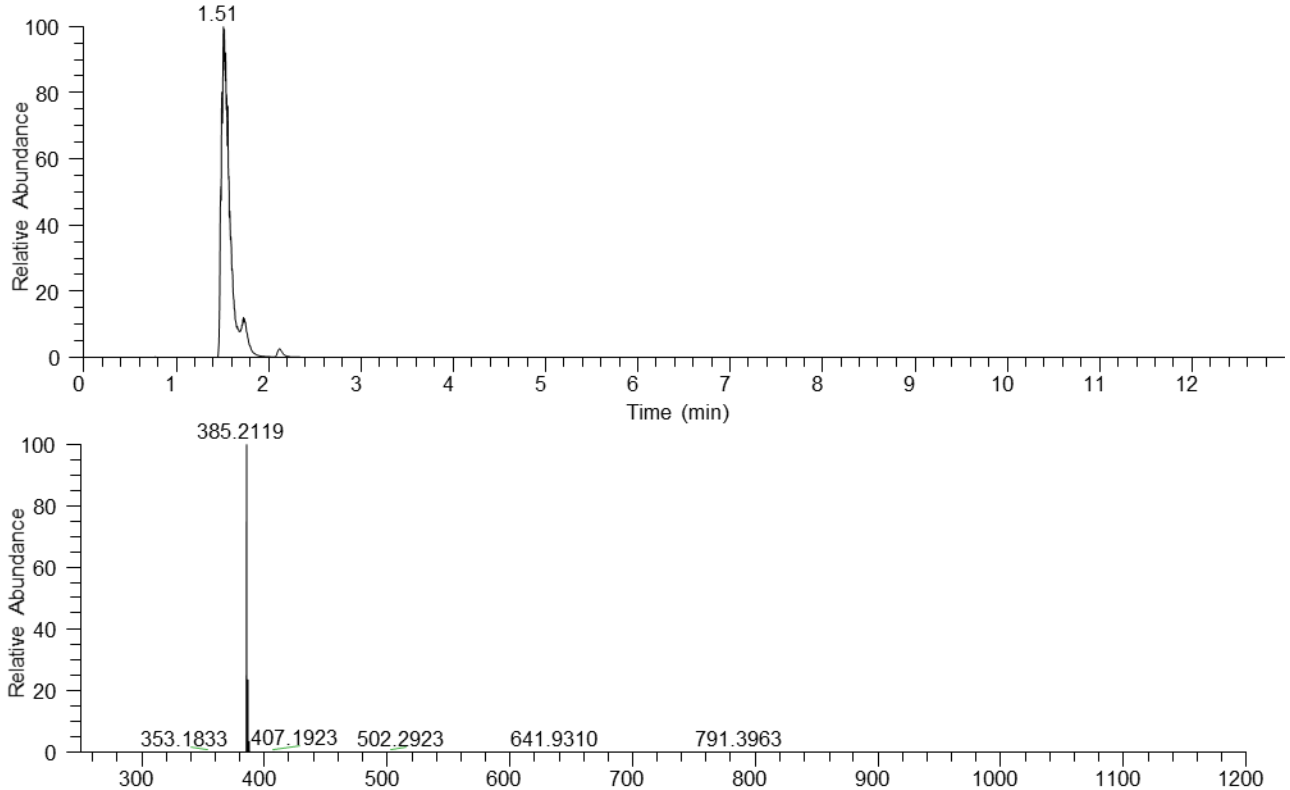

Figure S55. UPLC-HRESIMS data for corynoxine A (**15**).

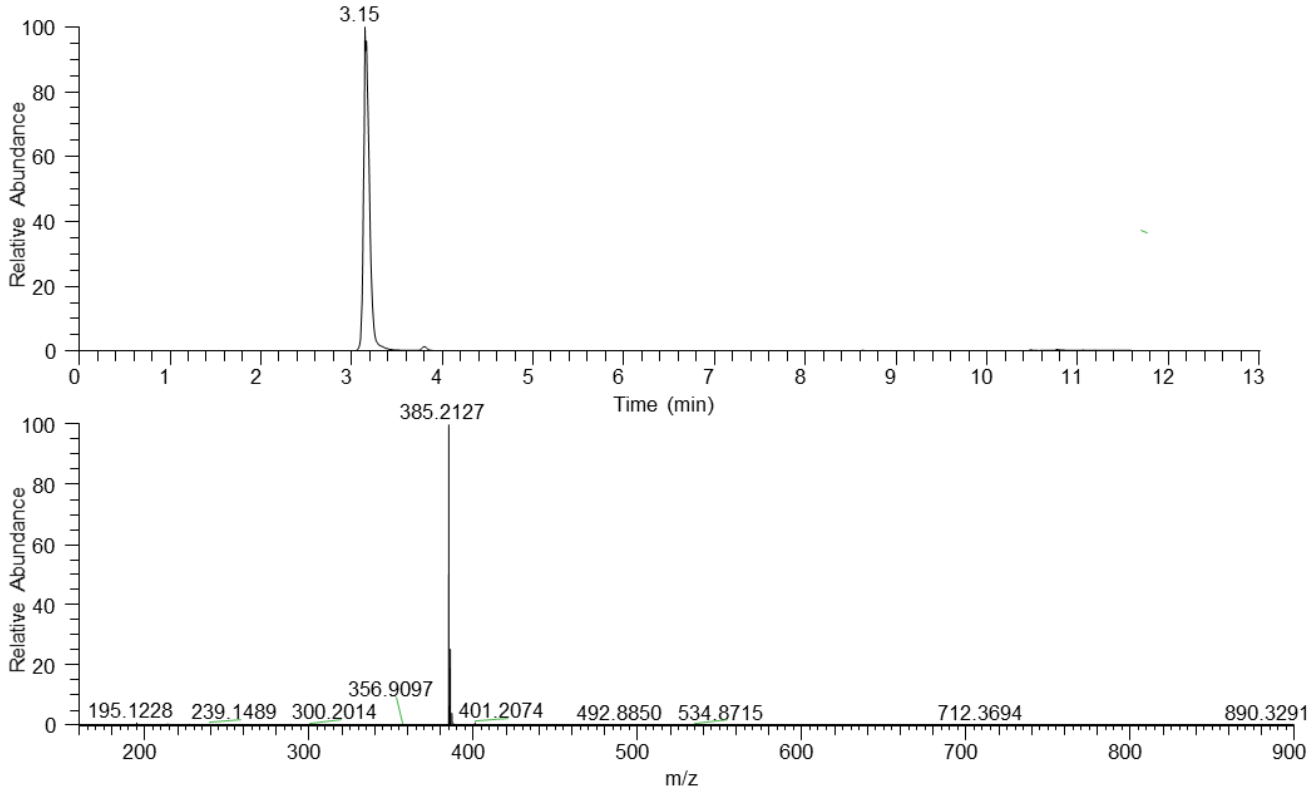

Figure S56. UPLC-HRESIMS data for corynoxine B (**16**).

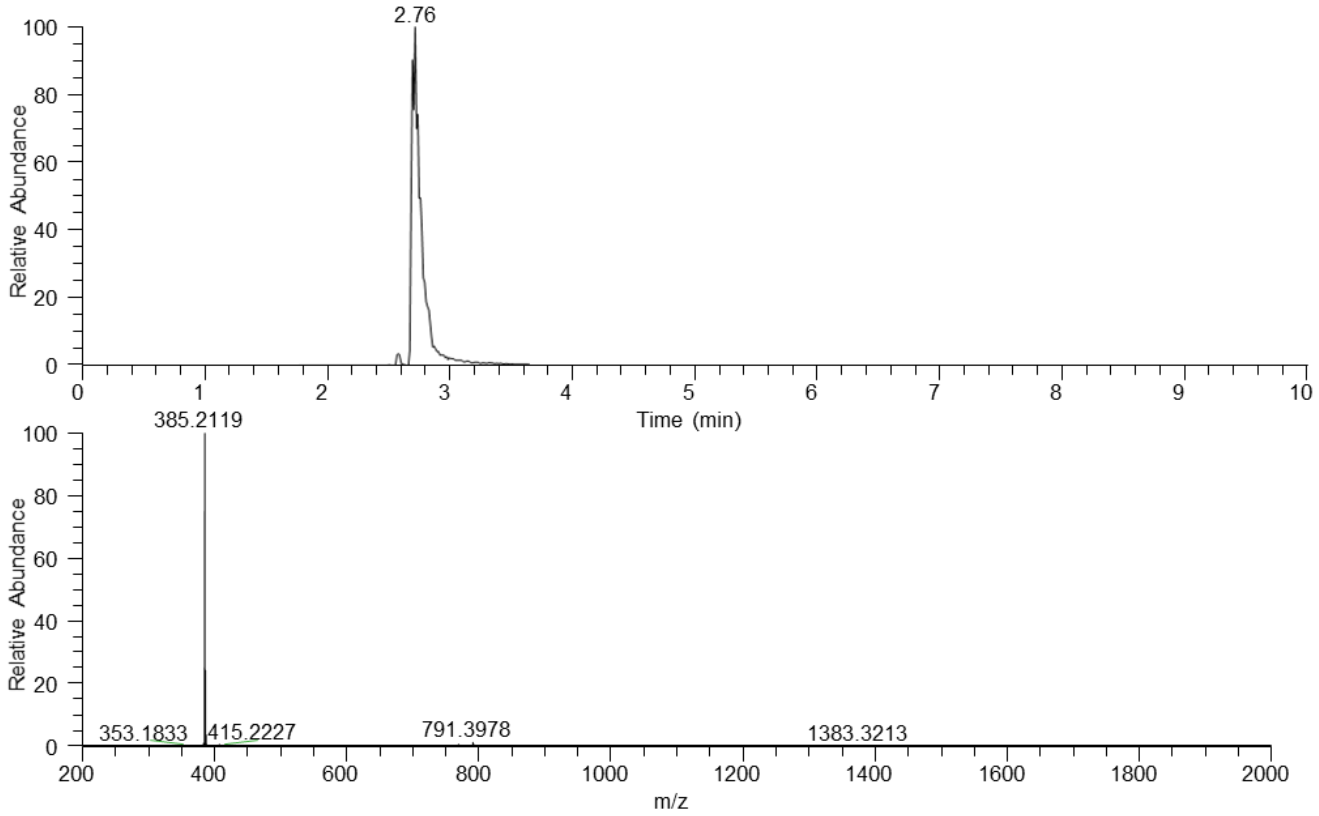

Figure S57. UPLC-HRESIMS data for 3-epirhynchophylline (**17**).

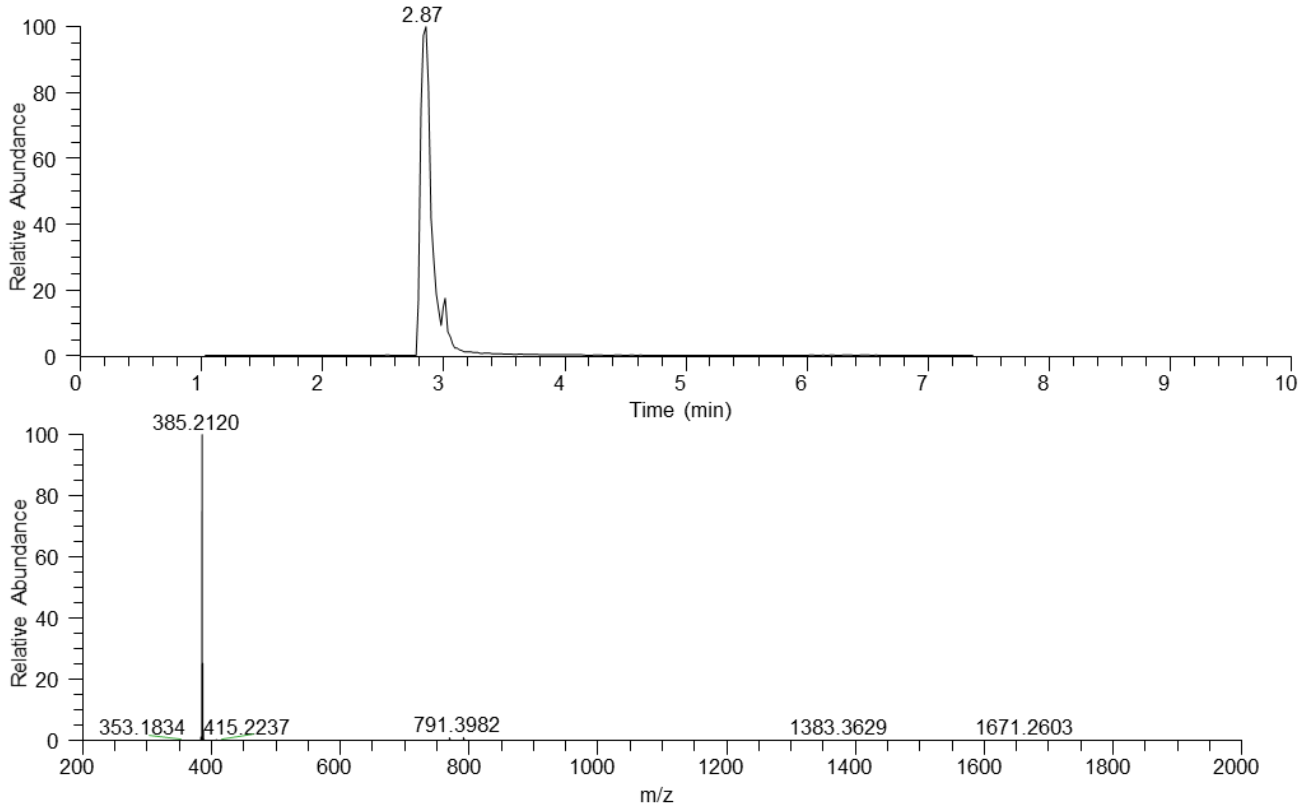

Figure S58. UPLC-HRESIMS data for 3-epicorynoxine B (**18**).

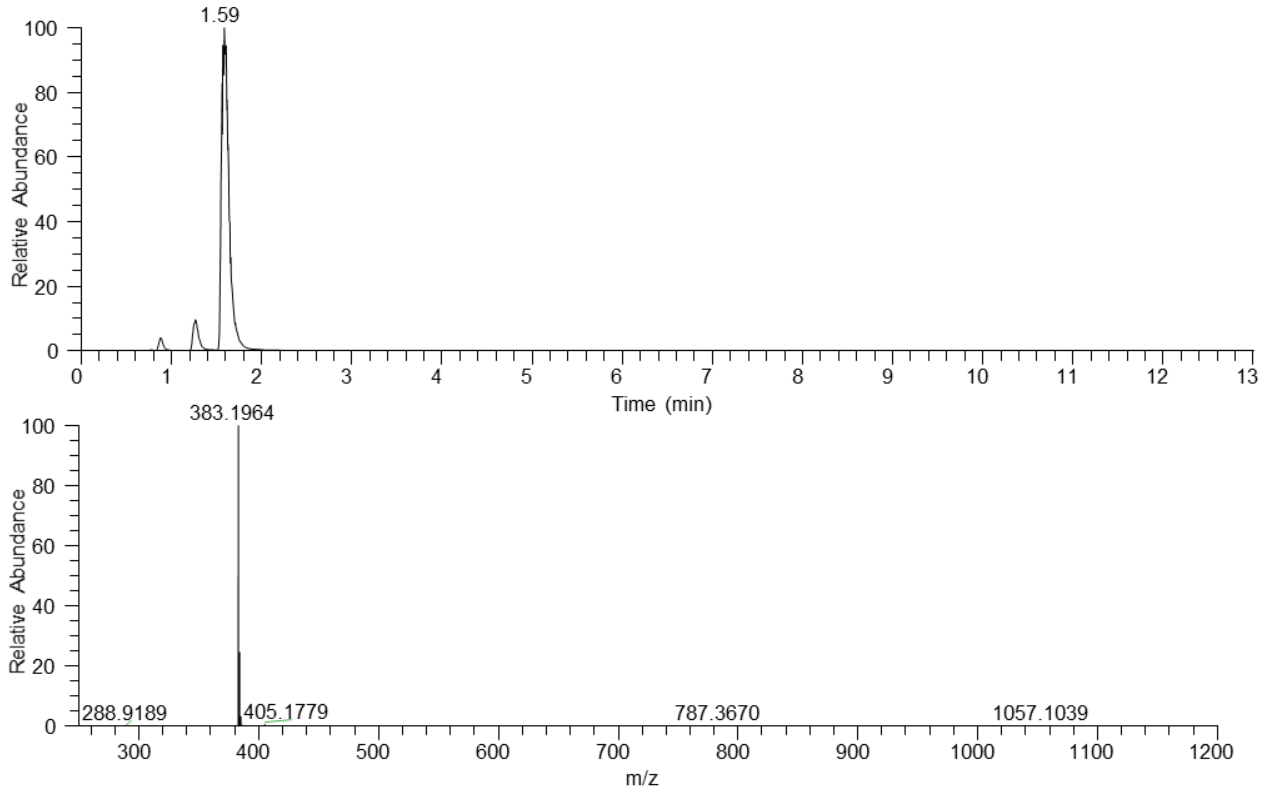

Figure S59. UPLC-HRESIMS data for corynoxeine (**19**)

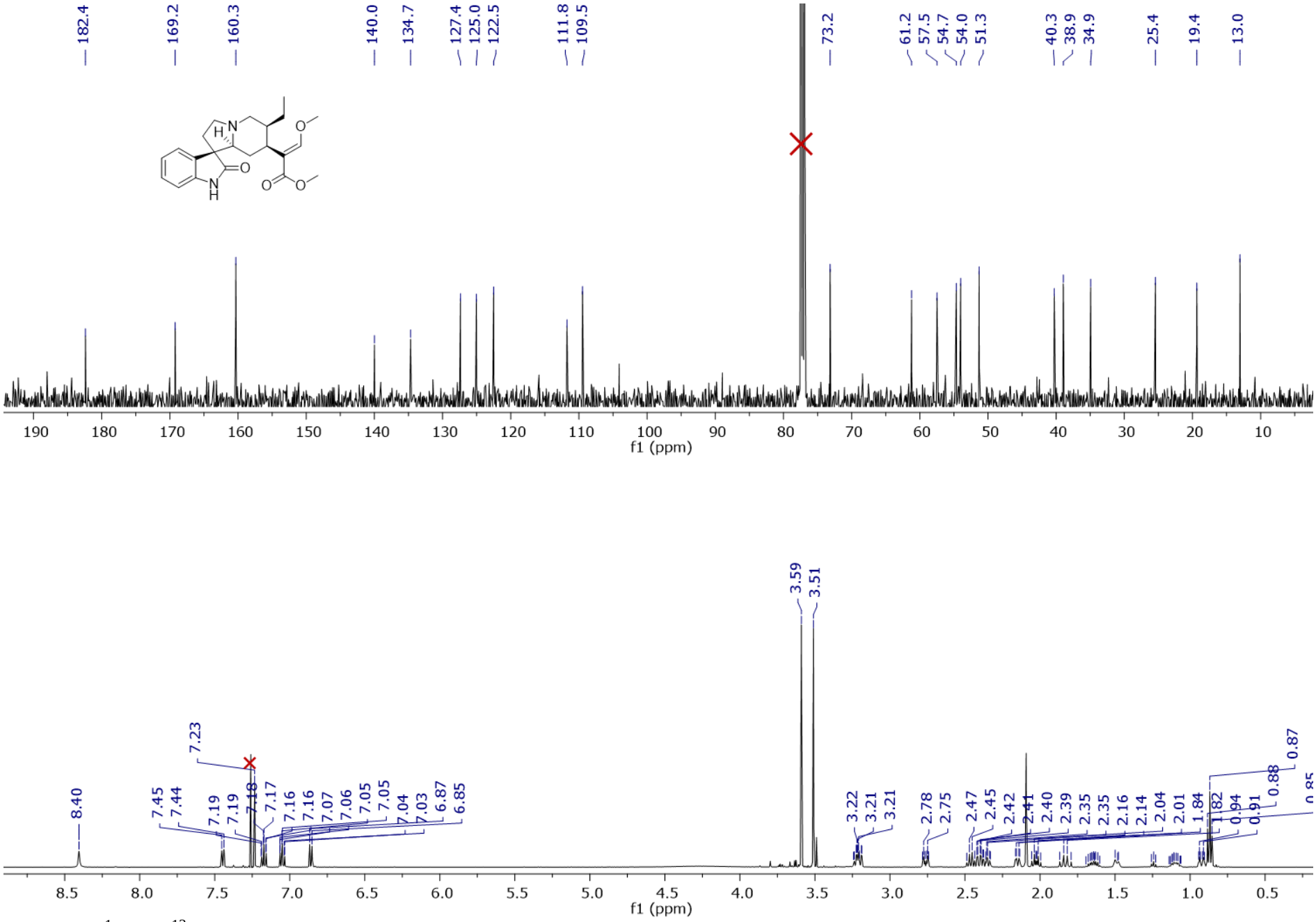

Figure S60. ^{1}H and ^{13}C NMR spectra for corynoxine A (**15**) ($CDCl_3$, 500 MHz and 125 MHz, respectively).

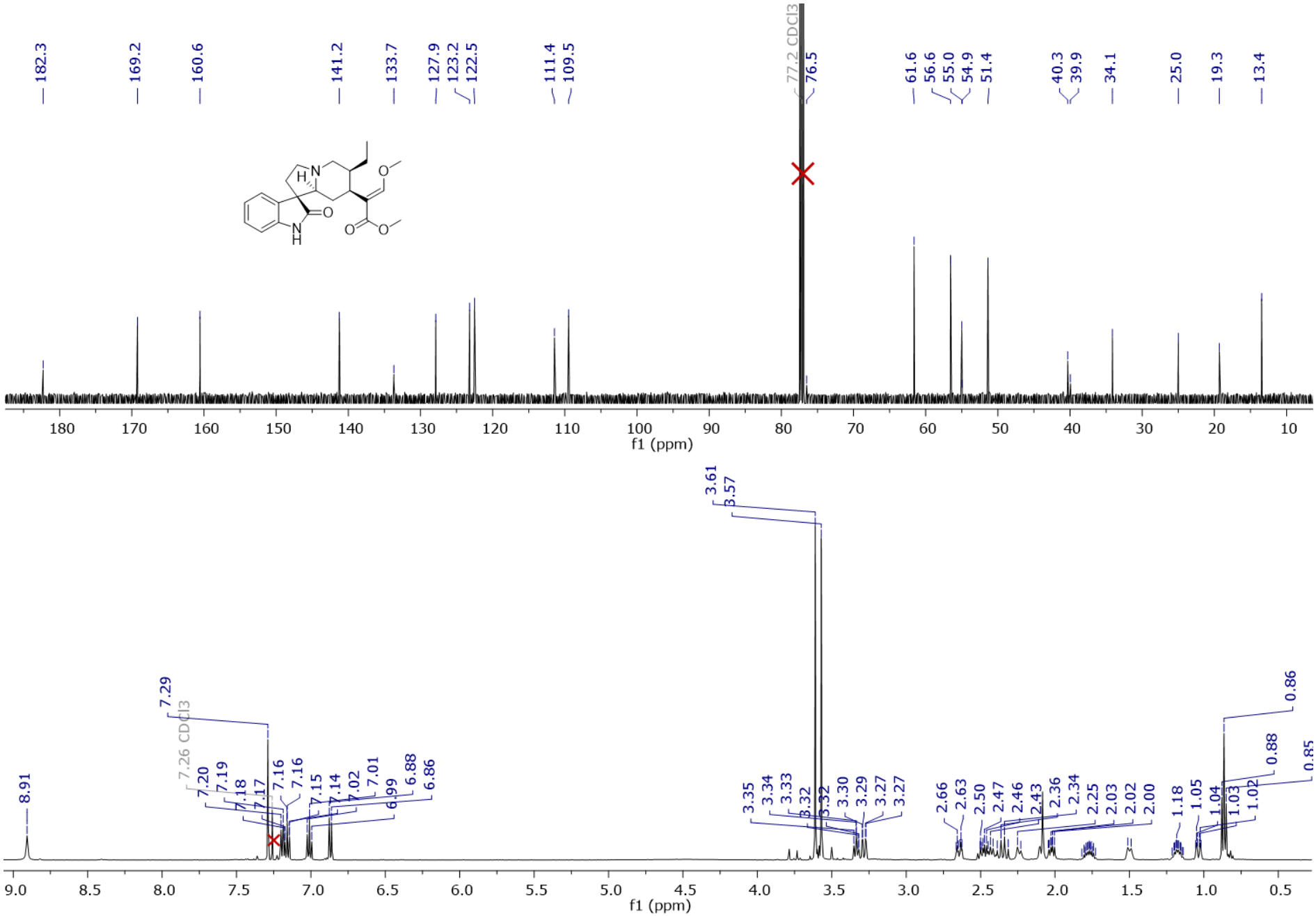

Figure S61. ^{1}H and ^{13}C NMR spectra for corynoxine B (**16**) ($CDCl_3$, 500 MHz and 125 MHz, respectively).

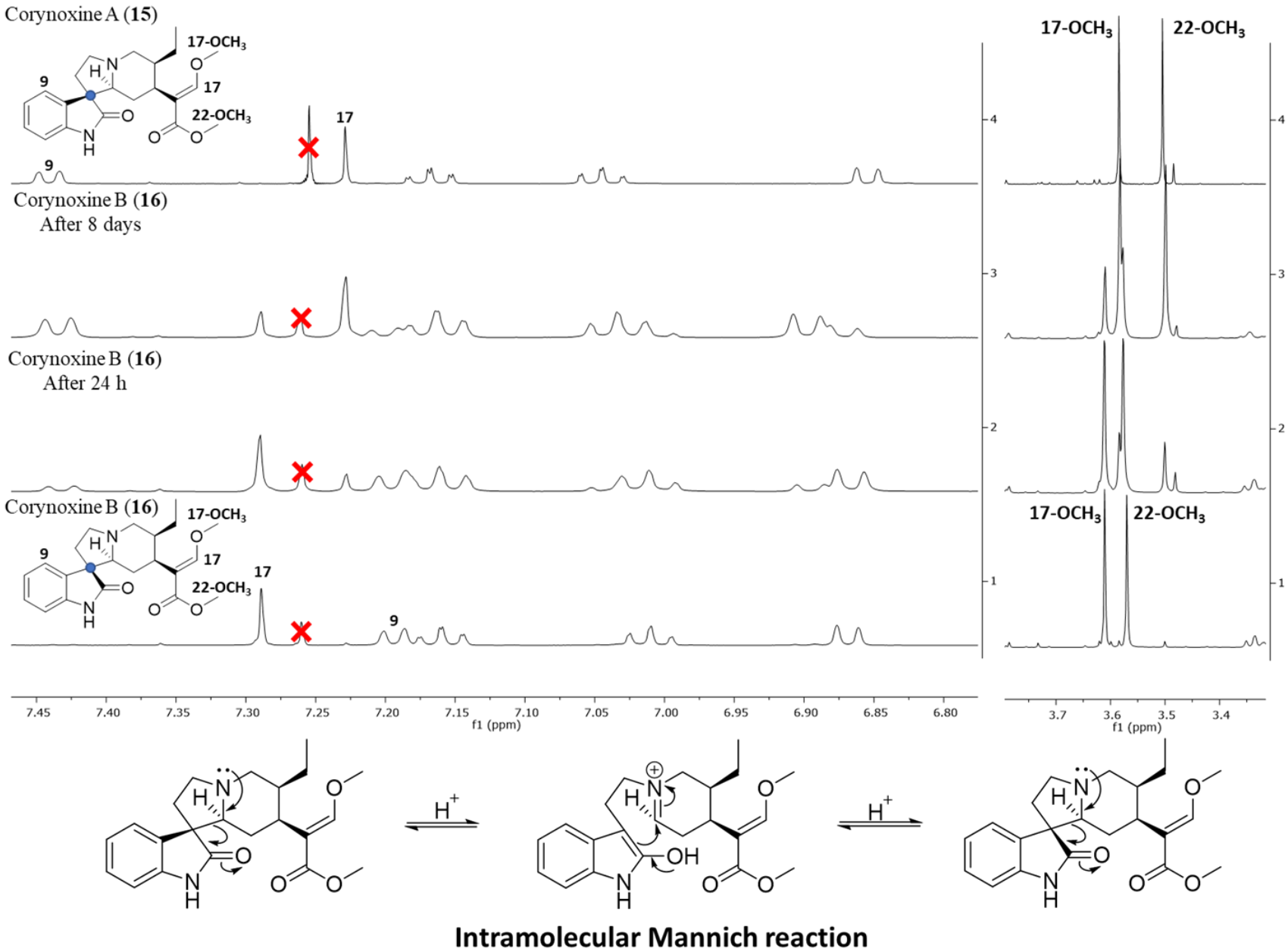

Figure S62. Monitoring the epimerization of corynoxine B (**16**) to corynoxine A (**15**) by ^{1}H NMR ($CDCl_3$, 500 MHz), and the proposed mechanism of epimerization via an intramolecular Mannich reaction.

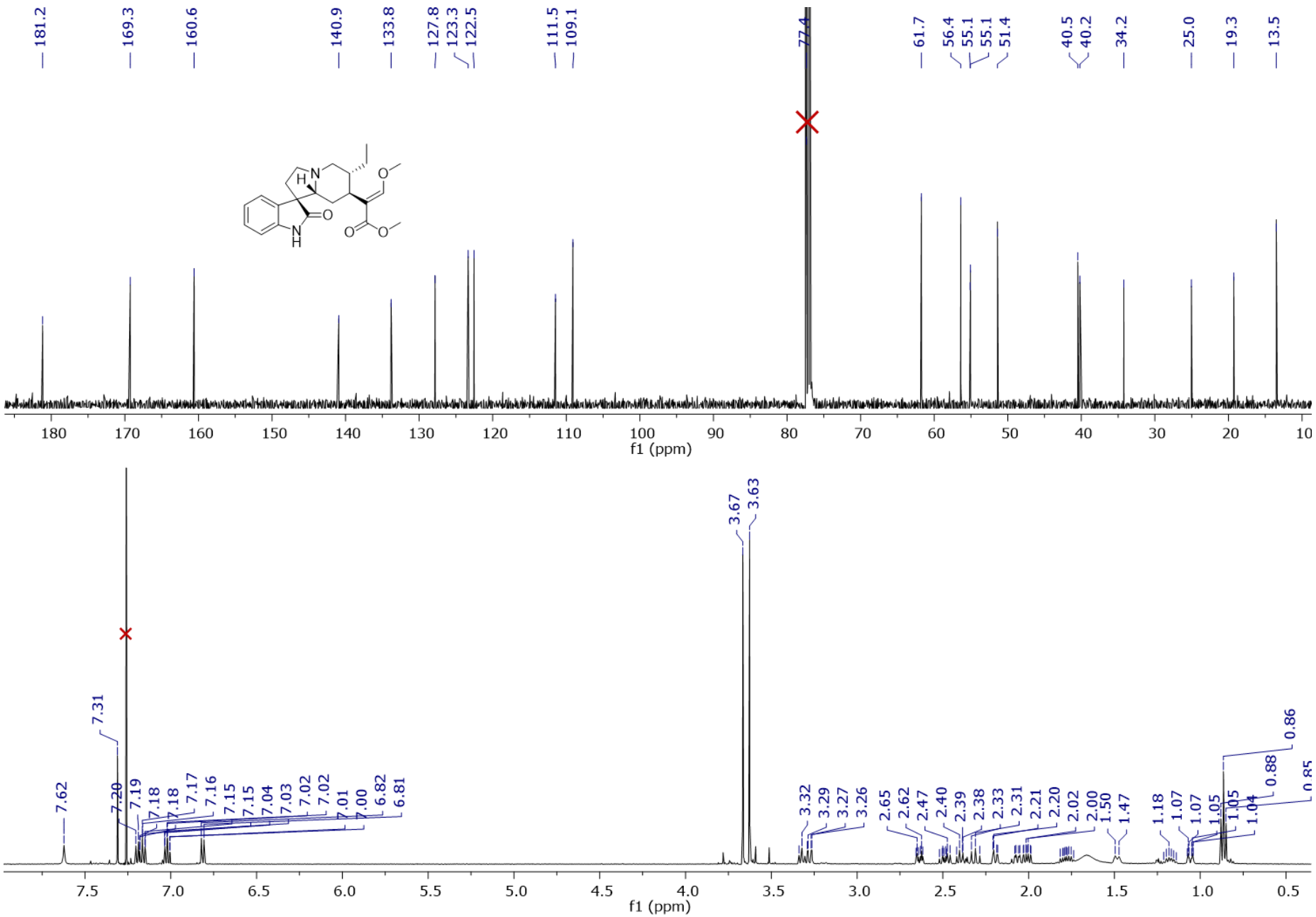

Figure S63. ^{1}H and ^{13}C NMR spectra for 3-epirhynchophylline (**17**) ($CDCl_3$, 500 MHz and 125 MHz, respectively).

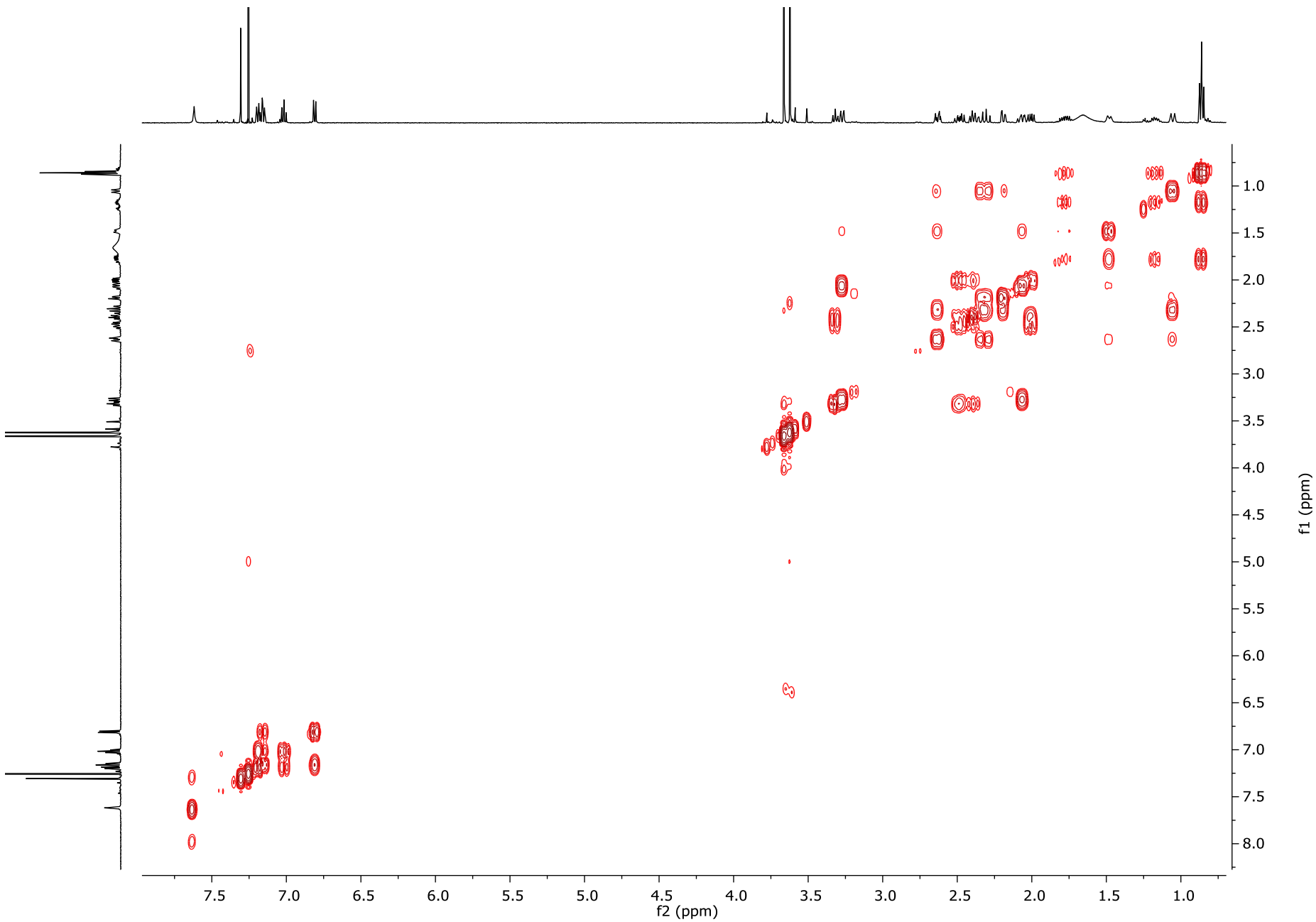

Figure S64. COSY spectrum for 3-epirhynchophylline (**17**) ($CDCl_3$, 500 MHz).

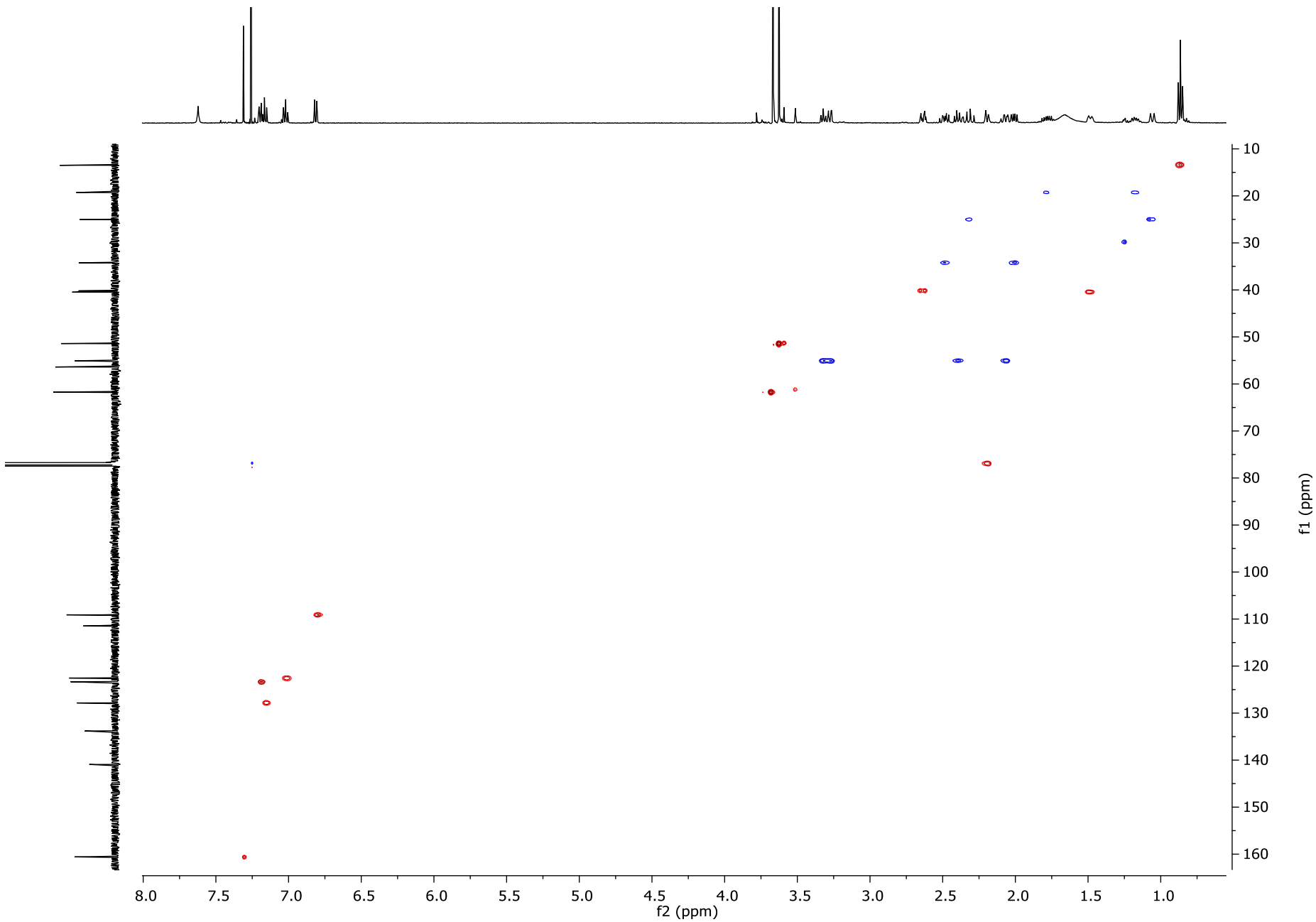

Figure S65. HSQC spectrum for 3-epirhynchophylline (**17**) ($CDCl_3$, 500 MHz).

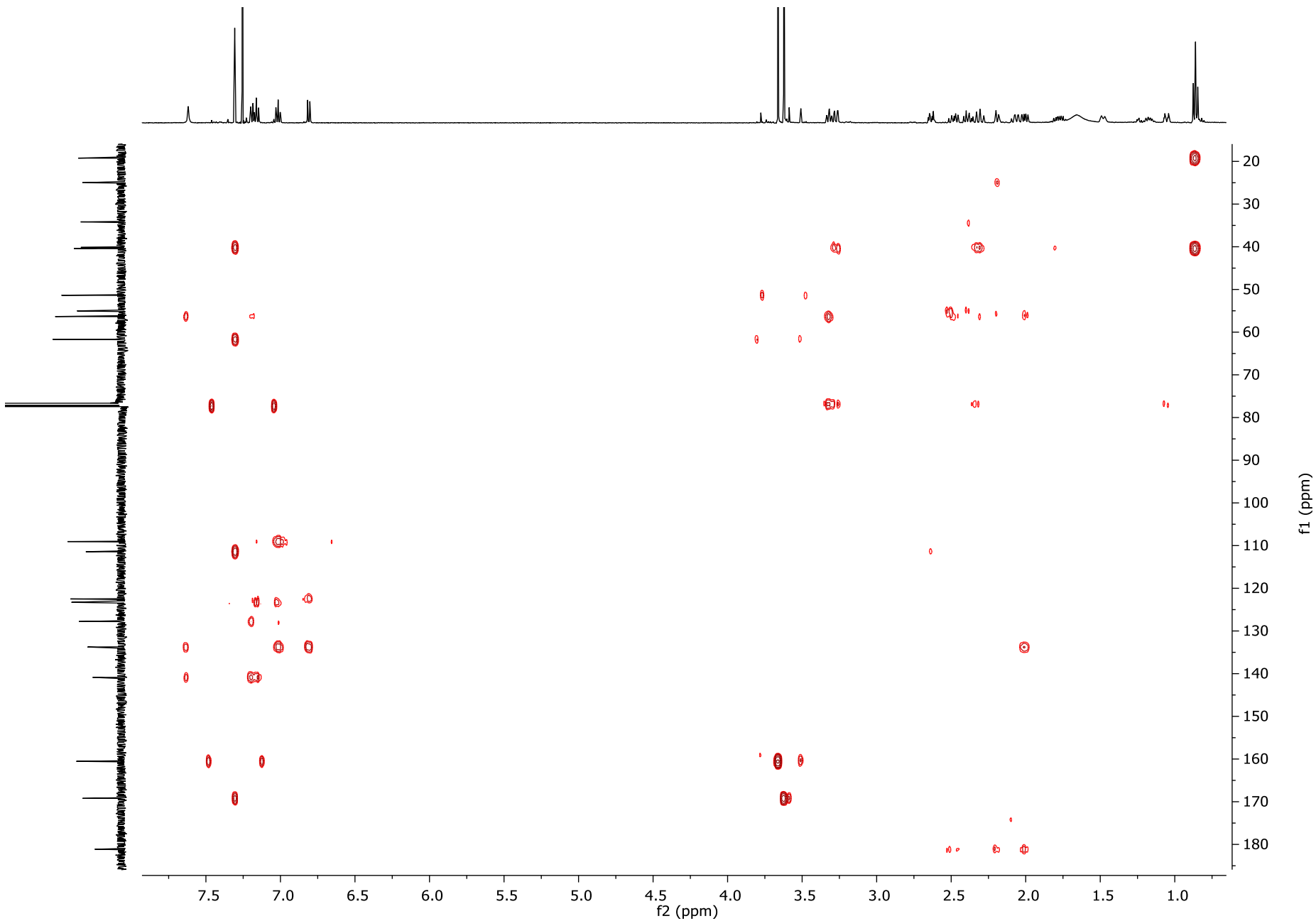

Figure S66. HMBC spectrum for 3-epirhynchophylline (**17**) ($CDCl_3$, 500 MHz).

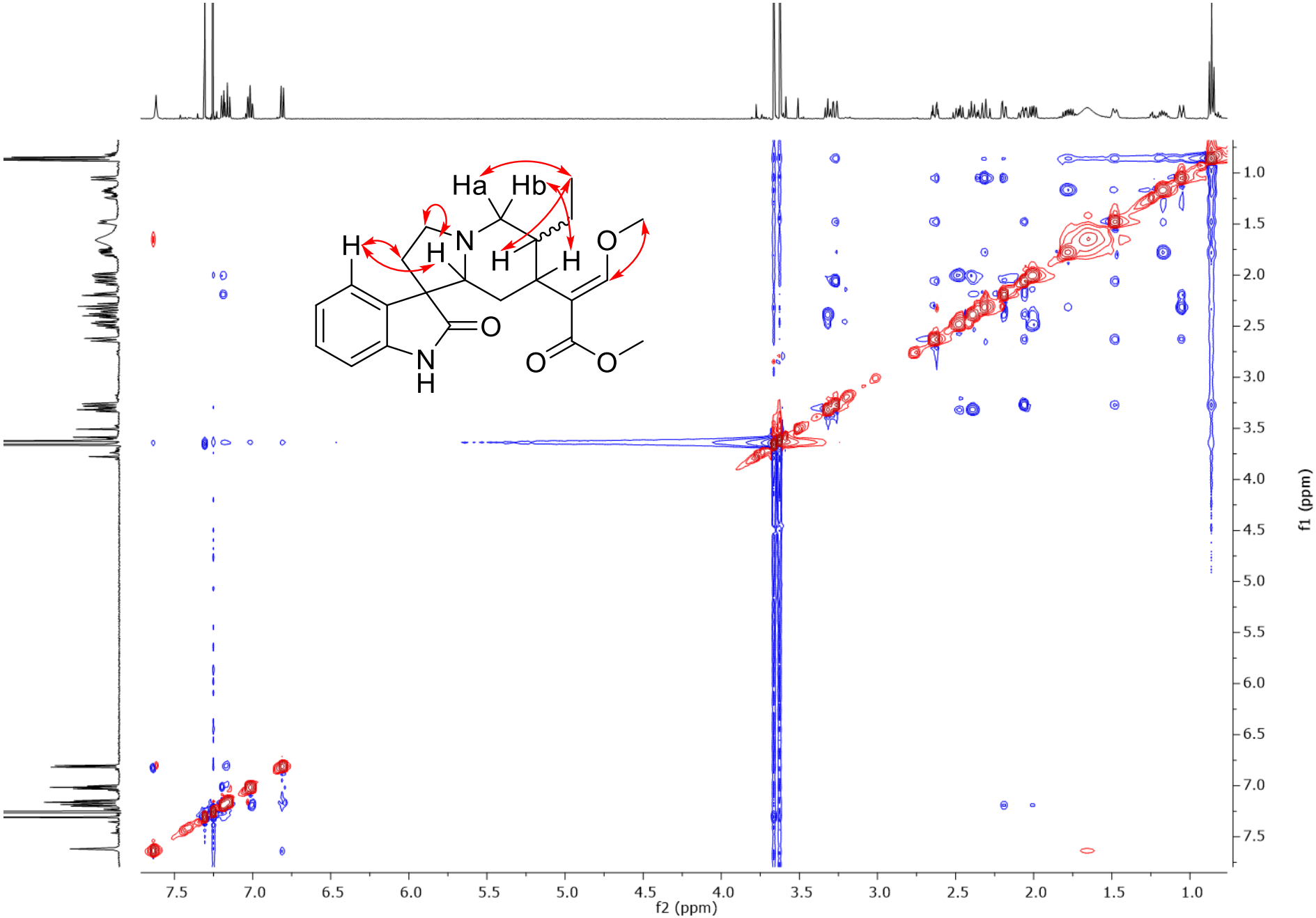

Figure S67. NOESY spectrum for 3-epirhynchophylline (**17**) ($CDCl_3$, 500 MHz).

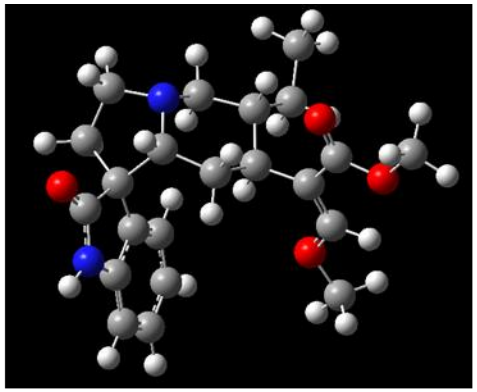

17a (*ΔG* 0.000 kcal/mol; *P* = 25.16%)

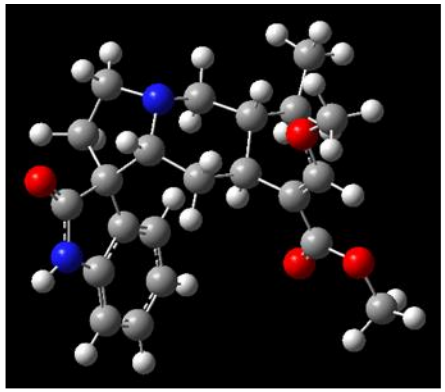

17b (*ΔG* 0.131 kcal/mol; *P* = 20.14%)

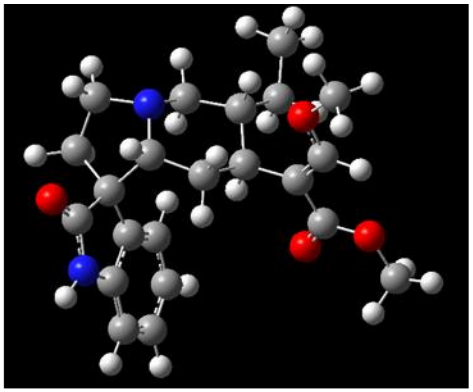

17c (*ΔG* 0.132 kcal/mol; *P* = 20.12%)

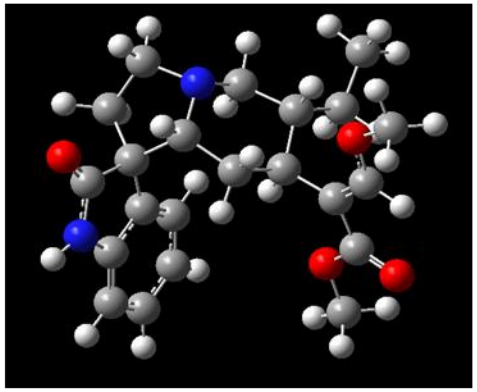

17d (*ΔG* 0.553 kcal/mol; *P* = 9.88%)

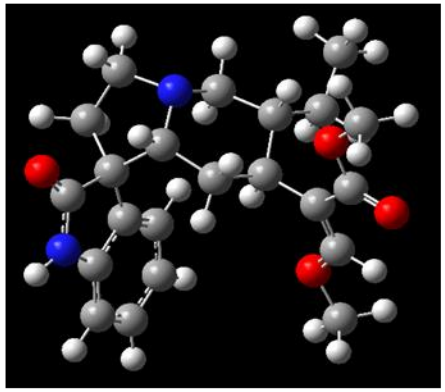

17e (*ΔG* 0.556 kcal/mol; *P* = 9.84%)

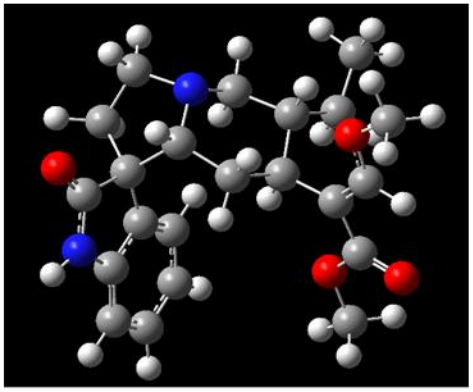

17f (*ΔG* 0.557 kcal/mol; *P* = 9.82%)

Figure S68. Six conformers used for the prediction of the ECD spectrum for **17**. The Boltzmann distributions are expressed as a percentage of population (*P*); the number of excited states considered for the calculation was n = 30.

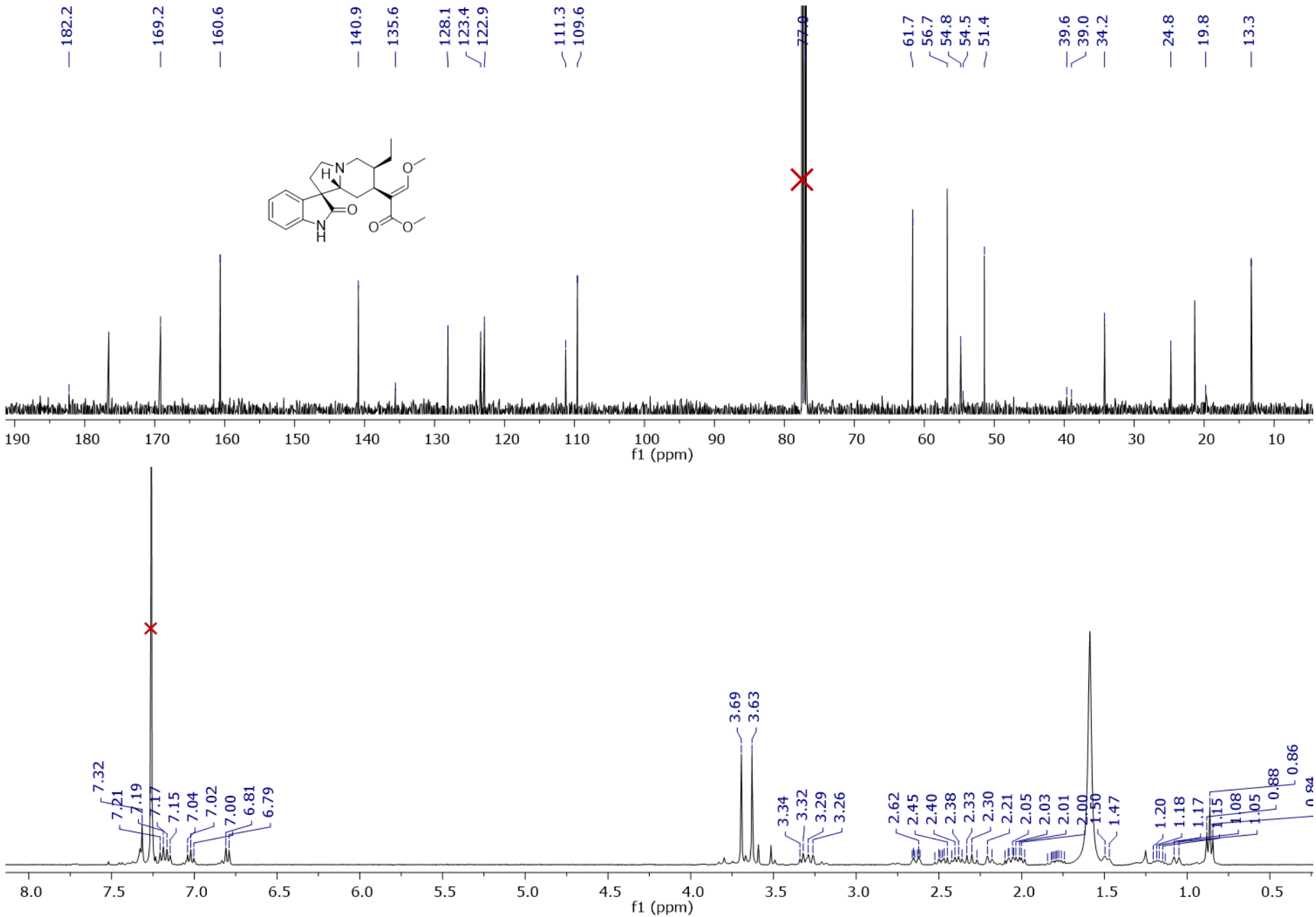

Figure S69. ^{1}H and ^{13}C NMR spectra for 3-epicorynoxine B (**18**) ($CDCl_3$, 500 MHz and 125 MHz, respectively).

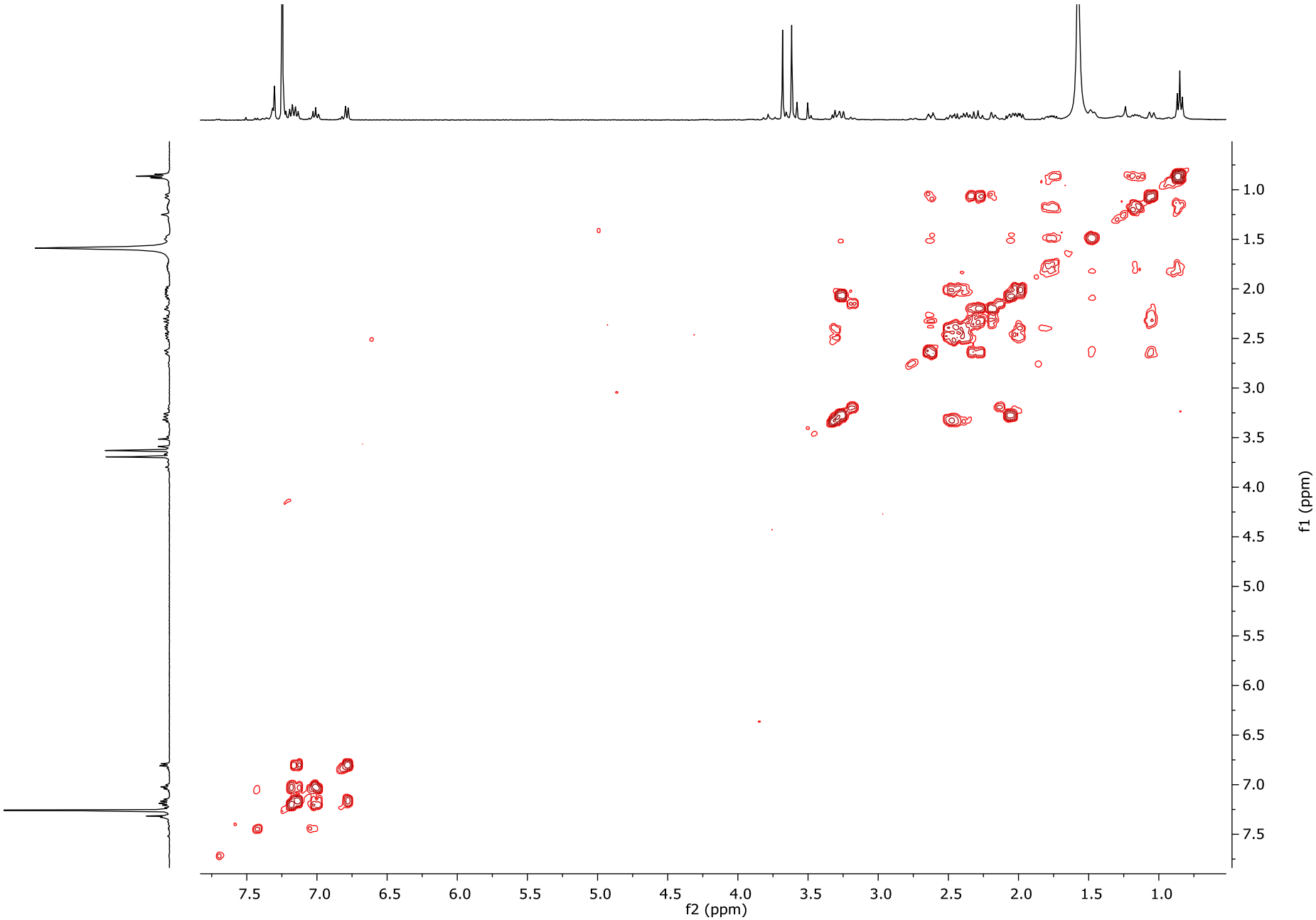

Figure S70. COSY spectrum for 3-epicorynoxine B (**18**) ($CDCl_3$, 500 MHz).

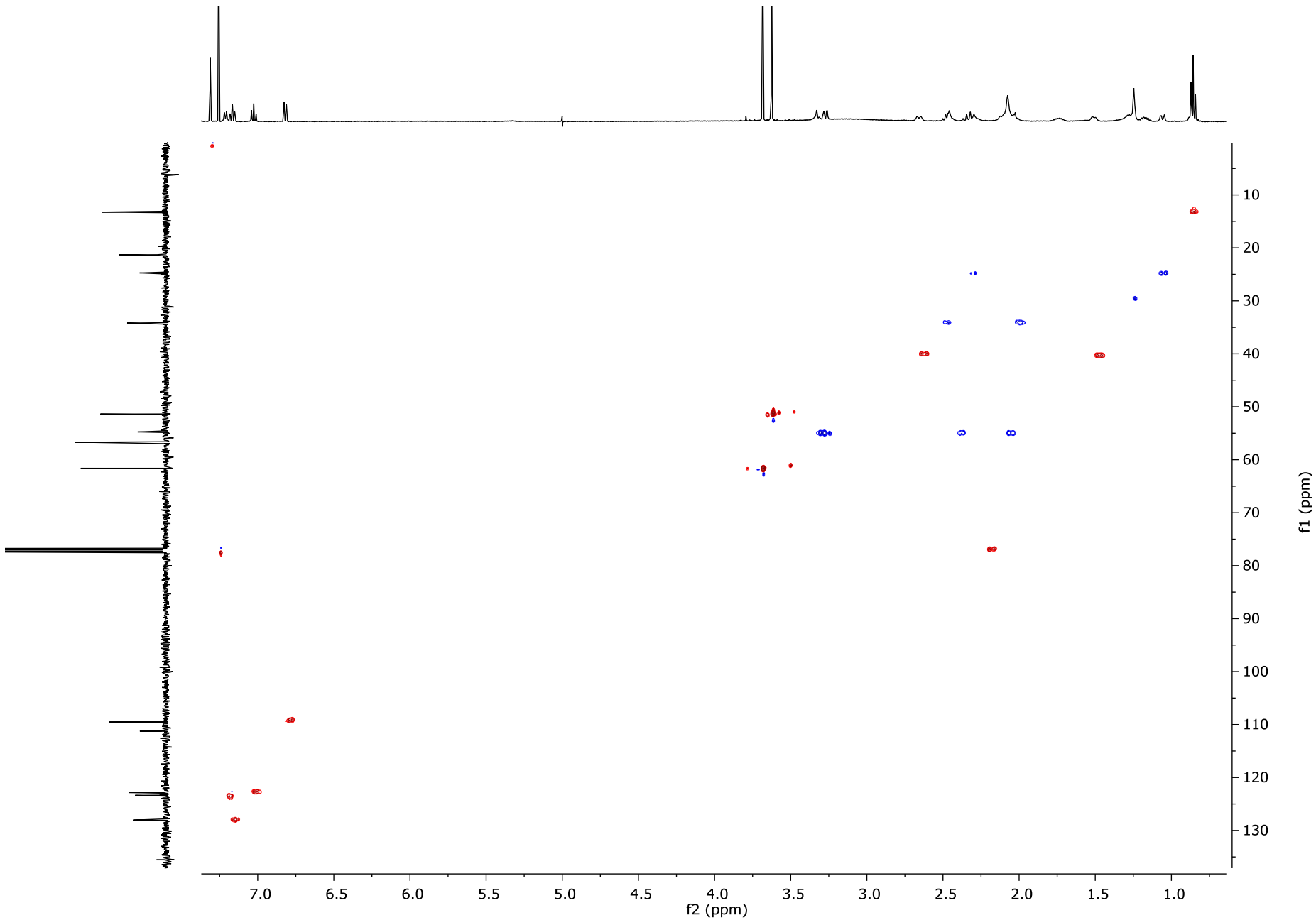

Figure S71. HSQC spectrum for 3-epicorynoxine B (**18**) ($CDCl_3$, 500 MHz).

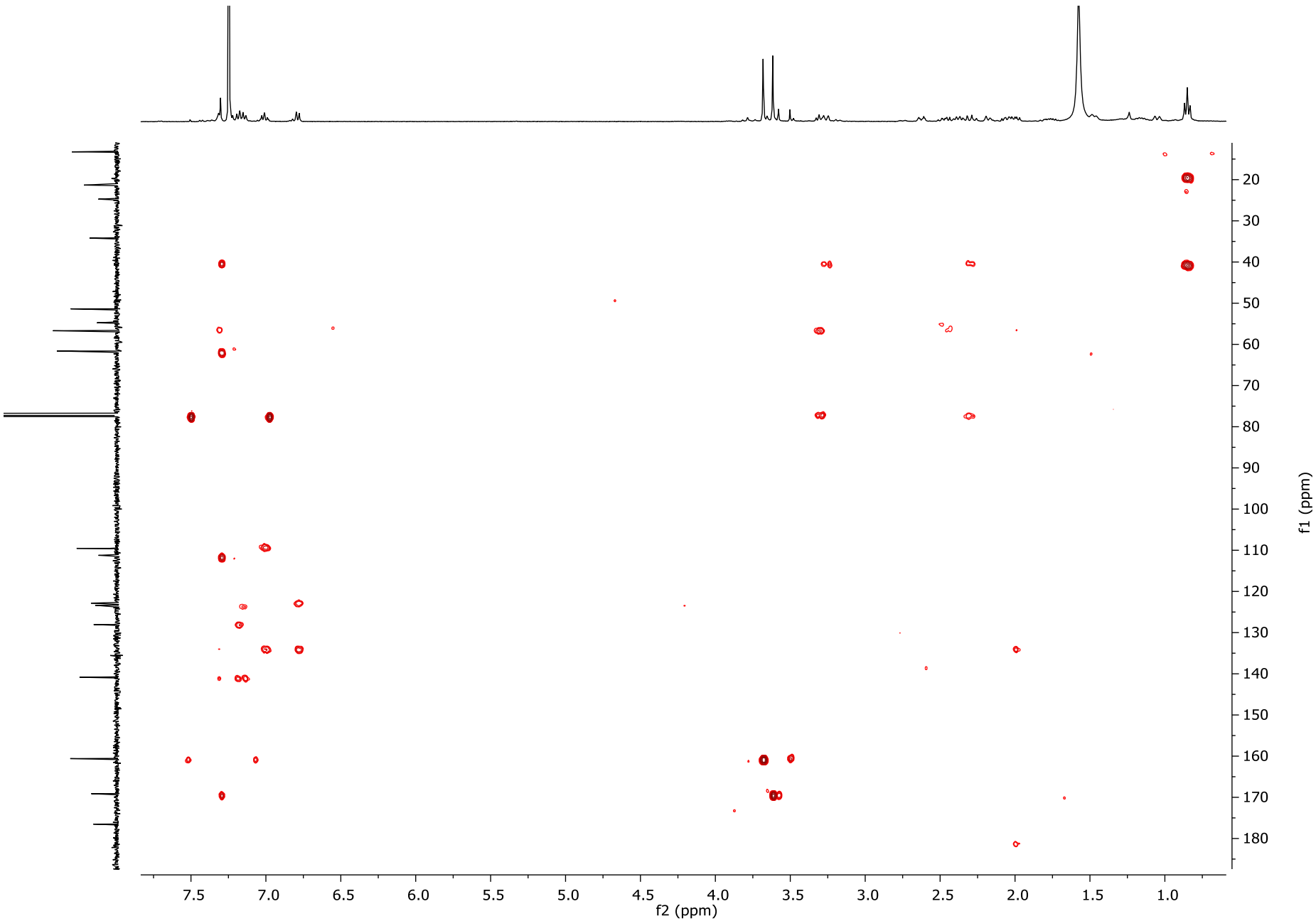

Figure S72. HMBC spectrum for 3-epicorynoxine B (**18**) ($CDCl_3$, 500 MHz).

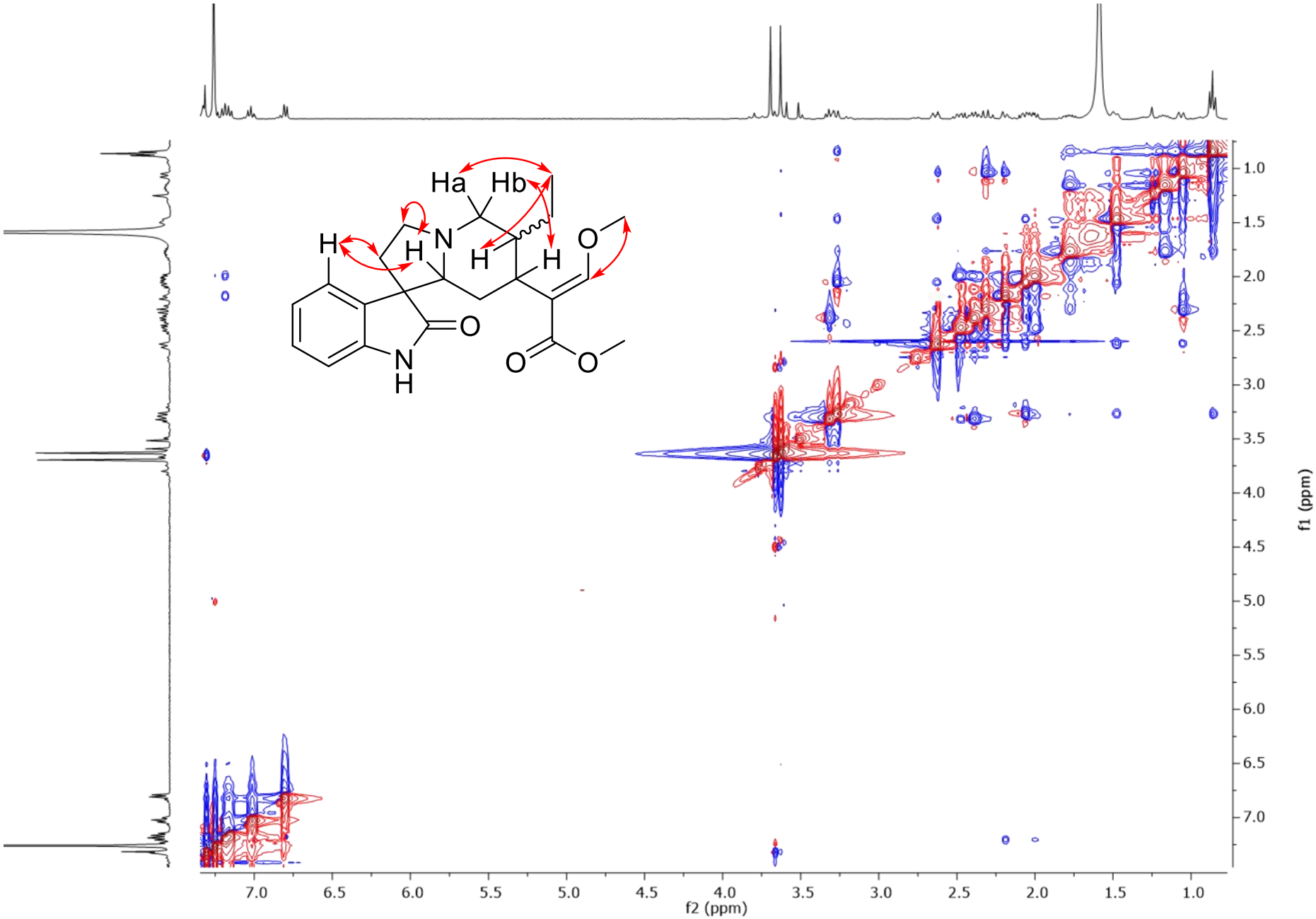

Figure S73. NOESY spectrum for 3-epicorynoxine B (**18**) ($CDCl_3$, 500 MHz).

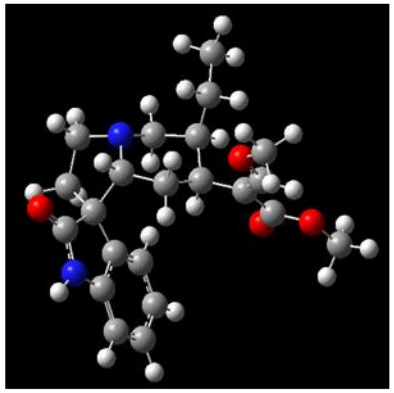

18a (ΔG 0.000 kcal/mol; P = 65.03%)

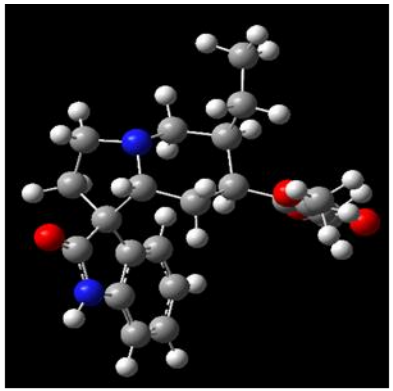

18b (ΔG 0.367 kcal/mol; P = 34.97%)

Figure S74. Two conformers used for the prediction of the ECD spectrum for **18**. The Boltzmann distributions are expressed as a percentage of population (P); the number of excited states considered for the calculation was n = 30.

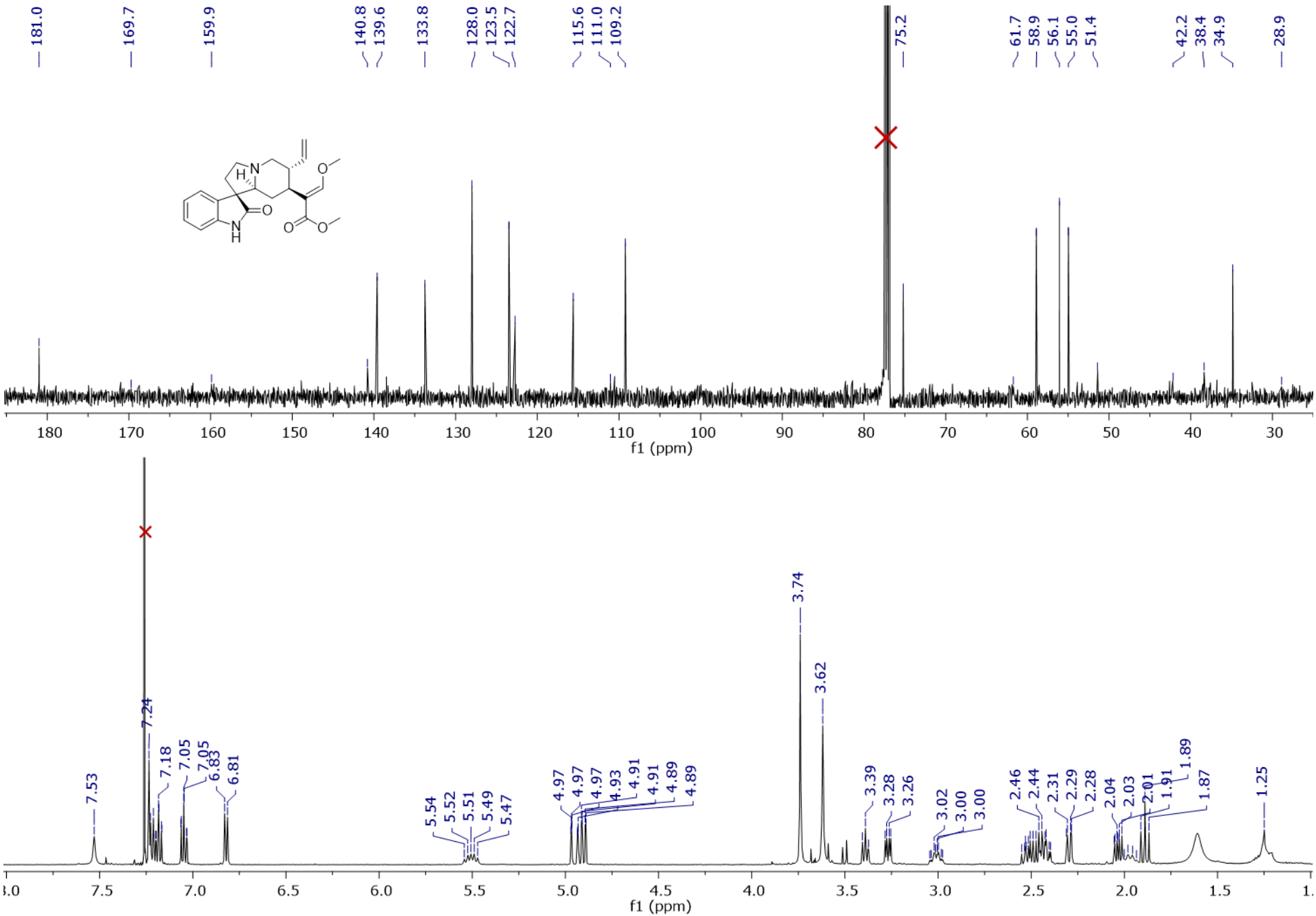

Figure S75. ^{1}H and ^{13}C NMR spectra for corynoxeine (**19**) ($CDCl_3$, 500 MHz and 125 MHz, respectively).

Table S8. Comparison of NMR Data for Compounds 15-19 ($CDCl_3$, 125 MHz and 500 MHz)

	corynoxine A (**15**)			corynoxine B (**16**)			3-epirhynchophylline (**17**)			3-epicorynoxine B (**18**)			corynoxeine (**19**)		
position	δ_C	type	δ_H (*J* in Hz)	δ_C	type	δ_H (*J* in Hz)	δ_C	type	δ_H (*J* in Hz)	δ_C	type	δ_H (*J* in Hz)	δ_C	type	δ_H (*J* in Hz)
2	182.4	C		182.3	C		181.2	C		182.2	C		181.0	C	
3	73.2	CH	2.41, dd (11.3, 2.7)	76.5	CH	2.24, bd (11.2)	77.4	CH	2.19, dd (11.4, 2.4)	77.0	CH	2.19, d (10.9)	75.2	CH	2.30, dd (11.3, 2.5)
5	54.0	CH_2	3.23, dd (8.7, 2.2) 3.20, dd (11.0, 2.16)	54.9	CH_2	3.33, m 2.50, m	55.1	CH_2	3.33, d (8.5) 2.40, m	54.8	CH_2	3.32, t (8.0) 2.39, m	55.0	CH_2	3.39, t (8.3) 2.47, m
6	34.9	CH_2	2.46, q (8.7) 2.03, dt (12.9, 8.5)	34.1	CH_2	2.46, m 2.03, m	34.2	CH_2	2.49, ddd (12.8, 10.0, 8.1) 2.01, ddd (12.9, 7.9, 1.3)	34.2	CH_2	2.49, m 2.01, dd (12.9, 8.3)	34.9	CH_2	2.52, m 2.04, ddd (13.6, 7.2, 1.8)
7	57.5	C		56.6	C		56.4	C		56.7	C		58.9	C	
8	134.7	C		133.7	C		133.8	C		135.6	C		133.8	C	
9	125.0	CH	7.45, d (7.4)	123.2	CH	7.19, d (7.4)	123.3	CH	7.20, d (7.5)	123.4	CH	7.20, d (7.8)	123.5	CH	7.22, d (7.8)
10	122.5	CH	7.05, td (7.6, 1.0)	122.5	CH	7.01, td (7.5, 1.0)	122.5	CH	7.02, td (7.6, 1.0)	122.9	CH	7.02, td (7.5)	122.7	CH	7.05, td (7.6, 1.0)
11	127.4	CH	7.17, td (7.7, 1.3)	127.9	CH	7.16, td (7.7, 1.0)	127.8	CH	7.16, td (7.7, 1.2)	128.1	CH	7.17, t (7.7)	128.0	CH	7.18, td (7.7, 1.2)
12	109.5	CH	6.86, d (7.7)	109.5	CH	6.87, d (7.7)	109.1	CH	6.81, d (7.7)	109.6	CH	6.80, d (7.7)	109.2	CH	6.82, d (7.7)
13	140.0	C		141.2	C		140.9	C		140.9	C		140.8	C	
14	25.4	CH_2	2.36, ddd (12.8, 9.4, 2.3) 0.92, dt (13.2, 3.0)	25.0	CH_2	2.37, td (12.5, 12.1) 1.04, dt (12.3, 2.8)	25.0	CH_2	2.31, m 1.06, dt (12.4, 2.6)	24.8	CH_2	2.30, m 1.06, d (12.0)	28.9	CH_2	2.47, m 1.89 t (10.9)
15	38.9	CH	2.76, dt (13.3, 3.6)	39.9	CH	2.64, dt (12.9, 3.4)	40.2	CH	2.64, dt (12.9, 3.4)	39.0	CH	2.64, qt (12.8, 2.9)	38.4	CH	3.01, qd (11.5, 3.8)
16	111.8	C	-	111.4	C	-	111.5	C	-	111.3	C	-	111.0	C	
17	160.3	CH	7.23, s	160.6	CH	7.29, s	160.6	CH	7.31, s	160.6	CH	7.32, s	159.9	CH	7.24, s
18	13.0	CH_3	0.87, t (7.4)	13.4	CH_3	0.86, t (7.4)	13.5	CH_3	0.86, t (7.4)	13.3	CH_3	0.86, t (7.3)	115.6	CH_2	4.95, ddd (17.2, 2.01, 0.8) 4.90, dd (10.2, 2.1)
19	19.4	CH_2	1.10, dqd (15.7, 7.8, 2.9) 1.65, dq (14.3, 7.2)	19.3	CH_2	1.77, ddq (14.2, 11.1, 7.1) 1.18, m	19.3	CH_2	1.78, ddq (13.6, 11.2, 7.2) 1.18, dq (14.7, 7.7)	19.8	CH_2	1.80, m 1.17, dq (14.5, 7.3)	139.6	CH_2	5.51, dt (18.0, 9.1)
20	40.3	CH	1.49, dt (11.4, 2.6)	40.3	CH	1.50, d (11.0)	40.5	CH	1.48, bd (11.1)	39.6	CH	1.48, d (10.6)	42.2	CH	1.97. dd (12.8, 10.3)
21	54.7	CH_2	2.15, dd (11.2, 2.7)	55.0	CH_2	3.28, dd (11.1, 2.1) 2.11, dd (9.8, 2.4	55.1	CH_2	3.28, dd (11.1, 2.1) 2.07, dd (11.2, 3.3)	54.5	CH_2	3.28, dd (11.6) 2.07, m	56.1	CH_2	3.27, dd (10.8, 4.1)
22	169.2	C	-	169.2	C	-	169.3	C		169.2	C		169.7	C	
17-OCH_3	61.2	CH_3	3.51, s	61.6	CH_3	3.57, s	61.7	CH_3	3.67, s	61.7	CH_3	3.69, s	61.7	CH_3	3.74, s
22-OCH_3	51.3	CH_3	3.59, s	51.4	CH_3	3.61, s	51.4	CH_3	3.63, s	51.4	CH_3	3.63, s	51.4	CH_3	3.62, s
NH			8.40, s			8.91, s			7.62, s			-			7.53, s

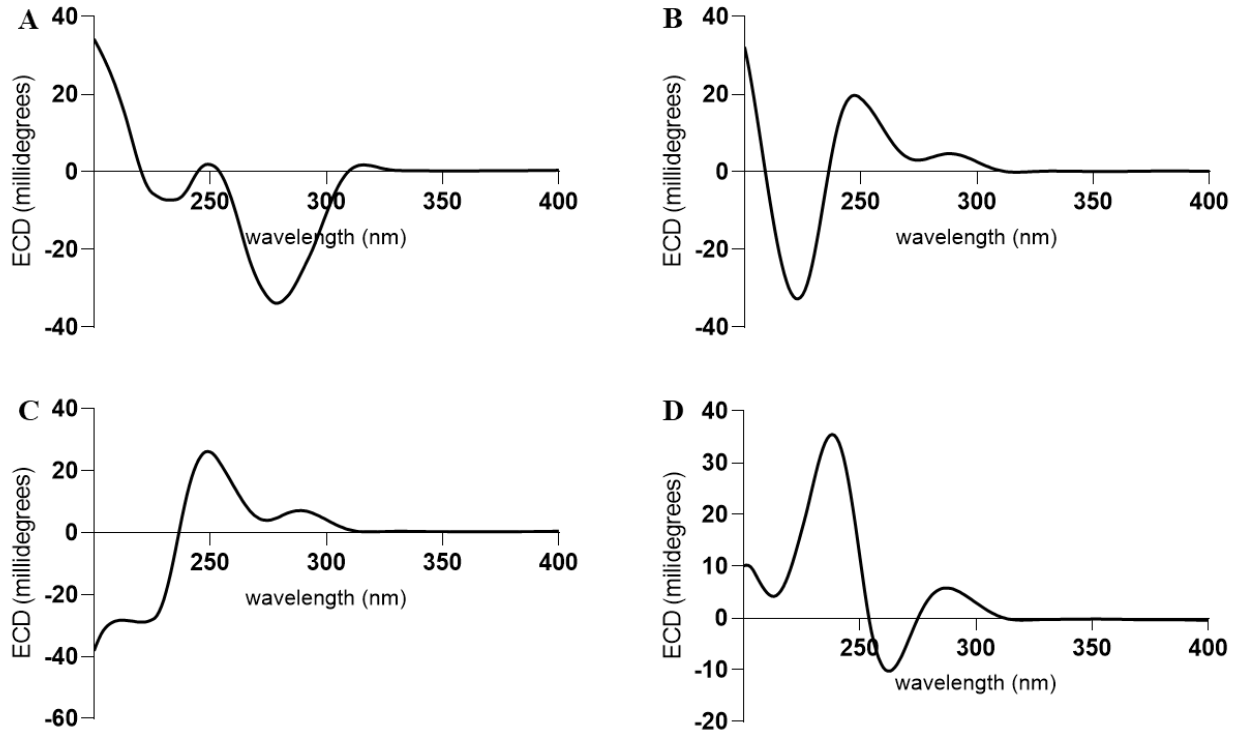

Figure S76. Comparison of the ECD spectra acquired in CH_3OH for A) corynoxine A (**15**), B) 3-epirhynchophylline (**17**), C) 3-epicorynoxine B (**18**), and D) corynoxeine (**19**).

Table S9. Confidence level data for the comparison of calculated and experimental VCD spectra.

Compound	S_E[a]	S_{-E}[b]	ESI[c]
Mitragynine (**1**)	70.0	4.6	65.4
Isopaynantheine (**6**)	59.9	8.6	51.2
Epiallo-isopaynantheine (**7**)	62.3	8.6	53.7
Corynoxine A (**15**)	67.2	7.3	59.9
3-epirhynchophylline (**17**)	57.7	8.7	48.9
3-epicorynoxine B (**18**)	58.2	8.9	49.3

[a]VCD spectral similarity for the proposed configuration. [b]VCD spectral similarity for the opposite proposed configuration. [c]Enantiomeric similarity index.

VCD Measurements. The samples were dissolved in $CHCl_3$ and placed in a BaF_2 cell with a path-length of 100 μm. In both cases, the baseline was generated by subtracting the spectrum of the solvent acquired under the same conditions.

Computational Methods. The minimum energy structures were built with Spartan'10 software. The conformational analysis was performed using the Monte Carlo search protocol under the MMFF94 molecular mechanics force field. The conformers were submitted to Gaussian'09 for calculation of their geometry optimization, performed using the B3LYP/cc-pVTZ level of theory. The optimized values were used to calculate vibrational frequencies, dipole transition moments, and rotational strengths. Individual VCD spectra were obtained as the sum of Lorentzian bands with a half-width of 9 cm^{-1} for each frequency value.

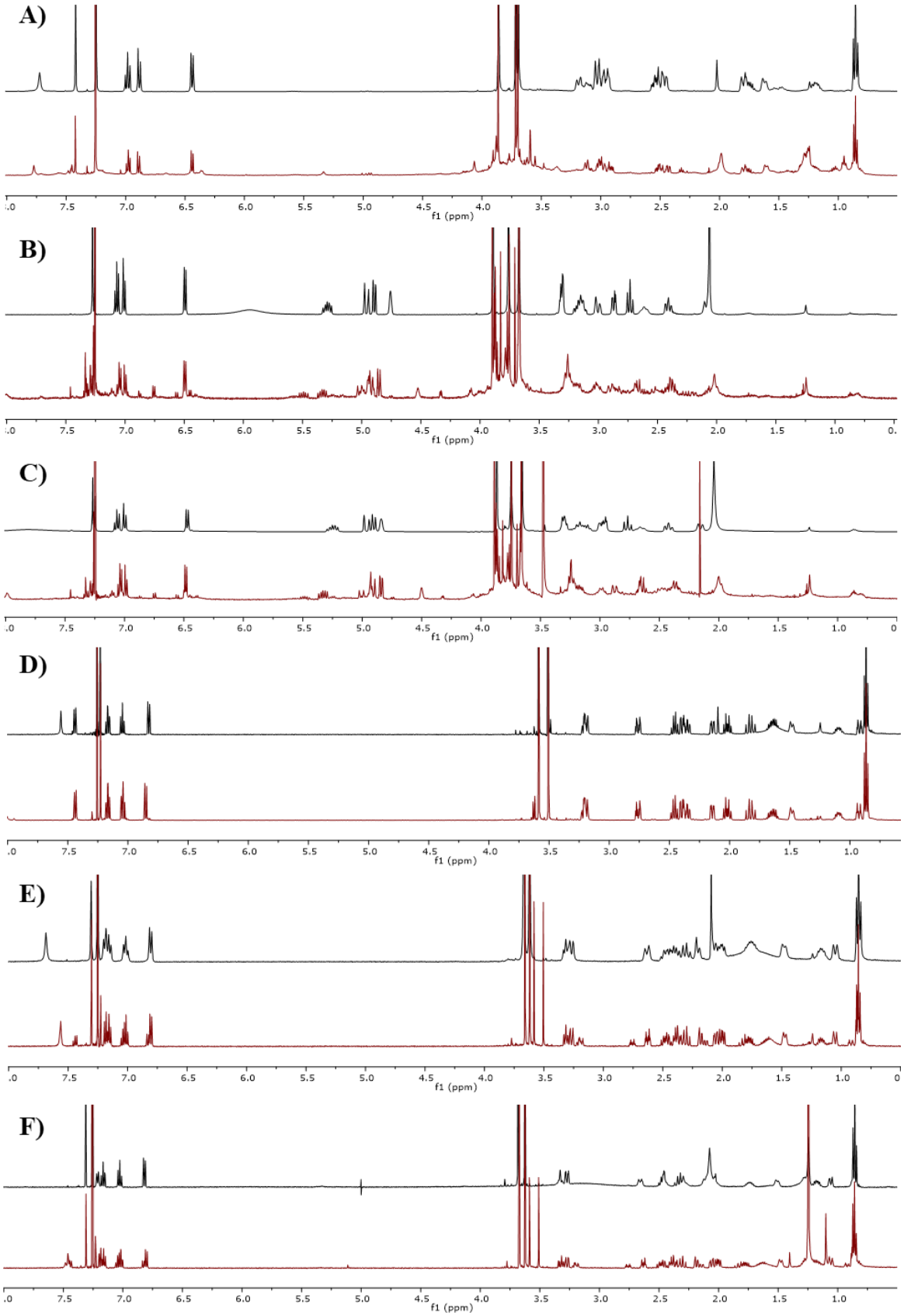

Figure S77. Comparison of the ^{1}H NMR before (black) and after (red) the acquisition of the VCD experiment. A) mitragynine (**1**), B) isopaynantheine (**6**), C) epiallo-isopaynantheine (**7**), D) corynoxine A (**15**), E) 3-epirhyncophylline (**17**), and F) 3-epicorynoxine B (**18**).